AD-A208 765

NAVAL POSTGRADUATE SCHOOL

Monterey, California

DTIC
ELECTE
JUN 0 9 1989
S D
H

THESIS

Synoptic Forcing of East Asian
Cold Surges

by

Randy J. Lefevre

March 1989

Thesis Advisor: Roger T. Williams

Approved for public release; distribution is unlimited.

89 6 09 024

Unclassified

Security Classification of this page

REPORT DOCUMENTATION PAGE

1a Report Security Classification Unclassified	1b Restrictive Markings
2a Security Classification Authority	3 Distribution Availability of Report
2b Declassification/Downgrading Schedule	Approved for public release; distribution is unlimited.
4 Performing Organization Report Number(s)	5 Monitoring Organization Report Number(s)
6a Name of Performing Organization Naval Postgraduate School; 6b Office Symbol (If Applicable) 63	7a Name of Monitoring Organization Naval Postgraduate School
6c Address (city, state, and ZIP code) Monterey, CA 93943-5000	7b Address (city, state, and ZIP code) Monterey, CA 93943-5000
8a Name of Funding/Sponsoring Organization; 8b Office Symbol (If Applicable)	9 Procurement Instrument Identification Number
8c Address (city, state, and ZIP code)	10 Source of Funding Numbers: Program Element Number; Project No; Task No; Work Unit Accession No.
11 Title (Include Security Classification) Synoptic Forcing of East Asian Cold Surges	
12 Personal Author(s) Randy J. Lefevre	
13a Type of Report Master's Thesis; 13b Time Covered From To	14 Date of Report (year, month,day) March 1989; 15 Page Count 122
16 Supplementary Notation The views expressed in this thesis are those of the author and do not reflect the official policy or position of the Department of Defense or the U.S. Government.	

17 Cosati Codes			18 Subject Terms (continue on reverse if necessary and identify by block number)
Field	Group	Subgroup	Winter Monsoon; Cold Surge; Eady Model; Planetary-scale Forcing; Synoptic-scale Forcing; Normal Modes; Rossby Waves; Primitive Equation Model; Spectral Model

19 Abstract (continue on reverse if necessary and identify by block number

A linearized, global spectral model with eight levels was used to determine whether the nonlinear interaction between a planetary-scale wave (wavenumber four) and a rapidly growing synoptic-scale wave (wavenumber seven) could produce a northeasterly wind, characteristic of East Asian cold surges. The amplitude of the synoptic-scale wave, or generic cyclone, was produced by a nonlinear Eady model of the atmosphere that included friction. The resulting nonlinear forcing was applied to either the first law of thermodynamics, the vorticity equation, or both.

The thermal forcing did not produce a significant cold surge response. The vorticity forcing produced a respectable cold surge within 48 hours. The results of this study indicate the planetary-synoptic wave interaction is a possible method for initiating East Asian cold surges.

20 Distribution/Availability of Abstract [X] unclassified/unlimited [ ] same as report [ ] DTIC users	21 Abstract Security Classification Unclassified
22a Name of Responsible Individual Roger T. Williams	22b Telephone (Include Area code) (408) 646-2296; 22c Office Symbol 63Wu

DD FORM 1473, 84 MAR 83 APR edition may be used until exhausted

All other editions are obsolete

security classification of this page Unclassified

Approved for public release; distribution is unlimited.

Synoptic Forcing of East Asian Cold Surges

by

Randy J. Lefevre
Captain, United States Air Force
B.A., Sonoma State University, California, 1982

Submitted in partial fulfillment of the
requirements for the degree of

MASTER OF SCIENCE IN METEOROLOGY

from the

NAVAL POSTGRADUATE SCHOOL
March 1989

Author: _____
Randy J. Lefevre

Approved by: _____
Roger T. Williams, Thesis Advisor

_____
Chih-Pei Chang, Second Reader

_____
Robert J. Renard, Chairman
Department of Meteorology

_____
Gordon E. Schacher,
Dean of Science and Engineering

ABSTRACT

A linearized, global spectral model with eight levels was used to determine whether the nonlinear interaction between a planetary-scale wave (wavenumber four) and a rapidly growing synoptic-scale wave (wavenumber seven) could produce a northeasterly wind, characteristic of East Asian cold surges. The amplitude of the synoptic-scale wave, or generic cyclone, was produced by a nonlinear Eady model of the atmosphere that included friction. The resulting nonlinear forcing was applied to either the first law of thermodynamics, the vorticity equation, or both.

The thermal forcing did not produce a significant cold surge response. The vorticity forcing produced a respectable cold surge within 48 hours. The results of this study indicate the planetary-synoptic wave interaction is a possible method for initiating East Asian cold surges.

DTIC
COPY
INSPECTED
6

Accession For
NTIS GRA&I ☑
DTIC TAB ☐
Unannounced ☐
Justification
By
Distribution/
Availability Codes
Dist | Avail and/or Special
A-1

TABLE OF CONTENTS

I. INTRODUCTION 1

II. SIMPLE BETA-PLANE SOLUTION 8

III. MODEL DESCRIPTION 14

A. VERTICAL STRUCTURE 18

B. SPECTRAL FORMULATION 22

IV. FORCING FUNCTIONS 24

A. PHASE I - ROSSBY WAVE FORCING 24

B. PHASE II - IMPULSE FORCING 26

C. PHASE III - GENERIC CYCLONE FORCING 28

1. Thermal Forcing 28

2. Vorticity Forcing 33

V. DESCRIPTION OF GENERIC CYCLONE MODEL 38

VI. ANALYSIS OF RESULTS 43

A. NORMAL MODE ANALYSIS 43

B. PHASE I RESULTS 48

1. Experiment 1 50

2. Experiment 2 60

3. Experiment 3 62

4. Experiment 4 62

5. Experiment 5 69

6. Experiment 6 71

7. Experiment 7 72

8. Phase I Summary 78

C. PHASE II RESULTS 78
1. Experiment 8 79
2. Experiment 9 84
3. Phase II Summary 90
D. PHASE III RESULTS 91
1. Experiment 10 94
2. Experiment 11 101
3. Experiment 12 102
4. Phase III Summary 102
VII. CONCLUSION 104
LIST OF REFERENCES 106
INITIAL DISTRIBUTION LIST 108

LIST OF TABLES

TABLE 6.1. EQUIVALENT DEPTH OF VERTICAL MODES 43

TABLE 6.2. ROSSBY WAVE FREQUENCY AND PERIOD OF VERTICAL MODES 49

TABLE 6.3A. ALPHA SQUARED ($M^{-1} X 10^{-12}$) FOR HIGH FREQUENCY MODES 49

TABLE 6.3B. ALPHA SQUARED ($M^{-1} X 10^{-12}$) FOR LOW FREQUENCY MODES 49

TABLE 6.4. PHASE I EXPERIMENTS 50

TABLE 6.5. PHASE II EXPERIMENTS 79

TABLE 6.6. PHASE III EXPERIMENTS 91

LIST OF FIGURES

Figure 1.1. Average Wintertime Surface Wind (Boyle and Chen, 1987).....3

Figure 1.2. Average Wintertime 20 kPa Wind (Boyle and Chen, 1987).....3

Figure 1.3. Climatological January 50 kPa Height Field (Boyle and Chen, 1987).....4

Figure 1.4. Wind Velocity Vectors for a Barotropic Model (Lim and Chang, 1981).....6

Figure 3.1. Vertical Structure of the Primitive Equation Model.....20

Figure 4.1. Vertical Structure of Forced Rossby Wave Solution.....25

Figure 4.2. Latitudinal Structure of Forced Rossby Wave Solution.....26

Figure 4.3. Temporal Structure of the Impulse Forcing.....27

Figure 5.1. Marginal Stability Curve of Eady Model, Including Friction.....40

Figure 6.1. Vertical Profile of Normal Mode 1.....44

Figure 6.2. Vertical Profile of Normal Mode 2.....44

Figure 6.3. Vertical Profile of Normal Mode 3.....45

Figure 6.4. Vertical Profile of Normal Mode 4.....45

Figure 6.5. Vertical Profile of Normal Mode 5.....46

Figure 6.6. Vertical Profile of Normal Mode 6.....46

Figure 6.7. Vertical Profile of Normal Mode 7.....47

Figure 6.8. Vertical Profile of Normal Mode 8.....47

Figure 6.9. Wind Vectors at 24 Hours for Phase I, Experiment 1.....51

Figure 6.10. Wind Vectors at 48 Hours for Phase I, Experiment 1.....51

Figure 6.11. Wind Vectors at 72 Hours for Phase I, Experiment 1.....52

Figure 6.12. Wind Vectors at 96 Hours for Phase I, Experiment 1.....52

Figure 6.13. Wind Vectors at 120 Hours for Phase I, Experiment 1 53
Figure 6.14. Wind Vectors at 144 Hours for Phase I, Experiment 1 53
Figure 6.15. Wind Vectors at 168 Hours for Phase I, Experiment 1 54
Figure 6.16. Wind Vectors at 192 Hours for Phase I, Experiment 1 54
Figure 6.17. Wind Vectors at 216 Hours for Phase I, Experiment 1 55
Figure 6.18. Wind Vectors at 240 Hours for Phase I, Experiment 1 55
Figure 6.19. Wind Vectors at 24 Hours for Phase I, Experiment 1, Mode 1 57
Figure 6.20. Wind Vectors at 240 Hours for Phase I, Experiment 1, Mode 1 58
Figure 6.21. Wind Vectors at 24 Hours for Phase I, Experiment 1, Mode 2 59
Figure 6.22. Wind Vectors at 240 Hours for Phase I, Experiment 1, Mode 2 59
Figure 6.23. Wind Vectors at 24 Hours for Phase I, Experiment 2 61
Figure 6.24. Wind Vectors at 240 Hours for Phase I, Experiment 2 61
Figure 6.25. Wind Vectors at 24 Hours for Phase I, Experiment 4 63
Figure 6.26. Wind Vectors at 48 Hours for Phase I, Experiment 4 63
Figure 6.27. Wind Vectors at 72 Hours for Phase I, Experiment 4 64
Figure 6.28. Wind Vectors at 96 Hours for Phase I, Experiment 4 64
Figure 6.29. Wind Vectors at 120 Hours for Phase I, Experiment 4 65
Figure 6.30. Wind Vectors at 144 Hours for Phase I, Experiment 4 65
Figure 6.31. Wind Vectors at 168 Hours for Phase I, Experiment 4 66
Figure 6.32. Wind Vectors at 192 Hours for Phase I, Experiment 4 66
Figure 6.33. Wind Vectors at 216 Hours for Phase I, Experiment 4 67
Figure 6.34. Wind Vectors at 240 Hours for Phase I, Experiment 4 67
Figure 6.35. Wind Vectors at 24 Hours for Phase I, Experiment 4, Mode 1 68
Figure 6.36. Wind Vectors at 24 Hours for Phase I, Experiment 4, Mode 2 69
Figure 6.37. Wind Vectors at 24 Hours for Phase I, Experiment 5 70

Figure 6.38. Wind Vectors at 240 Hours for Phase I, Experiment 5 70
Figure 6.39. Wind Vectors at 24 Hours for Phase I, Experiment 6 71
Figure 6.40. Wind Vectors at 240 Hours for Phase I, Experiment 6 72
Figure 6.41. Wind Vectors at 24 Hours for Phase I, Experiment 7 73
Figure 6.42. Wind Vectors at 48 Hours for Phase I, Experiment 7 73
Figure 6.43. Wind Vectors at 72 Hours for Phase I, Experiment 7 74
Figure 6.44. Wind Vectors at 96 Hours for Phase I, Experiment 7 74
Figure 6.45. Wind Vectors at 120 Hours for Phase I, Experiment 7 75
Figure 6.46. Wind Vectors at 144 Hours for Phase I, Experiment 7 75
Figure 6.47. Wind Vectors at 168 Hours for Phase I, Experiment 7 76
Figure 6.48. Wind Vectors at 192 Hours for Phase I, Experiment 7 76
Figure 6.49. Wind Vectors at 216 Hours for Phase I, Experiment 7 77
Figure 6.50. Wind Vectors at 240 Hours for Phase I, Experiment 7 77
Figure 6.51. Wind Vectors at 24 Hours for Phase II, Experiment 8 79
Figure 6.52. Wind Vectors at 48 Hours for Phase II, Experiment 8 80
Figure 6.53. Wind Vectors at 72 Hours for Phase II, Experiment 8 80
Figure 6.54. Wind Vectors at 96 Hours for Phase II, Experiment 8 81
Figure 6.55. Wind Vectors at 120 Hours for Phase II, Experiment 8 81
Figure 6.56. Wind Vectors at 144 Hours for Phase II, Experiment 8 82
Figure 6.57. Wind Vectors at 168 Hours for Phase II, Experiment 8 82
Figure 6.58. Wind Vectors at 192 Hours for Phase II, Experiment 8 83
Figure 6.59. Wind Vectors at 216 Hours for Phase II, Experiment 8 83
Figure 6.60. Wind Vectors at 240 Hours for Phase II, Experiment 8 84
Figure 6.61. Wind Vectors at 24 Hours for Phase II, Experiment 9 85
Figure 6.62. Wind Vectors at 48 Hours for Phase II, Experiment 9 86

Figure 6.63. Wind Vectors at 72 Hours for Phase II, Experiment 9 86
Figure 6.64. Wind Vectors at 96 Hours for Phase II, Experiment 9 87
Figure 6.65. Wind Vectors at 120 Hours for Phase II, Experiment 9 87
Figure 6.66. Wind Vectors at 144 Hours for Phase II, Experiment 9 88
Figure 6.67. Wind Vectors at 168 Hours for Phase II, Experiment 9 88
Figure 6.68. Wind Vectors at 192 Hours for Phase II, Experiment 9 89
Figure 6.69. Wind Vectors at 216 Hours for Phase II, Experiment 9 89
Figure 6.70. Wind Vectors at 240 Hours for Phase II, Experiment 9 90
Figure 6.71. Latitudinal Structure of Phase III Forcings.....92
Figure 6.72. Temporal Structure of Phase III Forcings.....92
Figure 6.73. Normalized Vertical Structure of Thermal Forcing of Phase III.....93
Figure 6.74. Normalized Vertical Structure of Vorticity Forcing of Phase III.....93
Figure 6.75. Wind Vectors at 24 Hours for Phase III, Experiment 10.....94
Figure 6.76. Wind Vectors at 48 Hours for Phase III, Experiment 10.....95
Figure 6.77. Wind Vectors at 72 Hours for Phase III, Experiment 10.....95
Figure 6.78. Wind Vectors at 96 Hours for Phase III, Experiment 10.....96
Figure 6.79. Wind Vectors at 120 Hours for Phase III, Experiment 10.....96
Figure 6.80. Wind Vectors at 144 Hours for Phase III, Experiment 10.....97
Figure 6.81. Wind Vectors at 168 Hours for Phase III, Experiment 10.....97
Figure 6.82. Wind Vectors at 192 Hours for Phase III, Experiment 10.....98
Figure 6.83. Wind Vectors at 216 Hours for Phase III, Experiment 10.....98
Figure 6.84. Wind Vectors at 240 Hours for Phase III, Experiment 10.....99

Figure 6.85. Wind Vectors at 24 Hours for Phase III, Experiment 10, Mode 1 100
Figure 6.86. Wind Vectors at 24 Hours for Phase III, Experiment 10, Mode 2 100
Figure 6.87. Wind Vectors at 24 Hours for Phase III, Experiment 11 101
Figure 6.88. Wind Vectors at 240 Hours for Phase III, Experiment 11 102

I. INTRODUCTION

The monsoon is a three-dimensional, planetary scale wind regime that exhibits a strong seasonal dependence. According to the Glossary of Meteorology (Huschke, 1959), "the primary cause (of the monsoon) is the much greater annual variation of temperature over large land areas compared with neighboring ocean surfaces, causing an excess of pressure over the continents in the winter and a deficit in summer." The variation in temperature results from the position of the sun during each season. The shapes of the continents and their variable topographies produce considerable regional and temporal variability of monsoons.

The northeasterly monsoon that occurs in East Asia during the winter is one of the most energetic circulations of the atmosphere. Even though the regional characteristics of the winter monsoon occur in East and Southeast Asia, the influence on other components of circulation can reach global scales (Lau and Chang, 1987). Because of the large scale effects on the atmosphere, the East Asian winter monsoon has been an area of active research. Recent areas of investigation include the role of the East Asian winter monsoon in midlatitude-tropical and inter-hemispheric interactions, monsoonal variations, and the forcing mechanisms responsible for small scale monsoonal variations.

The East Asian winter monsoon is associated with the thermally direct Hadley circulation, or cell, that occurs over the area in winter. The ascending branch of the Hadley cell, and major monsoonal convective zone, migrates from its summertime position over India to the maritime continent of Borneo/Indonesia (Ramage, 1971). The latent heat released in the upper levels, due to intense convection over the maritime continent, is transferred poleward. The cold

Siberian high pressure system, or anticyclone, is the heat sink area for the upper-level poleward moving warm air. The Siberian anticyclone, in conjunction with the descending branch of the Hadley cell, produces a large area of subsidence, and thus dominates the Southeast Asian winter (Ramage, 1971). The Himalayas block the southward movement of extremely cold surface air from the Siberian anticyclone. The only effective outflow region is to the southeast.

Boyle and Chen (1987) documented the wintertime surface and 20 kPa wind fields for the period 1973 to 1984. The predominant northeasterly flow, at the surface, associated with the East Asian winter monsoon is shown in Fig. 1.1. The blacked out regions correspond to terrain heights above 1000 m. A vector length of 5° longitude corresponds to a ten meters per second wind, and the isotach contour interval is 2.5 $m \cdot s^{-1}$. The intense subtropical jet stream over Southeast Asia, shown in Fig. 1.2, is caused by the intense baroclinic zone between the warm tropics and frigid Siberian area. A wind vector length of 5° corresponds to a 100 $m \cdot s^{-1}$ wind, and the isotach interval is 10 $m \cdot s^{-1}$. The climatological averaged January 50 kPa geopotential height and wind field (Fig. 1.3) shows a dominant long wave trough centered over the Sea of Japan.. The contour interval is 80 m.

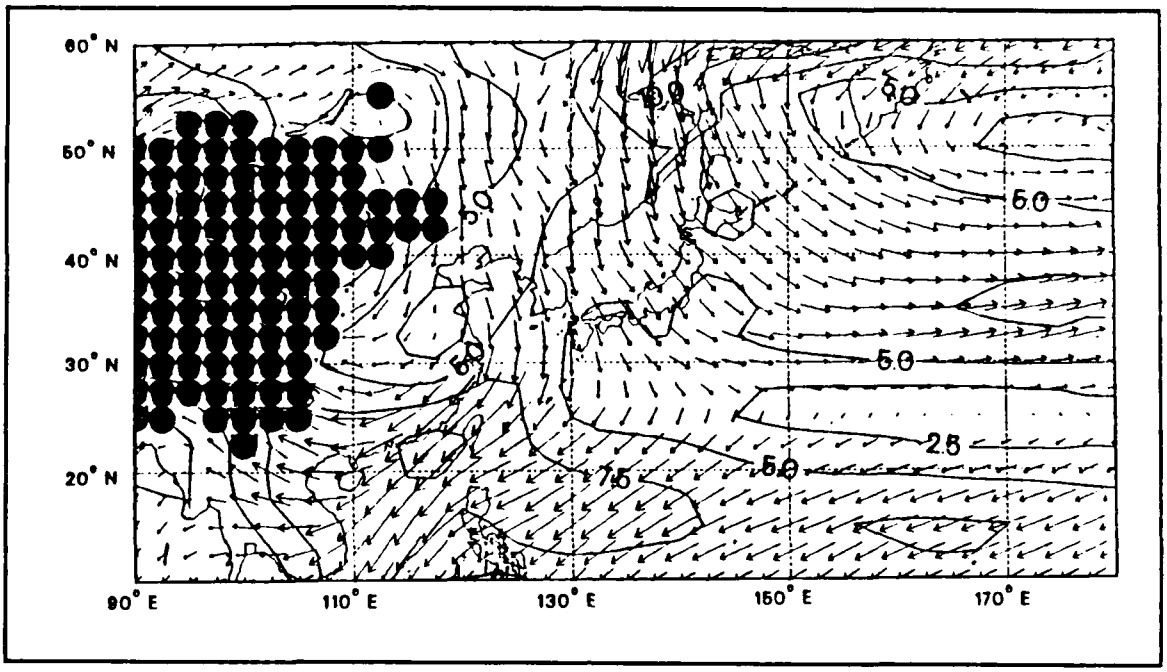

Figure 1.1. Average Wintertime Surface Wind (Boyle and Chen, 1987)

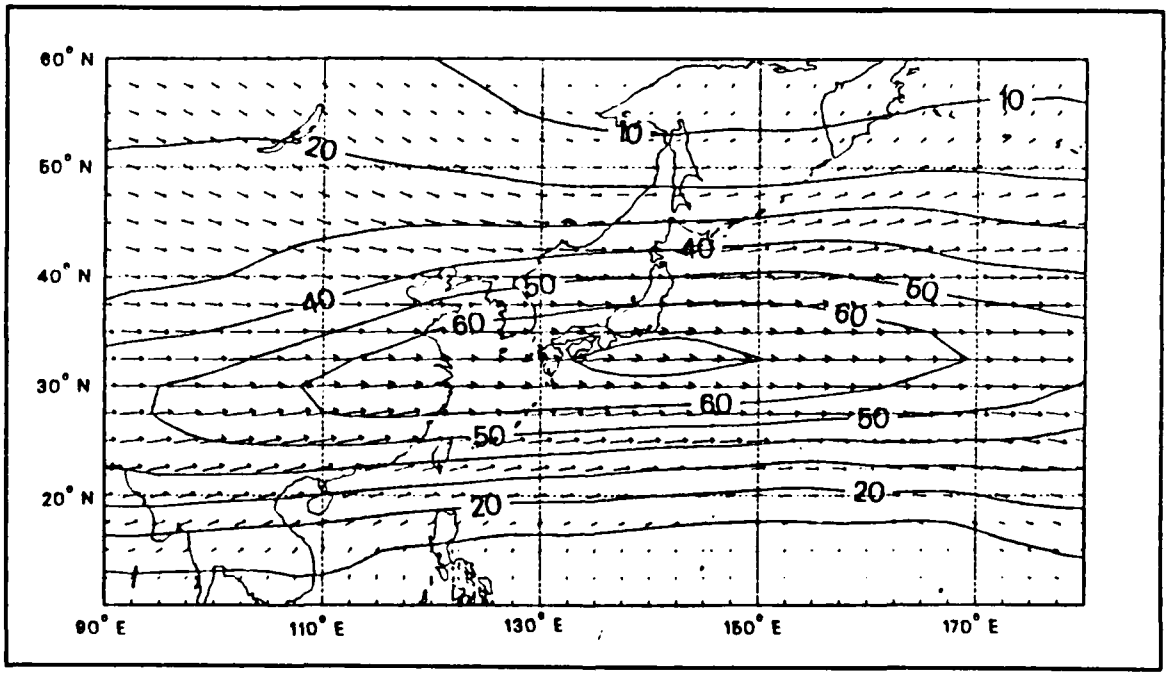

Figure 1.2. Average Wintertime 20 kPa Wind (Boyle and Chen, 1987)

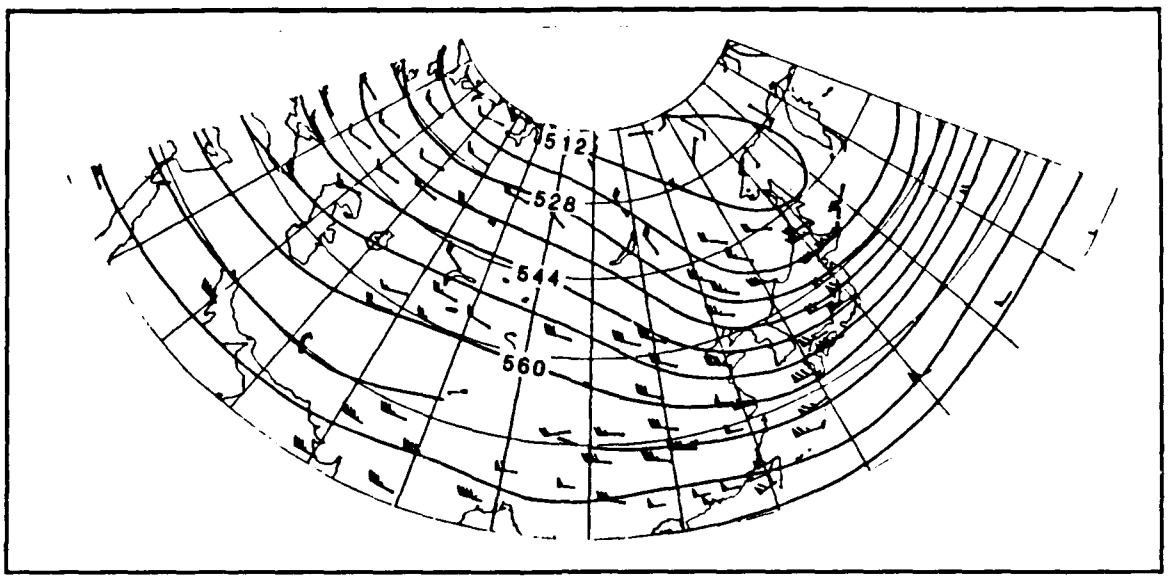

Figure 1.3. Climatological January 50 kPa Height Field (Boyle and Chen, 1987)

The Hadley circulation, and the effect of the Himalayas, set up the planetary circulation of the winter monsoon. However, Boyle and Chen (1987) indicate that transient synoptic-scale waves shape the final form of the Siberian High. As synoptic waves propagate along the longwave trough, surface cyclones and anticyclones develop due to the intense baroclinicity. Cyclones usually develop off the west coast of Japan in the area of strong upper-level positive vorticity advection and low-level warm air advection, and track to the northeast. Anticyclones develop near the southern extent of the Siberian High, due to the upper-level negative vorticity advection and low-level cold air advection, and track toward the southwest over China. When the pressure gradient between the China anticyclone and the cyclone off Japan tightens rapidly, significant ageostrophic motion results. The cross-isobaric ageostrophic flow accelerates toward lower pressure near the cyclone to the east and to the Intertropical Convergence Zone (ITCZ) to the south. The northeasterly cold wind is the "cold surge" in the winter monsoon. Cold surges

usually reach the equatorial South China Sea in 12 to 24 hours. The enhanced northerly flow intensifies the tropical convection over the maritime continent, and thus strengthens the Hadley circulation. The cold surge ends when the midlatitude trough-ridge pattern moves far enough east to diminish the China anticyclone, and consequently the pressure gradient. Boyle and Chen (1987) emphasize that cold surges are caused by the interaction of synoptic and planetary waves. They conclude that cold surges are dynamically forced, and thus must be considered separate entities from the Siberian anticyclone.

The East Asian cold surge has two stages. They are separated by a few hours to one day, depending on the location of the observing site (Lim and Chang, 1981; Chang et al., 1983). The first stage is the pressure surge. It is the leading edge of the air accelerating towards the equator. The pressure surge propagates with the speed of internal gravity waves. The second stage is a frontal passage that moves with advective speeds. It is defined by a sharp decrease in surface temperature and dew-point temperature.

The onset of the East Asian cold surges are defined in many ways (Boyle and Chen, 1987). The three most common definitions are: 1) A drop in surface temperature at Hong Kong of five degrees Celsius, or more; 2) An increase of the surface pressure gradient between coastal and central China of at least 0.5 kPa; and 3) A prevalent northerly surface flow over the South China Sea with speeds exceeding five meters per second(Lau and Chang, 1987).

The cause or nature of East Asian cold surges has been examined by Lim and Chang (1981), Baker (1983), Bashford (1985) and Harris (1985). Lim and Chang (1981) used linearized shallow-water equations on an equatorial beta-plane to simulate the response of the tropics to a midlatitude pressure surge. They did not

include planetary boundary layer friction or orography. Lim and Chang (1981) found that synoptic scale forcing in the midlatitudes produced Rossby-type waves that propagated into the tropics. The northeast-southwest tilt in the pressure field, typical of Rossby waves, and the northeasterly flow similar to cold surge events is shown in Fig. 1.4.

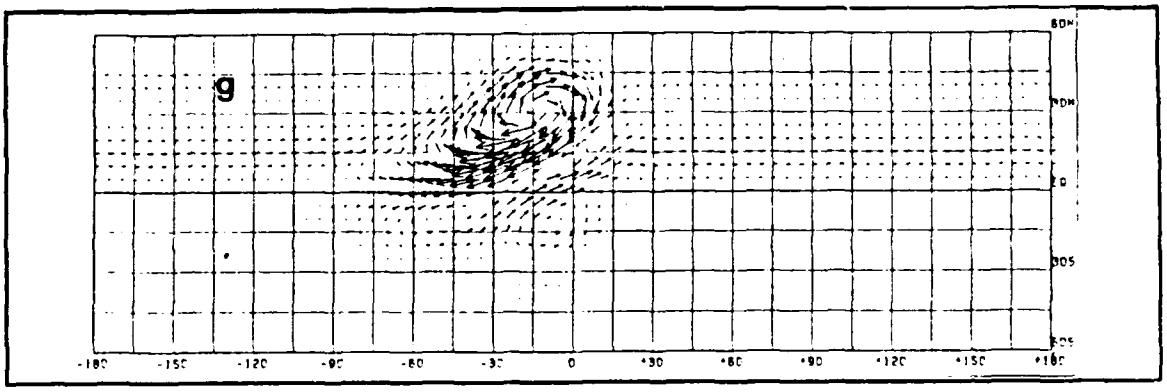

Figure 1.4. Wind Velocity Vectors for a Barotropic Model (Lim and Chang, 1981)

Baker (1983) used a global, six-layer, primitive equation model to examine the interaction of a midlatitude baroclinic wave with topography. Baker's results indicated that well developed baroclinic waves could initiate a cold surges, but the surges were limited, and weak. Baker concluded that other forcing mechanisms were required to simulate cold surges.

Bashford (1985) used an eight-layer, spectral, primitive equation model with an analytical heat source to study the effects of planetary scale motion on cold surges. The heat source function of Bashford's baroclinic model were similar to that used by Lim and Chang (1981) in their barotropic model. Bashford found that a planetary wave (wavenumber three) with a deep thermal forcing could produce a cold surge response.

Harris (1985) used the same model as Baker (1983) to study the interaction of a baroclinic wave (wavenumber eight) with a planetary wave (wavenumber four). Harris found the synoptic wave alone did not produce a cold surge, but the synoptic-planetary-wave interaction produced a significant cold surge response. Harris' results may be tainted because the planetary wave extended unrealistically far south.

This study will use a global, eight-layer, primitive equation model, and will be conducted in three phases. The first phase will examine the effect of a forcing with a single frequency derived from a forced Rossby wave, midlatitude beta-plane solution. The second phase will repeat Bashford's (1985) experiment with an impulse forcing that includes a spectrum of frequencies. This effort will attempt to reproduce the results of Lim and Chang (1981). The third phase will examine the interaction of a planetary wave (wavenumber four) with a synoptic wave (wavenumber seven). The synoptic wave, or generic cyclone, will be produced by a nonlinear Eady model of the atmosphere (Peng, 1982). The basic state or mean flow of the planetary wave, and the phase speed of the synoptic wave, are both equal to zero. Instead of combining the two waves together within the global model, as done by Harris (1985), this study will compute the nonlinear interactions analytically. The resulting wave (wavenumber three) is used in the linear, global model. To aid in the analysis of each experiment, the solutions from the global model will be projected onto the vertical normal modes.

II. SIMPLE BETA-PLANE SOLUTION

Since the baroclinic, primitive equation model used in this study is linear, and the mean or basic flow is zero, the full baroclinic atmosphere can be represented by the sum of vertical normal modes. The behavior of each vertical mode solution is similar to a barotropic shallow water system with the appropriate mean, or equivalent, depth (Lim and Chang, 1987). In other words, each mode of the baroclinic system will behave like a shallow water system. To simulate the variation in the Coriolis parameter, and simplify the mathematics, the system of shallow water equations is solved on a midlatitude beta-plane. The validity of using a midlatitude beta-plane is discussed by Lindzen (1967).

The scaled shallow water equations on the midlatitude beta-plane, with a forcing function added to the continuity equation, are:

$$\frac{\partial \phi'}{\partial t} + \mathbf{V}_\psi \cdot \nabla \phi' + gHD = -\frac{gH}{f_0} S \tag{2.1}$$

$$\frac{\partial \zeta}{\partial t} + \mathbf{V}_\psi \cdot \nabla (\zeta + \beta_0 y) + f_0 D = 0 \tag{2.2}$$

$$\nabla^2 \phi' - f_0 \zeta = 0 \tag{2.3}$$

where:

ϕ'	-	perturbation in the geopotential height field
ψ	-	geostrophic streamfunction
H	-	mean (basic) height field or equivalent depth
D	-	divergence
V	-	two dimensional wind velocity vector

ζ	-	vorticity
f_0	-	Coriolis parameter (constant)
t	-	time
β_0	-	gradient of Coriolis parameter in the north-south direction
y	-	north-south position
S	-	forcing function

If the vorticity is assumed geostrophic, then $\zeta = \nabla^2\psi$, and Eq. 2.3 yields $\psi = \phi'/f_0$ or $\phi' = f_0\psi$. When ϕ' is introduced into Eqs. 2.1 and 2.2, and the nonlinear terms are eliminated, Eqs. 2.1 and 2.2 become:

$$f_0\frac{\partial\psi}{\partial t} + gHD = -\frac{gH}{f_0}S \tag{2.4}$$

$$\frac{\partial\zeta}{\partial t} + \beta_0\frac{\partial\psi}{\partial x} + f_0 D = 0 \tag{2.5}$$

When the divergence is eliminated between Eqs. 2.4 and 2.5, the quasigeostrophic potential vorticity equation results:

$$\frac{\partial}{\partial t}\left(\zeta - \frac{f_0^2}{gH}\psi\right) + \beta_0\frac{\partial\psi}{\partial x} = S \tag{2.6}$$

Eq. 2.6 is solved by writing the streamfunction and forcing function as follows:

$$\psi = \Psi(y)\, e^{i(Kx - \omega t)} \tag{2.7}$$

$$S = i\, s(y)\, e^{i(Kx - \omega t)} \tag{2.8}$$

where K is the dimensional wavenumber, and ω is the frequency. The latitudinal structure of the forcing function is:

$$s(y)=\begin{cases} S_0\cos^2\left(\frac{\pi y}{2W}\right) & |y|\le W \\ 0 & |y|>W \end{cases} \tag{2.9}$$

where S_0 is the magnitude of the forcing, and W is half of the width of the forcing in the north-south direction.

When Eqs. 2.7 and 2.8 are substituted into Eq. 2.6, the following ordinary differential equation results:

$$\frac{d^2\Psi}{dy^2}+\alpha^2\Psi=-\frac{s(y)}{\omega} \tag{2.10}$$

where:

$$\alpha^2=-K^2-\frac{f_0^2}{gH}-\frac{K\beta_0}{\omega} \tag{2.11}$$

or:

$$\omega=\frac{-K\beta_0}{K^2+\alpha^2+\frac{f_0^2}{gH}} \tag{2.12}$$

The homogeneous solution to Eq. 2.10 is:

$$\Psi(y)=e^{\pm i\alpha y} \tag{2.13}$$

Since the latitudinal structure is symmetrical about y = 0, Eq. 2.10 will only be solved for $|y|\le -W$ and $y<-W$. When $y<-W$, the negative exponent of Eq. 2.13 is used, and when $y>W$ the positive exponent is used. If $\alpha^2>0$, the particular solution to Eq 2.10 for the interval $|y|\le W$ is:

$$\Psi(y)=\frac{S_0}{2\alpha^2}+\frac{S_0}{2}\frac{\cos\left(\frac{\pi y}{W}\right)}{\alpha^2-\left(\frac{\pi}{W}\right)^2} \tag{2.14}$$

When Eqs. 2.13 and 2.14 are combined, the general solution (with $\alpha^2 > 0$) is:

$$\Psi(y) = \frac{S_0}{2}\left(\frac{1}{\alpha^2} + \frac{\cos\left(\frac{\pi y}{W}\right)}{\alpha^2 - \left(\frac{\pi}{W}\right)^2}\right) + C_1\left(e^{i\alpha y} + e^{-i\alpha y}\right) \qquad |y| \le W \tag{2.15}$$

$$\Psi(y) = C_2 e^{-i\alpha y} \qquad y < -W \tag{2.16}$$

Since $\alpha^2 > 0$, α can be positive or negative. When $\alpha > 0$, the solution to Eq. 2.16 will have a north-south phase structure that tilts from the northeast to the southwest for $y < -W$. A northeast-southwest tilt in phase structure will propagate energy away from the source region. This can be shown by applying a radiation condition which requires that the wave have a group velocity moving away from the source. If $\alpha < 0$, the solution to Eq. 2.16 will have a phase structure that tilts from the northwest to the southeast, and will propagate energy toward the source region. For the region $y > W$, $\alpha < 0$ will produce a northwest-southeast tilt in the phase structure, and propagate energy northward away from the source region.

The two constants are determined by equating Eqs. 2.15 and 2.16, and also equating their derivatives, at $y = -W$. When Eqs. 2.15 and 2.16 are substituted into the real part of Eq. 2.10, the complete propagating solution is:

$$\Psi = \frac{S_0}{2}\left(\frac{1}{\alpha^2} + \frac{\cos\left(\frac{\pi y}{W}\right)}{\alpha^2 - \left(\frac{\pi}{W}\right)^2}\right)\cos(Kx - \omega t) -$$

$$\frac{S_0}{2}\left(\frac{1}{\alpha^2} - \frac{1}{\alpha^2 - \left(\frac{\pi}{W}\right)^2}\right)\cos(\alpha y)\cos(Kx + \alpha W - \omega t) \qquad |y| \le W \tag{2.17}$$

$$\Psi = \frac{S_0}{2}\sin(\alpha W)\left(\frac{1}{\alpha^2} - \frac{1}{\alpha^2 - \left(\frac{\pi}{W}\right)^2}\right)\sin(Kx + \alpha y - \omega t) \qquad y < -W \tag{2.18}$$

If $\alpha^2 < 0$ and $\alpha^2 = -\mu^2$, Eq. 2.10 becomes:

$$\frac{d^2\Psi}{dy^2} - \mu^2\Psi = -\frac{s(y)}{\omega} \tag{2.19}$$

and Eq. 2.11 becomes:

$$\mu^2 = K^2 + \frac{f_0^2}{gH} + \frac{K\beta_0}{\omega} \tag{2.20}$$

The homogeneous solution of Eq. 2.19 is:

$$\Psi(y) = e^{\pm\mu y} \tag{2.21}$$

and the particular solution for $|y| \le W$ is:

$$\Psi(y) = -\frac{S_0}{2\mu^2} - \frac{S_0}{2}\frac{\cos\left(\frac{\pi y}{W}\right)}{\mu^2 + \left(\frac{\pi}{W}\right)^2} \tag{2.22}$$

When $y < -W$, the positive exponent of Eq. 2.21 is used.

When Eqs. 2.21 and 2.22 are combined, the general solution (with $\alpha^2 < 0$ or $\mu^2 > 0$) is:

$$\Psi(y) = -\frac{S_0}{2}\left(\frac{1}{\mu^2} + \frac{\cos\left(\frac{\pi y}{W}\right)}{\mu^2 + \left(\frac{\pi}{W}\right)^2}\right) + C_1(e^{\mu y} + e^{-\mu y}) \qquad |y| \le W \tag{2.23}$$

$$\Psi(y) = C_2 e^{\mu y} \qquad y < -W \tag{2.24}$$

Since $\mu^2 > 0$, μ can be positive or negative. When $\mu > 0$, the solution to Eq. 2.24 will trap energy near the source. If $\mu < 0$, then the solution would grow to infinity for large $|y|$.

The constants can be solved in the same manner as used to get Eqs. 2.17 and 2.18. When Eqs. 2.23 and 2.24 are substituted into the real part of Eq. 2.10, the complete trapped solution is:

$$\Psi = \frac{S_0}{2}\left[-\frac{1}{\mu^2} - \frac{\cos\left(\frac{\pi y}{W}\right)}{\mu^2 + \left(\frac{\pi}{W}\right)^2} + e^{-\mu W}\cosh(\mu y)\left(\frac{1}{\mu^2} - \frac{1}{\mu^2 + \left(\frac{\pi}{W}\right)^2}\right)\right]\cos(Kx - \omega t) \qquad |y| \le W \tag{2.25}$$

$$\Psi = \frac{S_0}{2}\sinh(\mu W)\left(\frac{1}{\mu^2} - \frac{1}{\mu^2 + \left(\frac{\pi}{W}\right)^2}\right)e^{\mu y}\sin(Kx - \omega t) \qquad y < -W \tag{2.26}$$

The derivation above indicates that under certain conditions, or frequencies, the solution to the shallow water equations can either propagate energy away from the source region, or trap energy near the source. The experiments in Phase I will examine the effects of forcing the primitive equation model with a variety of frequencies.

III. MODEL DESCRIPTION

The model used in this study is a baroclinic spectral transform primitive equation model as described by Haltiner and Williams (1980), and used by McAtee (1984). The model discussion of this chapter is taken directly from McAtee. The model is configured to include friction, diabatic heating and a vorticity forcing. The specifics of how diabatic heating and vorticity are included in the model will be discussed in the next section. Friction is not included in this study. The basic equations of the model, in sigma coordinates, are as follows:

$$\frac{\partial \zeta}{\partial t} = -\nabla \cdot (\zeta + f)\mathbf{V} - \mathbf{k} \cdot \nabla \times \left(RT\nabla q + \dot{\sigma}\frac{\partial \mathbf{V}}{\partial \sigma} \right) + \mathbf{k} \cdot \nabla \times \mathbf{F} + \Lambda \tag{3.1}$$

$$\frac{\partial D}{\partial t} = \mathbf{k} \cdot \nabla \times (\zeta + f)\mathbf{V} - \nabla \cdot \left(RT\nabla q + \dot{\sigma}\frac{\partial \mathbf{V}}{\partial \sigma} \right) - \nabla^2 \left(\phi + \frac{\mathbf{V}^2}{2} \right) + \nabla \cdot \mathbf{F} \tag{3.2}$$

$$\frac{\partial q}{\partial t} = -D - \mathbf{V} \cdot \nabla q - \frac{\partial \dot{\sigma}}{\partial \sigma} \tag{3.3}$$

$$\frac{\partial \theta}{\partial t} = -\mathbf{V} \cdot \nabla \theta - \dot{\sigma}\frac{\partial \theta}{\partial \sigma} + Q \tag{3.4}$$

$$\frac{\partial \phi}{\partial \sigma} = -\frac{RT}{\sigma} \tag{3.5}$$

where:

ζ	-	vorticity
D	-	divergence
T	-	temperature
t	-	time

θ	-	potential temperature
Π	-	surface pressure
$\mathbf{V}$	-	horizontal velocity vector
ϕ	-	geopotential height
R	-	gas constant
C_p	-	specific heat at constant pressure
f	-	Coriolis parameter
σ	-	vertical coordinate ($\sigma = \frac{P - P_T}{\Pi - P_T}$)
$\dot{\sigma}$	-	vertical velocity ($\dot{\sigma} = \frac{d\sigma}{dt}$)
q	-	ln(P)
P	-	pressure
P_T	-	pressure at the top of the model
F	-	frictional force
Q	-	diabatic heat forcing function
Λ	-	vorticity forcing function

The continuity equation (3.3) is rewritten by integrating with respect to sigma, and applying the boundary conditions $\dot{\sigma}(0) = \dot{\sigma}(1) = 0.0$. Thus the integral of Eq. 3.3 may be written:

$$\frac{\partial q}{\partial t} = -\overline{D} + \overline{G} \tag{3.6}$$

where:

$$(\overline{\ }) = \int_0^1 (\ )d\sigma$$

$$G = \mathbf{V} \cdot \nabla q$$

The vertical velocity, $\dot{\sigma}$, is derived diagnostically by substituting Eq. 3.6 into Eq. 3.3, integrating in the vertical, and using $\dot{\sigma}(0) = 0$.

$$\dot{\sigma} = \left(\overline{D} + \overline{G}\right)\sigma - \int_0^{\sigma} \left(\overline{D} + \overline{G}\right) d\sigma \tag{3.7}$$

The first law of thermodynamics, Eq. 3.4, is written:

$$\frac{\partial T}{\partial t} = -\mathbf{V}\cdot\nabla T - \sigma^{\kappa}\,\dot{\sigma}\frac{\partial\left(T\sigma^{-\kappa}\right)}{\partial\sigma} + \kappa T\left(\frac{\partial q}{\partial t} + \mathbf{V}\cdot\nabla q\right) + Q \tag{3.8}$$

where κ equals R/C_p. To apply semi-implicit differencing, it is necessary to divide the temperature into parts as follows:

$$T = T^*(\sigma) + T'\left(\sigma,\lambda,\varphi,t\right) \tag{3.9}$$

where:

T^*	-	appropriately averaged temperature
T'	-	*perturbation temperature*
λ	-	longitude
φ	-	latitude

The basic equations are conveniently written in spherical coordinates by defining the following operator:

$$\alpha(a,b) \equiv \frac{1}{\cos^2\varphi}\frac{\partial a}{\partial\lambda} + \frac{1}{\cos\varphi}\frac{\partial b}{\partial\varphi} \tag{3.10}$$

Using Eqs. 3.9 and 3.10, the basic equations can be written as follows:

$$\frac{\partial\zeta}{\partial t} = -\alpha(A,B) + \Lambda \tag{3.11}$$

$$\frac{\partial D}{\partial t} = -\alpha(A,B) - \nabla^2\left(E + \phi + RT^*q\right) \tag{3.12}$$

$$\frac{\partial T}{\partial t} = -\alpha\left(UT', VT'\right) + DT' - \sigma^{\kappa}\,\dot{\sigma}\frac{\partial\left(T\sigma^{\kappa}\right)}{\partial\sigma} + \kappa T\left(G - \overline{G} - \overline{D}\right) + Q \tag{3.13}$$

$$\frac{\partial q}{\partial t} = -\left(\overline{D} + \overline{G}\right) \tag{3.14}$$

$$\sigma\frac{\partial\phi}{\partial\sigma} = -RT \tag{3.15}$$

where:

$$A = \left(\zeta + f\right)U + \dot{\sigma}\frac{\partial V}{\partial\sigma} + \frac{RT'}{r^2}\cos^2\varphi\,\frac{\partial q}{\partial\lambda} - \frac{\cos\varphi}{r}F_{\varphi}$$

$$B = \left(\zeta + f\right)V - \dot{\sigma}\frac{\partial U}{\partial\sigma} - \frac{RT'}{r^2}\frac{\partial q}{\partial\lambda} + \frac{\cos\varphi}{r}F_{\lambda}$$

$$G = \frac{U}{\cos^2\varphi}\frac{\partial q}{\partial\lambda} + V\frac{1}{\cos\varphi}\frac{\partial q}{\partial\varphi}$$

$$E = \frac{U^2 + V^2}{2\cos^2\varphi}$$

$$U = \frac{u\cos\varphi}{r}$$

$$V = -\frac{v\cos\varphi}{r}$$

and:

u - zonal component of the velocity vector (**V**)

v - meridional component of the velocity vector (**V**)

r - mean radius of the Earth

Eqs. 3.10 through 3.15 are the basic equations used in the model. These equations are represented spectrally in the horizontal and finite differenced in the vertical.

A. VERTICAL STRUCTURE

The vertical structure of the model follows the development given by Arakawa and Suarez (1983). The variables are staggered in σ so that ζ, D, U, V and T are carried at the mid-point of each layer, where $\sigma = \hat{\sigma}_k$. The variable $\dot{\sigma}$ is carried at the top and bottom of each layer, where $\sigma = \sigma_k$. The vertical structure is illustrated in Fig. 3.1. The finite difference form of Eqs. 3.10 through 3.15 are:

$$\frac{\partial \zeta}{\partial t} = -\alpha_k(A,B) + \Lambda_k \tag{3.16}$$

$$\frac{\partial D_k}{\partial t} = \alpha_k(B,-A) - \nabla^2\left(\phi_k + RT^*q + E_k\right) \tag{3.17}$$

$$\frac{\partial q}{\partial t} = -\left(\overline{G} + \overline{D}\right) \tag{3.18}$$

$$\frac{\partial T_k}{\partial t} = -\alpha_k\left(UT',VT'\right)T' + T_k^*\left(G_k - \overline{G} - \overline{D}\right) - \frac{1}{\Delta\sigma_k}\left\{\dot{\sigma}_{k+1}B_k\left(\frac{P_k}{P_{k+1}}T_{k+1} - T_k\right) + \dot{\sigma}_k A_{k-1}\left(T_k - \frac{P_k}{P_{k-1}}T_{k-1}\right)\right\} + Q \tag{3.19}$$

$$\phi_k - \phi_{k+1} = C_p\left(P_{k+1} - P_k\right)\left(\frac{A_k T_k}{P_k} + \frac{B_k T_{k+1}}{P_{k+1}}\right) \tag{3.20}$$

$$\phi_{LM} = \phi_S + C_P T_{LM}^*\left(\frac{P^\kappa}{P_{LM}} - 1\right) \tag{3.21}$$

$$\dot{\sigma}_{k+1} = \sigma_{k+1}(G + D) - \sum_{j=1}^{k}\left(G_j + D_j\right)\Delta\sigma_j \tag{3.22}$$

where:

$$\hat{P}_k = \left(\sigma_{k+1}\Pi\right)^\kappa$$

$$P = \frac{\left(\frac{\Pi^\kappa}{1+\kappa}\right)\left(\sigma_{k+1}^{1+\kappa} - \sigma_k^{1+\kappa}\right)}{\sigma_{k+1} - \sigma_k}$$

$$A = (\zeta + f)U_k + \frac{\dot{\sigma}_{k+1}(V_{k+1} - V_k) + \dot{\sigma}_k(V_k - V_{k-1})}{2\Delta\sigma_k} + \left(\frac{RT'_k \cos^2\varphi}{r^2}\right)\frac{1}{\cos\varphi}\frac{\partial q}{\partial\varphi} - \left(\frac{\cos\varphi}{r}\right)F_\varphi$$

$$B = (\zeta + f)V_k + \frac{\dot{\sigma}_{k+1}(U_{k+1} - U_k) + \dot{\sigma}_k(U_k - U_{k-1})}{2\Delta\sigma_k} - \left(\frac{C_p RT'_k}{r}\right)\frac{1}{\cos\varphi}\frac{\partial q}{\partial\varphi} + \left(\frac{\cos\varphi}{r}\right)F_\lambda$$

$$G = \frac{\mathbf{V}_k \cdot \nabla\Pi}{\Pi}$$

$$D = \nabla \cdot \mathbf{V}_k$$

$$A_K = \frac{\hat{P}_k - P_k}{P_{k+1} - P_k}$$

$$B_k = \frac{P_{k+1} - \hat{P}_k}{P_{k+1} - P_k} = 1 - A_k$$

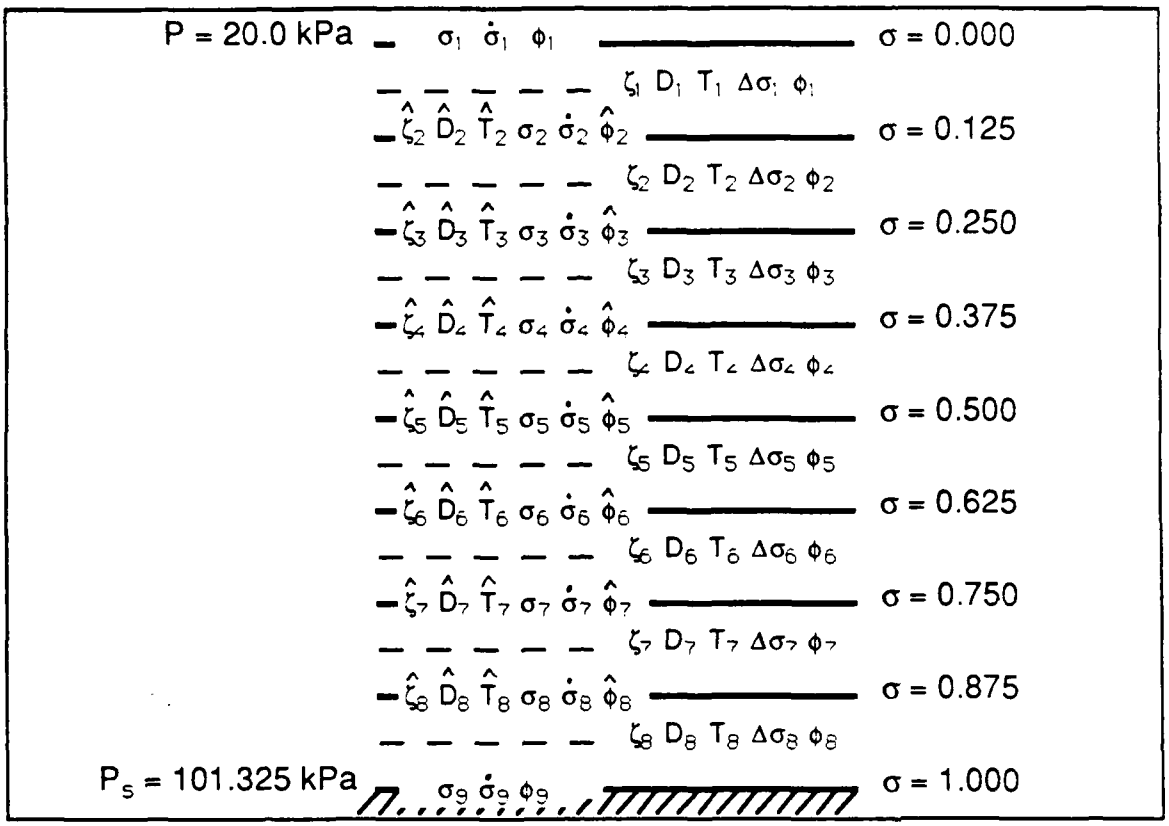

Figure 3.1. Vertical Structure of the Primitive Equation Model

Eqs. 3.16 through 3.22 are written in matrix form, so the terms on the right hand sides contain all the terms that are to be evaluated explicitly, and the terms on the left hand sides contain those terms that are to be evaluated implicitly. Eq. 3.20 is combined with an integrated finite difference form of Eq. 3.15 to obtain:

$$\phi = |C|T + \phi_s \tag{3.23}$$

where $|C|$ is a square matrix and the other quantities are column vectors. The finite difference form of the surface pressure tendency equation, Eq. 3.14, is :

$$\frac{\partial q}{\partial t} = \sum_k (G_k + D_k)\Delta\sigma_k \tag{3.24}$$

which can be written in matrix form as:

$$\frac{\partial q}{\partial t} = -N^T(G+D) \tag{3.25}$$

where N^T is the transpose of a constant column vector. Similarly, Eq. 3.22 is written:

$$\dot{\sigma} = Z(G+D) \tag{3.26}$$

The next to last term in Eq. 3.19 is:

$$\dot{\sigma}_{k+1}B_k\left(\frac{P_k}{P_{k+1}}T_{k+1} - T_k\right) + \dot{\sigma}_k A_{k-1}\left(T_k - \frac{P_k}{P_{k-1}}T_{k-1}\right) \tag{3.27}$$

For the purpose of semi-implicit formulation, the temperature is separated according to Eq. 3.9. The mean part of that term is written:

$$\dot{\sigma}_{k+1}B_k\left(\frac{P_k}{P_{k+1}}T^*_{k+1} - T_k\right) + \dot{\sigma}_k A_{k-1}\left(T^*_k - \frac{P_k}{P_{k-1}}T^*_{k-1}\right) = |\mathbf{M}|(G+D) \tag{3.28}$$

Eqs. 3.17, 3.19, 3.23 and 3.25 are now written:

$$\frac{\partial \mathbf{D}}{\partial t} + \nabla^2(\phi\ \ ' + |\mathbf{R}|\mathbf{T}^*q) = \alpha(B_r - A) - \nabla^2 E = \mathbf{K}_D \tag{3.29}$$

$$\frac{\partial q}{\partial t} + \mathbf{N}^T\mathbf{D} = -\mathbf{N}^T\mathbf{G} \tag{3.30}$$

$$\frac{\partial \mathbf{T}}{\partial t} + |\mathbf{Q}|\mathbf{D} = \mathbf{K}_T \tag{3.31}$$

$$\phi' = |\mathbf{C}|\,\mathbf{T} \tag{3.32}$$

where $|\mathbf{Q}| = |\mathbf{M}| + \kappa T^* N^T$ and $\phi' = \phi - \phi_S$. The variables $\mathbf{K}_D$ and $\mathbf{K}_T$ represent terms that are not explicitly separated out.

The semi-implicit time differencing is achieved by evaluating the terms on the left hand sides of Eqs. 3.29 through 3.31 implicitly. The remaining terms and

Eq. 3.32 are evaluated explicitly using leapfrog differencing. The difference equations are written:

$$\mathbf{D}_{n+1} + \Delta t \nabla^2 (|\mathbf{C}| \mathbf{T}_{n+1} + |\mathbf{R}| \mathbf{T}^* q_{n+1}) =$$

$$\mathbf{D}_{n-1} - \Delta t \nabla^2 (|\mathbf{C}| \mathbf{T}_{n-1} + |\mathbf{R}| \mathbf{T}^* q_{n-1}) + 2\Delta t (\mathbf{K}_D)_n \tag{3.33}$$

$$\mathbf{T}_{n+1} + \Delta t |\mathbf{Q}| \mathbf{D}_{n+1} = \mathbf{T}_{n-1} - \Delta t |\mathbf{Q}| \mathbf{D}_{n-1} - 2\Delta t (\mathbf{K}_T)_n \tag{3.34}$$

$$q_{n+1} + \Delta t \mathbf{N}^T \mathbf{D} = q_{n-1} - \Delta t \mathbf{N}^T \mathbf{D}_{n-1} - 2\Delta t \mathbf{N}^T \mathbf{G}_n \tag{3.35}$$

Now, the following equation for D is found by substituting Eqs. 3.34 and 3.35 into Eq. 3.33:

$$\mathbf{B}_- \mathbf{D}_{n+1} = \mathbf{B}_+ \mathbf{D}_{n-1} + 2\Delta t (\mathbf{K}_D)_n - 2\Delta t \nabla^2 (|\mathbf{C}| \mathbf{T}_{n-1} + |\mathbf{R}| \mathbf{T}^* q_{n-1} + |\mathbf{C}| (\mathbf{K}_T)_n) -$$

$$|\mathbf{R}| \mathbf{T}^* \mathbf{N}^T \mathbf{G}_n \tag{3.36}$$

where the matrix operator B is:

$$\mathbf{B}_\pm = \Delta t^2 (|\mathbf{C}||\mathbf{Q}| \pm |\mathbf{R}| \mathbf{T} \mathbf{N}^T) \nabla^2 + |\mathbf{I}| \tag{3.37}$$

and $|\mathbf{I}|$ is the identity matrix.

B. SPECTRAL FORMULATION

The equations 3.10 through 3.15 are represented spectrally in the horizontal. The variables are represented as follows:

$$C(\lambda, \varphi, \sigma, t) = \sum_{m=-J}^{J} \sum_{n=|m|}^{J} C_n^m(\sigma, t) P_n^m(\sin\varphi) e^{im\lambda} = \sum_{m=-J}^{J} \sum_{n=|m|}^{J} C_n^m Y_n^m \tag{3.38}$$

where C is some variable, and:

$$C_n^m(\ ) = (-1)^m C_n^{-m}$$

where m is the zonal wavenumber, n is the meridional index, and $n - |m|$ gives the number of zeros between the poles ($-1 < \sin \varphi < 1$) of the associated Legendre function. Triangular truncation is used in this study, with the truncation limit, J, equal to three. The non dimensional zonal coordinate index, λ, equals $(s - 1)/2$ where $1 < s < 16$. Note that the separation is such that the coefficients C_n^m are functions of time and the vertical and spherical harmonic Y_n^m are horizontal functions of space. The normalization and orthogonal properties of Y_n^m allow the coefficients to be obtained as follows:

$$C_n^m = \langle C, Y_n^m \rangle \equiv \frac{1}{4\pi} \int_0^{2\pi} \int_{-1}^{+1} C Y_n^m d\varphi d\lambda \tag{3.39}$$

The nonlinear terms are computed using the transform method following Haltiner and Williams (1980). The longitudinal direction is treated with a Fast Fourier Transform and the latitudinal direction uses Gaussian Quadrature. The number of latitudes, N, and longitudes, M, satisfy: $N > 3J/2 + 1$ and $M > 3(J - 1) + 1$. For this study, $N = 60$ and $M = 48$.

IV. FORCING FUNCTIONS

Chapter III of this paper describes the global spectral model. The vorticity equation (3.1) and the thermodynamic equation (3.4) use forcing functions, Λ and Q, respectively. This chapter describes the forcing functions.

A. PHASE I - ROSSBY WAVE FORCING

The thermal and vorticity forcing of Phase I follows the development of Chapter II. The forcing function is:

$$F=(F_A)(F_S)(F_\varphi)(F_R) \tag{4.1}$$

where F_A is the amplitude of either the thermal or vorticity forcing. The vertical structure (F_S), shown in Fig. 4.1, is:

$$F_S = \begin{cases} \dfrac{(1.0 - F_{A0})\sinh^2 \sigma_{LO}^2}{\sinh^2 1.0} & \sigma \geq \sigma_{max} \\ \dfrac{\tanh \sqrt{\sigma_{HI}}}{\tanh 1.0} & \sigma \leq \sigma_{max} \end{cases} \tag{4.2}$$

where F_{A0} is the amplitude of either forcing at the surface (for this study $F_{A0} = 0$), and:

$$\sigma_{LO} = \frac{\sigma - \sigma_{max}}{1.0 - \sigma_{max}} \tag{4.3}$$

$$\sigma_{HI} = \frac{\sigma - \sigma_{min}}{\sigma_{max} - \sigma_{min}} \tag{4.4}$$

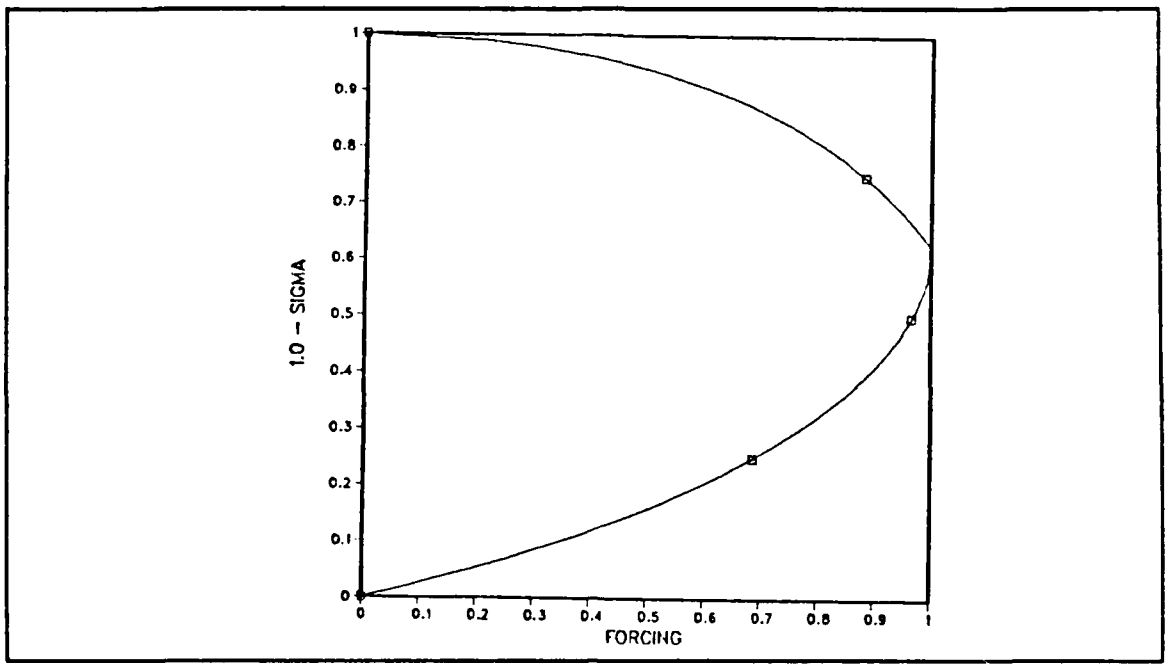

Figure 4.1. Vertical Structure of Forced Rossby Wave Solution

The meridional structure (F_φ) is:

$$F_\varphi = \sin^2\left(\frac{\pi(\varphi - Y_S)}{Y_N - Y_S}\right) \tag{4.5}$$

where φ is the latitude, and $Y_N - Y_S$ is the north–south period of forcing.

The development in Chapter II uses a $\cos^2$ latitudinal function, where the actual latitudinal forcing of the model is $\sin^2$. The difference is insignificant. The forcing is equal to zero in the Southern Hemisphere, and outside of the latitudinal limits in the Northern Hemisphere (Fig. 4.2).

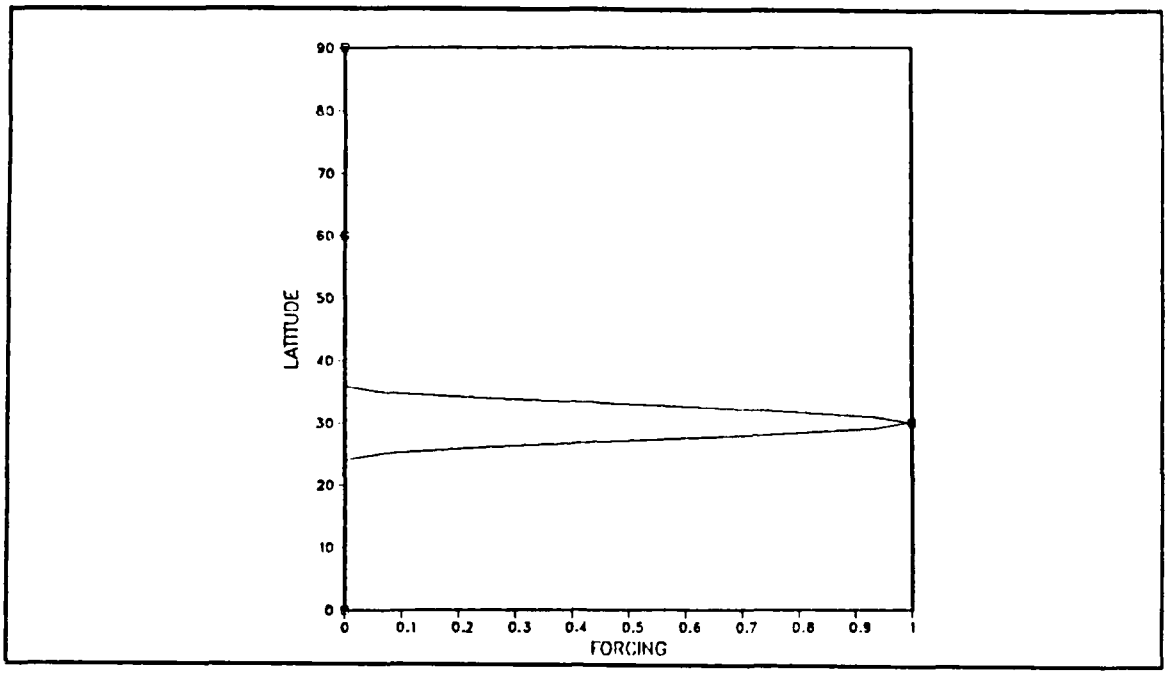

Figure 4.2. Latitudinal Structure of Forced Rossby Wave Solution

The amplitude, vertical and latitudinal components of the forcing function discussed so far are similar to Bashford (1985). Both the temporal and longitudinal structure of the forcing functions are included in the function F_R shown below:

$$F_R = \cos\left(\frac{2\pi(\lambda - X_W)}{X_E - X_W} - \omega t\right) \tag{4.6}$$

where $X_W - X_E$ is the East - West period of forcing, and λ is the longitude. The frequency (ω) is given by Eq. 2.11.

B. PHASE II - IMPULSE FORCING

Bashford (1985) used an impulse forcing in the thermal equation similar to Lim and Chang (1981). In this study the impulse is also added to the vorticity equation. Since this impulse forcing includes a spectrum frequencies, it is more realistic than the single-frequency forcing described in Phase I. The impulse forcing is given by:

$$F=(F_A)(F_S)(F_\varphi)(F_\lambda)(F_T) \tag{4.7}$$

where F_A, F_S, and F_φ are the same as Phase I. The longitudinal part (F_λ) is the same as Phase I, but it is separate from the temporal function. The impulse is generated by the temporal function (F_T):

$$F_T=\frac{t^2}{2\tau^3}e^{-\frac{t}{\tau}} \tag{4.8}$$

where t is time and τ is the time scale. The impulse peaks at $t = 2\tau$ and then decays exponentially to zero. The solutions in this study use τ = .5 day, so the peak of the impulse occurs at one day (Fig.4.3).

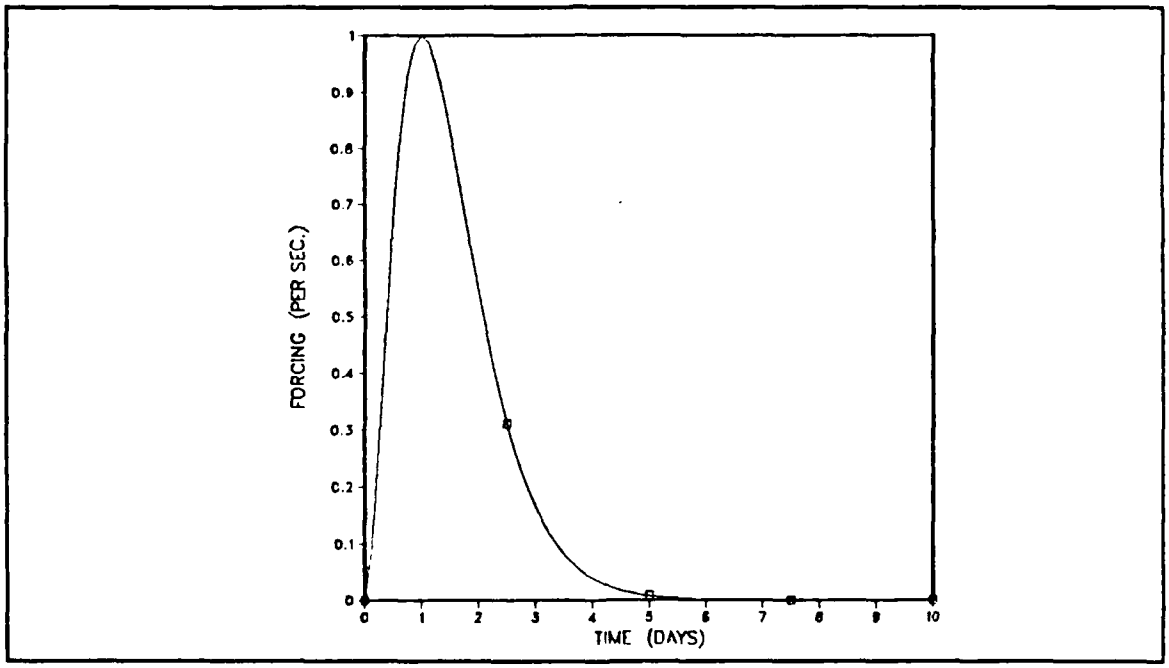

Figure 4.3. Temporal Structure of the Impulse Forcing

C. PHASE III - GENERIC CYCLONE FORCING

1. Thermal Forcing

The thermal forcing from the generic cyclone represents the nonlinear advection of the synoptic temperature field by planetary waves, and vice versa. The nonlinear advection terms are given below:

$$Q = - \mathbf{V}_L \cdot \nabla T_S - \mathbf{V}_S \cdot \nabla T_L \tag{4.9}$$

where:

V_L - two dimensional planetary wind vector

V_S - two dimensional synoptic wind vector

T_L - planetary scale temperature field

T_S - synoptic scale temperature field

Eq. 4.9 is written in scalar form as follows:

$$Q = - U_L \frac{\partial T_S}{\partial x} - V_L \frac{\partial T_S}{\partial y} - U_S \frac{\partial T_L}{\partial x} - V_S \frac{\partial T_L}{\partial y} \tag{4.10}$$

The quasistationary geopotential height field for the planetary wave is:

$$\phi_L = A(P,t) W(y) \cos(K_L x) \tag{4.11}$$

where A(P,t) is the amplitude factor for the planetary wave (constant for this study), and K_L is the planetary wave number (for this study $K_L = 4$). The latitudinal structure of the planetary wave is:

$$W(y) = \sin\left(\frac{\pi(y - Y_{PS})}{Y_{PN} - Y_{PS}}\right) \tag{4.12}$$

where $Y_{PS} - Y_{PN}$ is the north-south period of forcing for the planetary wave.

The geopotential height field for the synoptic wave is:

$$\phi_S = N(y)(a(P,t)\cos(K_S x - \nu t) + b(P,t)\sin(K_S x - \nu t)) \tag{4.13}$$

where a(P,t) and b(P,t) are the vertical amplitudes of the synoptic scale wave. The functions, a(P,t) and b(P,t), represent a baroclinic wave generated from an Eady model, to be discussed later. The value K_S is the synoptic wavenumber (for this study $K_S = 7$), and ν is the frequency. The latitudinal structure of the synoptic-scale wave is:

$$N(y) = \sin\left(\frac{\pi(y - Y_{SS})}{Y_{SN} - Y_{SS}}\right) \tag{4.14}$$

where $Y_{SN} - Y_{SS}$ is the north-south period of forcing for the synoptic wave.

The ideal gas law:

$$P = \rho RT \tag{4.15}$$

and the hydrostatic equation:

$$\frac{\partial P}{\partial Z} = -\rho g \tag{4.16}$$

are combined to yield:

$$T_S = -\frac{P}{R}\frac{\partial \phi_S}{\partial P} = -\frac{P}{R}N\left[\frac{\partial a}{\partial P}\cos(K_S x - \nu t) + \frac{\partial b}{\partial P}\sin(K_S x - \nu t)\right] \tag{4.17}$$

and:

$$T_L = -\frac{P}{R}\frac{\partial \phi_L}{\partial P} = -\frac{P}{R}\frac{\partial A}{\partial P}W\cos(K_L x) \tag{4.18}$$

The planetary wave amplitude function, A(P,t), is constant for this study so $T_L = 0$ and Eq. 4.10 simplifies to:

$$Q = -U_L\frac{\partial T_S}{\partial x} - V_L\frac{\partial T_S}{\partial y} \tag{4.19}$$

The planetary and synoptic vorticity fields are:

$$\zeta_L = \frac{1}{f}\nabla^2\phi_L = \frac{A}{f}\left(\frac{\partial^2 W}{\partial y^2} - K_L^2 W\right)\cos(K_L x) \tag{4.20}$$

$$\zeta_S = \frac{1}{f}\nabla^2\phi_S = \frac{1}{f}\left(\frac{\partial^2 N}{\partial y^2} - K_S^2 N\right)[a\cos(K_S x - \nu t) + b\sin(K_S x - \nu t)] \tag{4.21}$$

The planetary and synoptic zonal wind fields are:

$$U_L = -\frac{1}{f}\frac{\partial\phi_L}{\partial y} = -\frac{A}{f}\frac{\partial W}{\partial y}\cos(K_L x) \tag{4.22}$$

$$U_S = -\frac{1}{f}\frac{\partial\phi_S}{\partial y} = -\frac{1}{f}\frac{\partial N}{\partial y}[a\cos(K_S x - \nu t) + b\sin(K_S x - \nu t)] \tag{4.23}$$

The planetary and synoptic meridional wind fields are:

$$V_L = \frac{1}{f}\frac{\partial\phi_L}{\partial x} = -\frac{A}{f}WK_L\sin(K_L x) \tag{4.24}$$

$$V_S = \frac{1}{f}\frac{\partial\phi_S}{\partial x} = \frac{1}{f}NK_S[-a\sin(K_S x - \nu t) + b\cos(K_S x - \nu t)] \tag{4.25}$$

When Eqs. 4.17, 4.22 and 4.24 are substituted into Eq. 4.19, and simplified, the result is:

$$\begin{aligned} Q = -\frac{P}{R}\frac{A}{f}\Bigg[& -\frac{\partial W}{\partial y}N\frac{\partial a}{\partial P}K_S\cos(K_L x)\sin(K_S x - \nu t) + \\ & \frac{\partial W}{\partial y}N\frac{\partial b}{\partial P}K_S\cos(K_L x)\cos(K_S x - \nu t) + \\ & W\frac{\partial N}{\partial y}K_L\frac{\partial a}{\partial P}\sin(K_L x)\cos(K_S x - \nu t) + \\ & W\frac{\partial N}{\partial y}K_L\frac{\partial b}{\partial P}\sin(K_L x)\sin(K_S x - \nu t)\Bigg] \end{aligned} \tag{4.26}$$

Using the trigonometric identities:

$$\sin(\alpha-\beta)=\sin\alpha\cos\beta-\cos\alpha\sin\beta \tag{4.27}$$

$$\cos(\alpha-\beta)=\cos\alpha\cos\beta+\sin\alpha\sin\beta \tag{4.28}$$

Eq. 4.26 becomes:

$$\begin{aligned}Q=-\frac{P}{R}\frac{A}{f}\Bigg[&-\frac{\partial W}{\partial y}N\frac{\partial a}{\partial P}K_S\cos(K_L x)(\sin(K_S x)\cos(\nu t)-\cos(K_S x)\sin(\nu t))+\\&\frac{\partial W}{\partial y}N\frac{\partial b}{\partial P}K_S\cos(K_L x)(\cos(K_S x)\cos(\nu t)+\sin(K_S x)\sin(\nu t))+\\&W\frac{\partial N}{\partial y}K_L\frac{\partial a}{\partial P}\sin(K_L x)(\cos(K_S x)\cos(\nu t)+\sin(K_S x)\sin(\nu t))+\\&W\frac{\partial N}{\partial y}K_L\frac{\partial b}{\partial P}\sin(K_L x)(\sin(K_S x)\cos(\nu t)-\cos(K_S x)\sin(\nu t))\Bigg]\end{aligned} \tag{4.29}$$

Using the trigonometric identities:

$$\sin\alpha\cos\beta=\frac{1}{2}(\sin(\alpha+\beta)+\sin(\alpha-\beta)) \tag{4.30}$$

$$\cos\alpha\cos\beta=\frac{1}{2}(\cos(\alpha+\beta)+\cos(\alpha-\beta)) \tag{4.31}$$

$$\sin\alpha\sin\beta=\frac{1}{2}(\cos(\alpha-\beta)-\cos(\alpha+\beta)) \tag{4.32}$$

Eq. 4.29 becomes:

$$
\begin{aligned}
Q = -\frac{1}{2}\frac{P}{R}\frac{A}{f}\Bigg[& -\frac{\partial W}{\partial y}N\frac{\partial a}{\partial P}K_S\Big[\cos(\nu t)(\sin((K_S+K_L)x)+\sin((K_S-K_L)x))- \\
& \sin(\nu t)(\cos((K_S+K_L)x)+\cos((K_S-K_L)x))\Big]+ \\
& \frac{\partial W}{\partial y}N\frac{\partial b}{\partial P}K_S\Big[\cos(\nu t)(\cos((K_S+K_L)x)+\cos((K_S-K_L)x))+ \\
& \sin(\nu t)(\sin((K_S+K_L)x)+\sin((K_S-K_L)x))\Big]+ \\
& W\frac{\partial N}{\partial y}K_L\frac{\partial a}{\partial P}\Big[\cos(\nu t)(\sin((K_L+K_S)x)-\sin((K_S-K_L)x))+ \\
& \sin(\nu t)(\cos((K_S-K_L)x)-\cos((K_S+K_L)x))\Big]+ \\
& W\frac{\partial N}{\partial y}K_L\frac{\partial b}{\partial P}\Big[\cos(\nu t)(\cos((K_S-K_L)x)-\cos((K_S+K_L)x))- \\
& \sin(\nu t)(\sin((K_L+K_S)x)-\sin((K_S-K_L)x))\Big]\Bigg]
\end{aligned}
\tag{4.33}
$$

Eq. 4.33 describes the nonlinear interaction between the planetary-scale wave (wavenumber four) and the synoptic-scale wave (wavenumber seven). The resulting waves are wavenumber three ($K_S - K_L$) and wavenumber 11 ($K_S + K_L$). Since synoptic-scale waves do not propagate into the tropics (Harris, 1985), wavenumber 11 is ignored in Eq. 4.33. The resulting equation, (4.34), is the thermal forcing function, Q:

$$Q = -\frac{1}{2}\frac{P}{R}\frac{A}{f}\Bigg[-\frac{\partial W}{\partial y}N\frac{\partial a}{\partial P}K_S\Big[\cos(\nu t)\sin((K_S - K_L)x) - \sin(\nu t)\cos((K_S - K_L)x)\Big] +$$

$$\frac{\partial W}{\partial y}N\frac{\partial b}{\partial P}K_S\Big[\cos(\nu t)\cos((K_S - K_L)x) + \sin(\nu t)\sin((K_S - K_L)x)\Big] +$$

$$W\frac{\partial N}{\partial y}K_L\frac{\partial a}{\partial P}\Big[-\cos(\nu t)\sin((K_S - K_L)x) + \sin(\nu t)\cos((K_S - K_L)x)\Big] +$$

$$W\frac{\partial N}{\partial y}K_L\frac{\partial b}{\partial P}\Big[\cos(\nu t)\cos((K_S - K_L)x) + \sin(\nu t)\sin((K_S - K_L)x)\Big]\Bigg] \tag{4.34}$$

2. Vorticity Forcing

The vorticity forcing function represents the nonlinear advection of vorticity by both the planetary-scale and synoptic-scale waves. The nonlinear advection terms are:

$$\Lambda = -\mathbf{V}_L\cdot\nabla\zeta_S - \mathbf{V}_S\cdot\nabla\zeta_L \tag{4.35}$$

Eq. 4.35 is written in scalar form as follows:

$$\Lambda = -U_L\frac{\partial\zeta_S}{\partial x} - V_L\frac{\partial\zeta_S}{\partial y} - U_S\frac{\partial\zeta_L}{\partial x} - V_S\frac{\partial\zeta_L}{\partial y} \tag{4.36}$$

When Eqs. 4.20, 4.21, 4.22, 4.23, 4.24, and 4.25 are substituted into Eq. 4.36, the result is:

$$\Lambda = \frac{A}{f^2}\Bigg[\frac{\partial W}{\partial y}K_S\left(\frac{\partial^2 N}{\partial y^2} - K_S^2 N\right)\cos(K_L x)(-a\sin(K_S x - \nu t) + b\cos(K_S x - \nu t)) +$$

$$WK_L\left(\frac{\partial^3 N}{\partial y^3} - K_S^2\frac{\partial N}{\partial y}\right)\sin(K_L x)(a\cos(K_S x - \nu t) + b\sin(K_S x - \nu t)) -$$

$$\frac{\partial N}{\partial y}K_L\left(\frac{\partial^2 W}{\partial y^2} - K_L^2 W\right)\sin(K_L x)(a\cos(K_S x - \nu t) + b\sin(K_S x - \nu t)) -$$

$$NK_S\left(\frac{\partial^3 W}{\partial y^3} - K_L^2\frac{\partial W}{\partial y}\right)\cos(K_L x)(-a\sin(K_S x - \nu t) + b\cos(K_S x - \nu t))\Bigg] \tag{4.37}$$

When like terms are grouped together and the trigonometric identities in Eqs. 4.27 and 4.28 are used to simplify Eq. 4.37, Λ becomes:

$$\Lambda = \frac{A}{f^2}\Bigg[\Bigg[\frac{\partial W}{\partial y}K_S\left(\frac{\partial^2 N}{\partial y^2} - K_S^2 N\right) - NK_S\left(\frac{\partial^3 W}{\partial y^3} - K_L^2\frac{\partial W}{\partial y}\right)\Bigg]$$

$$\Bigg[\cos(K_L x)\Big(-a\sin(K_S x)\cos(\nu t) + a\cos(K_S x)\sin(\nu t) +$$

$$b\cos(K_S x)\cos(\nu t) + b\sin(K_S x)\sin(\nu t)\Big)\Bigg] +$$

$$\Bigg[WK_L\left(\frac{\partial^3 N}{\partial y^3} - K_S^2\frac{\partial N}{\partial y}\right) - \frac{\partial N}{\partial y}K_L\left(\frac{\partial^2 W}{\partial y^2} - K_L^2 W\right)\Bigg]$$

$$\Bigg[\sin(K_L x)\Big(a\cos(K_S x)\cos(\nu t) + a\sin(K_S x)\sin(\nu t) +$$

$$b\sin(K_S x)\cos(\nu t) - b\cos(K_S x)\sin(\nu t)\Big)\Bigg]\Bigg] \tag{4.38}$$

Using the trigonometric identities of Eqs. 4.30, 4.31 and 4.32, Eq. 4.38 becomes:

$$
\begin{aligned}
\Lambda = \frac{1}{2}\frac{A}{f^2}\Bigg[& \left[\frac{\partial W}{\partial y}K_S\left(\frac{\partial^2 N}{\partial y^2} - K_S^2 N\right) - NK_S\left(\frac{\partial^3 W}{\partial y^3} - K_L^2\frac{\partial W}{\partial y}\right)\right] \\
& \Big[(-\operatorname{asin}((K_S + K_L)x) - \operatorname{asin}((K_S - K_L)x))\cos(\nu t) + \\
& (\operatorname{acos}((K_S + K_L)x) + \operatorname{acos}((K_S - K_L)x))\sin(\nu t) + \\
& (\operatorname{bcos}((K_S + K_L)x) + \operatorname{bcos}((K_S - K_L)x))\cos(\nu t) + \\
& (\operatorname{bsin}((K_S + K_L)x) + \operatorname{bsin}((K_S - K_L)x))\sin(\nu t)\Big] + \\
& \left[WK_L\left(\frac{\partial^3 N}{\partial y^3} - K_S^2\frac{\partial N}{\partial y}\right) - \frac{\partial N}{\partial y}K_L\left(\frac{\partial^2 W}{\partial y^2} - K_L^2 W\right)\right] \\
& \Big[(\operatorname{asin}((K_S + K_L)x) - \operatorname{asin}((K_S - K_L)x))\cos(\nu t) + \\
& (\operatorname{acos}((K_S - K_L)x) - \operatorname{acos}((K_S + K_L)x))\sin(\nu t) + \\
& (\operatorname{bcos}((K_S - K_L)x) - \operatorname{bcos}((K_S + K_L)x))\cos(\nu t) - \\
& (\operatorname{bsin}((K_S + K_L)x) - \operatorname{bsin}((K_S - K_L)x))\sin(\nu t)\Big]\Bigg]
\end{aligned}
\tag{4.39}
$$

Eq. 4.39 describes the nonlinear interaction between the planetary wave (wavenumber four), and the synoptic wave (wavenumber seven). The resulting shortwave, wavenumber 11, is ignored. The final form of the vorticity forcing function is:

$$
\begin{aligned}
\Lambda = \frac{1}{2}\frac{A}{f^2}\Bigg[& \Bigg[\frac{\partial W}{\partial y} K_S \left(\frac{\partial^2 N}{\partial y^2} - K_S^2 N \right) - N K_S \left(\frac{\partial^3 W}{\partial y^3} - K_L^2 \frac{\partial W}{\partial y} \right) \Bigg] \\
& \Big[- a\sin((K_S - K_L)x)\cos(\nu t) + a\cos((K_S - K_L)x)\sin(\nu t) + \\
& b\cos((K_S - K_L)x)\cos(\nu t) + b\sin((K_S - K_L)x)\sin(\nu t) \Big] + \\
& \Bigg[W K_L \left(\frac{\partial^3 N}{\partial y^3} - K_S^2 \frac{\partial N}{\partial y} \right) - \frac{\partial N}{\partial y} K_L \left(\frac{\partial^2 W}{\partial y^2} - K_L^2 W \right) \Bigg] \\
& \Big[- a\sin((K_S - K_L)x)\cos(\nu t) + a\cos((K_S - K_L)x)\sin(\nu t) + \\
& b\cos((K_S - K_L)x)\cos(\nu t) + b\sin((K_S - K_L)x)\sin(\nu t) \Big] \Bigg]
\end{aligned}
\tag{4.40}
$$

V. DESCRIPTION OF GENERIC CYCLONE MODEL

The synoptic-scale geopotential height field is given by Eq. 4.13, where the vertical amplitudes, a(P,t) and b(P,t), are obtained from the growth of a generic cyclone. The intensity of the generic cyclone follows the development of midlatitude baroclinic disturbances in the atmosphere, using an Eady (1949) model. Eady assumed the atmosphere was a frictionless, continuously stratified fluid whose motion is adiabatic, hydrostatic and quasi-geostrophic. Eady's original study neglected the nonlinear wave interactions.

Peng (1982) applied spectral methods to the Eady (1949) model, but included frictional dissipation and nonlinear wave interactions. Peng found the behavior of the baroclinic wave depended on the stratification, S, frictional dissipation, γ, supercriticality of the vertical wind shear, Δ, and the fundamental zonal wave number, k. The Peng (1982) model of a baroclinic wave is used in this study to generate the generic cyclone.

The atmosphere is considered to be an infinite channeled Boussinesq fluid with a constant Brunt-Vaisala frequency, N_s. The top and bottom boundaries are rigid walls, separated by a distance, D. The lateral boundaries are also rigid walls, separated by a distance, L. The basic state is a zonal flow, U, with a constant vertical wind shear, λ. The quasi-geostrophic potential vorticity equation that describes the motion is:

$$\left(\frac{\partial}{\partial t} + \lambda z \frac{\partial}{\partial x}\right) q + J(\psi, q) = 0 \tag{5.1}$$

where:

$$J(f,g)=\frac{\partial f}{\partial x}\frac{\partial g}{\partial y}-\frac{\partial f}{\partial y}\frac{\partial g}{\partial x} \tag{5.2}$$

and the potential vorticity (q) is:

$$q=\frac{\partial^2\psi}{\partial x^2}+\frac{\partial^2\psi}{\partial y^2}+\frac{1}{S}\frac{\partial^2\psi}{\partial z^2} \tag{5.3}$$

with ψ being the disturbance streamfunction. The vertical variable (z) ranges from minus 1/2 at the bottom of the model, to 1/2 at the top.

The basic state stratification parameter, S, of the fluid is constant,and given by:

$$S=\frac{N_s^2 D^2}{f_0^2 L^2} \tag{5.4}$$

where:

N_s	-	Brunt-Vaisala frequency
D	-	vertical depth of the fluid
f_0	-	Coriolis parameter
L	-	width of the channel

The frictional dissipation, γ, is given by:

$$\gamma=\frac{E_v^{\frac{1}{2}}}{R_o} \tag{5.5}$$

where E_v is the Ekman number, and R_o is the Rossby number.

The supercriticality of flow, Δ, measures the vertical wind shear in excess of the critical vertical wind shear required for growth of the baroclinic wave, and is:

$$\Delta=\lambda-\lambda_c \tag{5.6}$$

where:

$$\lambda_c = \frac{4\gamma\mu^2 \tanh^{\frac{1}{2}}\mu}{k\left[(\mu - \tanh\mu)(1 - \mu\tanh\mu)\right]^{\frac{1}{2}}} \tag{5.7}$$

represents the marginal shear required for instability by linear theory, and:

$$\mu = \frac{1}{2} S^{\frac{1}{2}} \left(k^2 + \pi^2\right)^{\frac{1}{2}} \tag{5.8}$$

where k is the fundamental zonal wave number. The marginal stability curve, as a function of μ, for S = .0628 is given in Fig. 5.1.

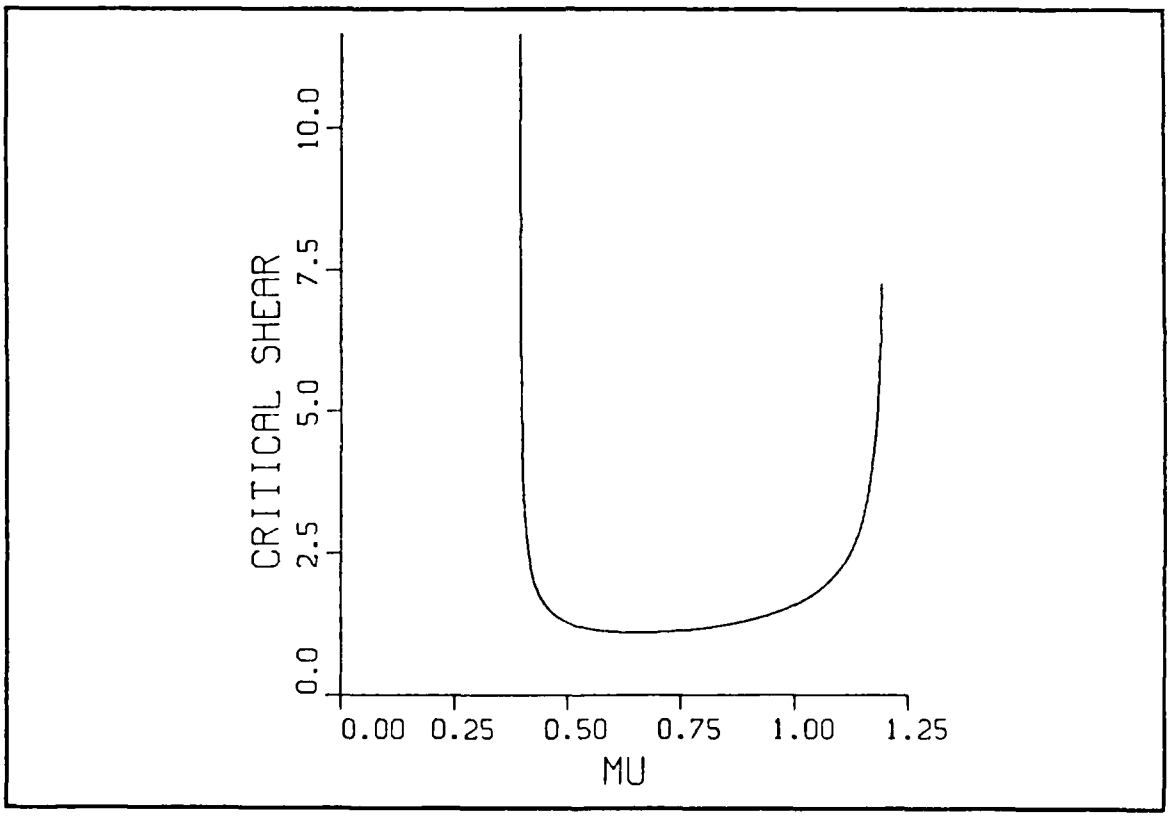

Figure 5.1. Marginal Stability Curve of Eady Model, Including Friction

The disturbance potential vorticity (q) is equal to zero throughout the lifetime of the cyclone in this model. Eq. 5.1 simplifies to:

$$\frac{\partial^2\psi}{\partial x^2}+\frac{\partial^2\psi}{\partial y^2}+\frac{1}{S}\frac{\partial^2\psi}{\partial z^2}=0 \tag{5.9}$$

The nondimensional boundary conditions for the model are:

$$\frac{\partial\psi}{\partial x}=0 \quad \text{at } y=0,1 \tag{5.10}$$

$$\frac{\partial^2\overline{\psi}}{\partial y\partial t}=0 \quad \text{at } y=0,1 \tag{5.11}$$

$$\left(\frac{\partial}{\partial t}+\lambda z\frac{\partial}{\partial x}\right)\frac{\partial\psi}{\partial z}-\lambda\frac{\partial\psi}{\partial x}+J\left(\psi,\frac{\partial\psi}{\partial z}\right)\pm S\gamma\left(\frac{\partial^2\psi}{\partial x^2}+\frac{\partial^2\psi}{\partial y^2}\right)=0 \quad \text{at } z=\pm 1/2 \tag{5.12}$$

where $\overline{\psi}$ is the zonal average streamfunction.

Eqs 5.9, 5.10, 5.11 and 5.12 form a closed system of equations. A Fourier series, Eq. 5.13, whose y structure satisfies Eqs. 5.10 and 5.11, is used to represent the horizontal streamfunction field:

$$\psi=\sum_m\sum_n\left(C_{mn}e^{imkx}+C^*_{mn}e^{-imkx}\right)\sin n\pi y+\sum_n C_{0n}\cos n\pi y \tag{5.13}$$

where m and n are the number of zonal and meridional modes, respectively. The complex amplitude coefficient (C_{mn}) of mode (m,n), and the complex conjugate (C^*_{mn}) of C_{mn}, are both functions of time. Since only one baroclinic wave is used in this study, Eq. 5.13 simplifies to:

$$\psi=\left(C_{11}e^{ikx}+C^*_{11}e^{-ikx}\right)\sin\pi y+C_{01}\cos\pi y \tag{5.14}$$

The amplitude coefficients, C_{11}, C^*_{11}, and C_{01} are determined by substituting Eq 5.14 into Eqs. 5.9, 5.10, 5.11 and 5.12. The system of equations is integrated in time using a fourth order Runge-Kutta method (Peng, 1982). The vertical

amplitude coefficients, a(P,t) and b(P,t), in Eq. 4.13 are related to the amplitude coefficients of Peng by:

$$C_{11} = a\cosh(\mu z) + b\sinh(\mu z) \tag{5.15}$$

The variables a and b are determined by solving Eq. 5.15 at $z = \pm 1/2$.

The nondimensional coefficients a and b are made dimensional by multiplying the them by 4 000 000 m (the characteristic length scale of the Eady model), 40 $m \cdot s^{-1}$ (the characteristic velocity scale), and .000 1 s^{-1} (the Coriolis parameter at 45° N).

VI. ANALYSIS OF RESULTS

A. NORMAL MODE ANALYSIS

The solutions of all three phases of this study will be analyzed using the vertical normal modes of the primitive equation model. Gill (1982) provides a good general discussion of normal mode analysis, and Lim and Chang (1987) derive the vertical modes of a shallow water equation model solved on an equatorial beta-plane.

The vertical normal modes of the primitive equation model used in this study are displayed in Figs. 6.1 to 6.8. There are eight vertical modes, consistent with the eight levels of the model. The first mode does not have a zero-crossing. and is considered a barotropic mode. The second mode has one zero-crossing. Since the amplitude of the second mode changes sign in the vertical, it is considered the baroclinic mode (Lim and Chang, 1987). The higher modes have successively more zero-crossings. The solutions to the primitive equation model at each level are projected onto these vertical profiles and summed to produce the modal output. The equivalent depth (H) of each vertical mode is provided in Table 6.1.

TABLE 6.1. EQUIVALENT DEPTH OF VERTICAL MODES

Vertical Mode	Equivalent Depth, m
1	7083.1
2	209.1
3	59.7
4	28.4
5	16.1
6	9.8
7	6.2
8	3.8

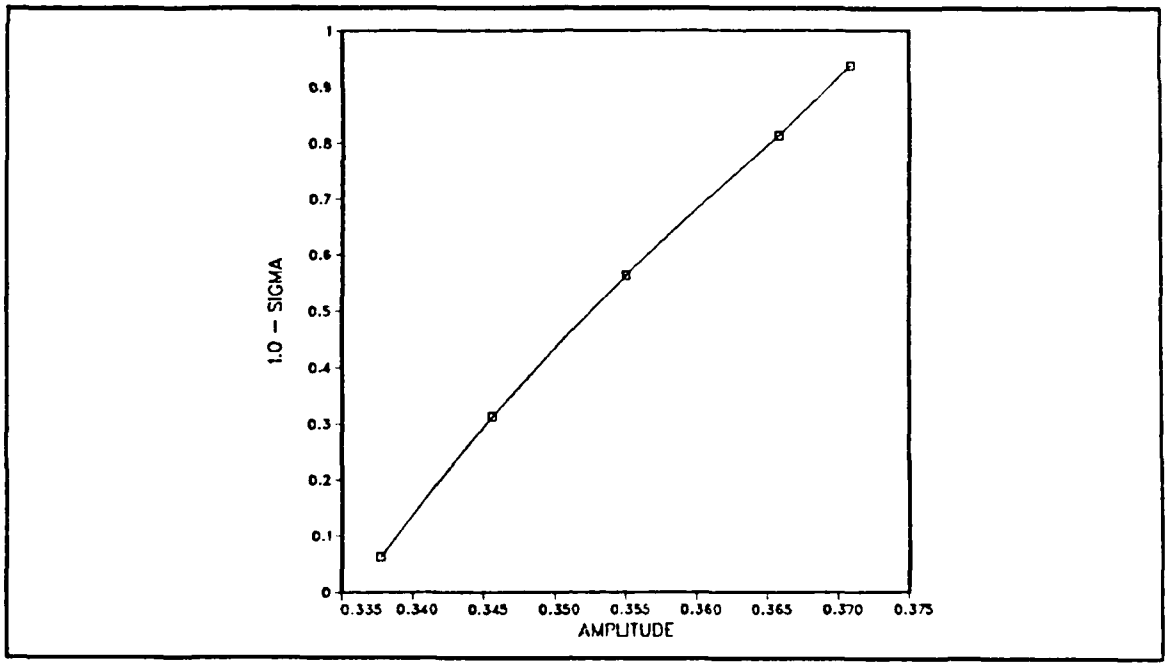

Figure 6.1. Vertical Profile of Normal Mode 1

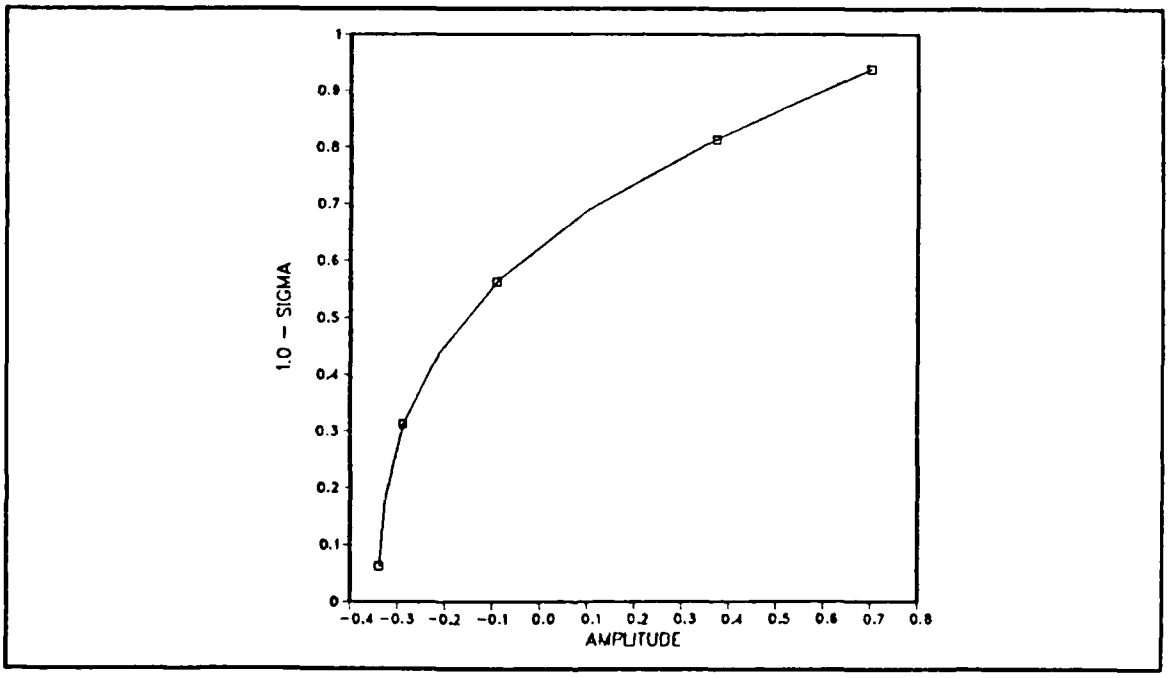

Figure 6.2. Vertical Profile of Normal Mode 2

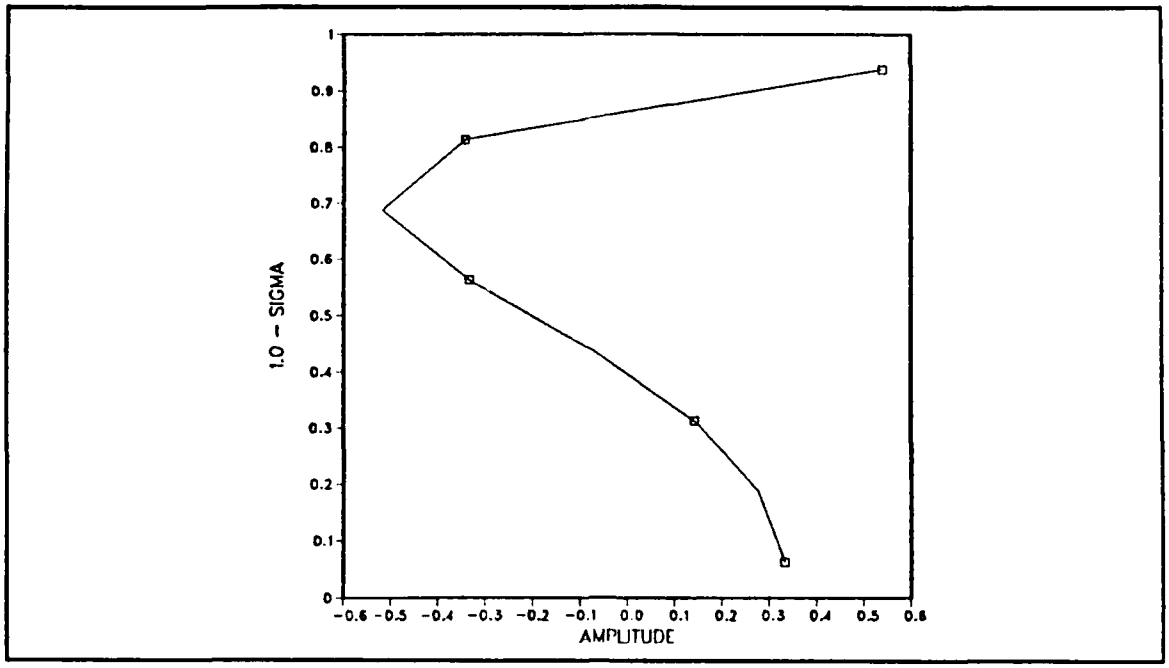

Figure 6.3. Vertical Profile of Normal Mode 3

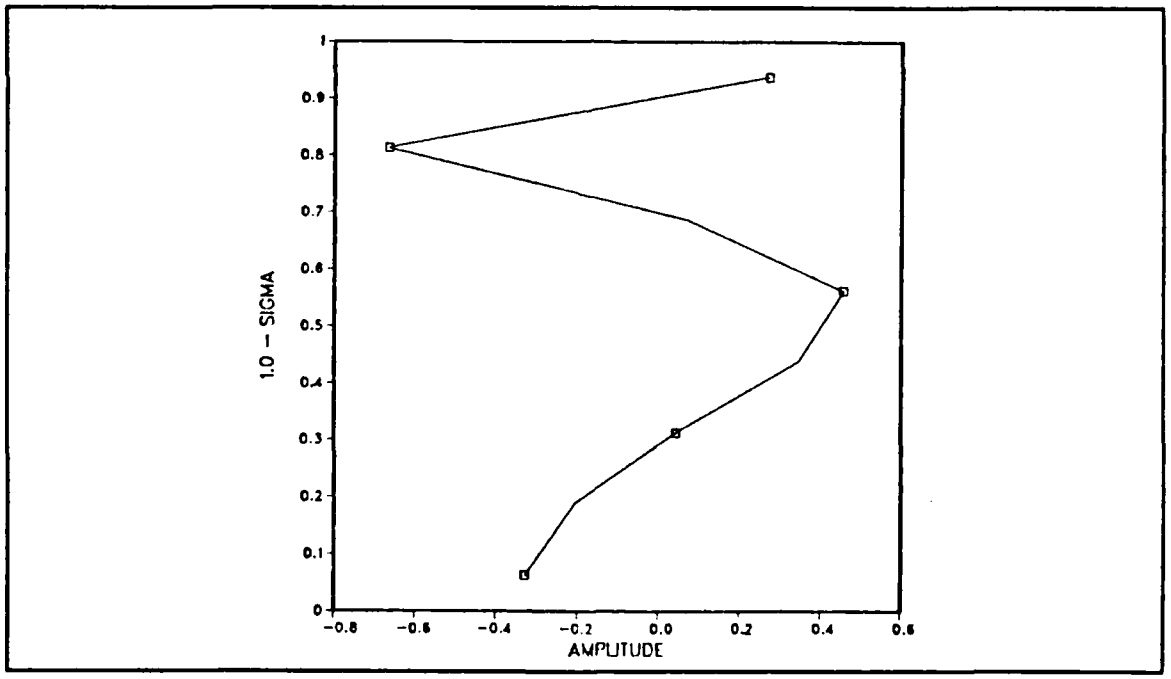

Figure 6.4. Vertical Profile of Normal Mode 4

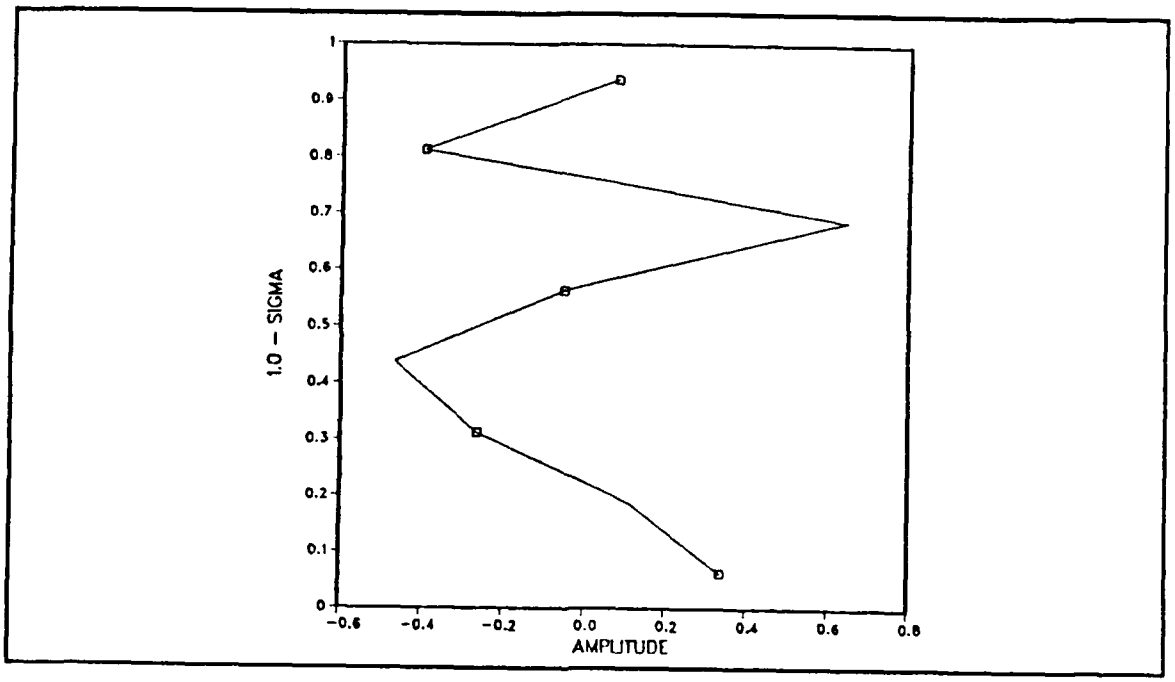

Figure 6.5. Vertical Profile of Normal Mode 5

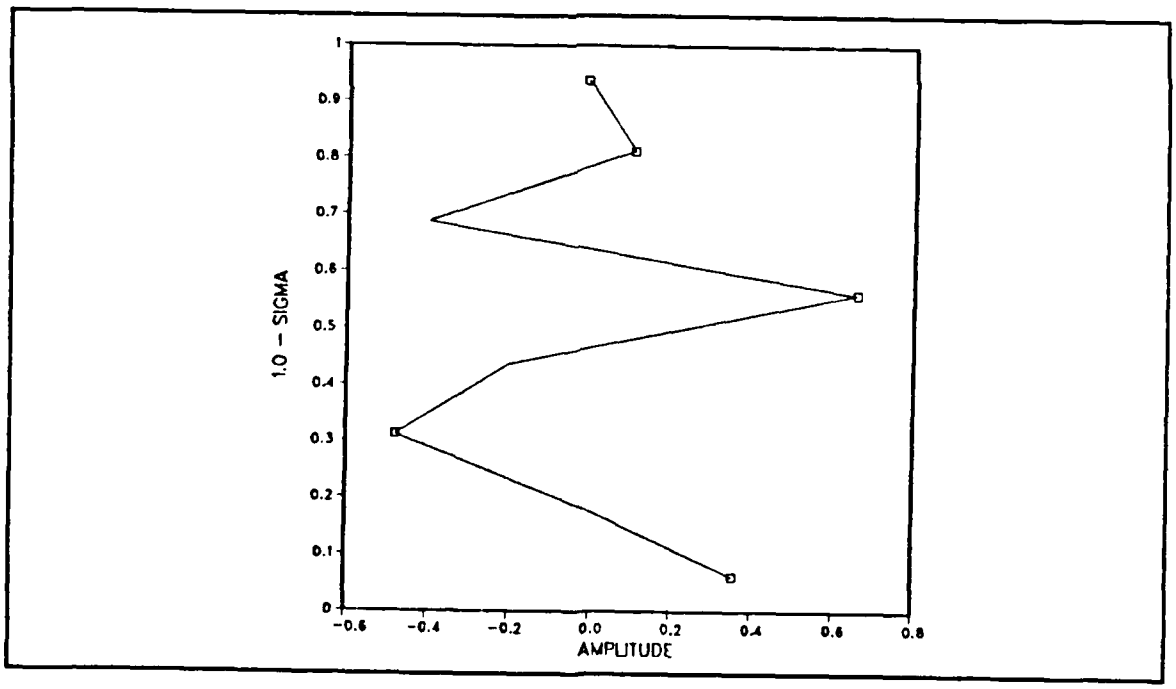

Figure 6.6. Vertical Profile of Normal Mode 6

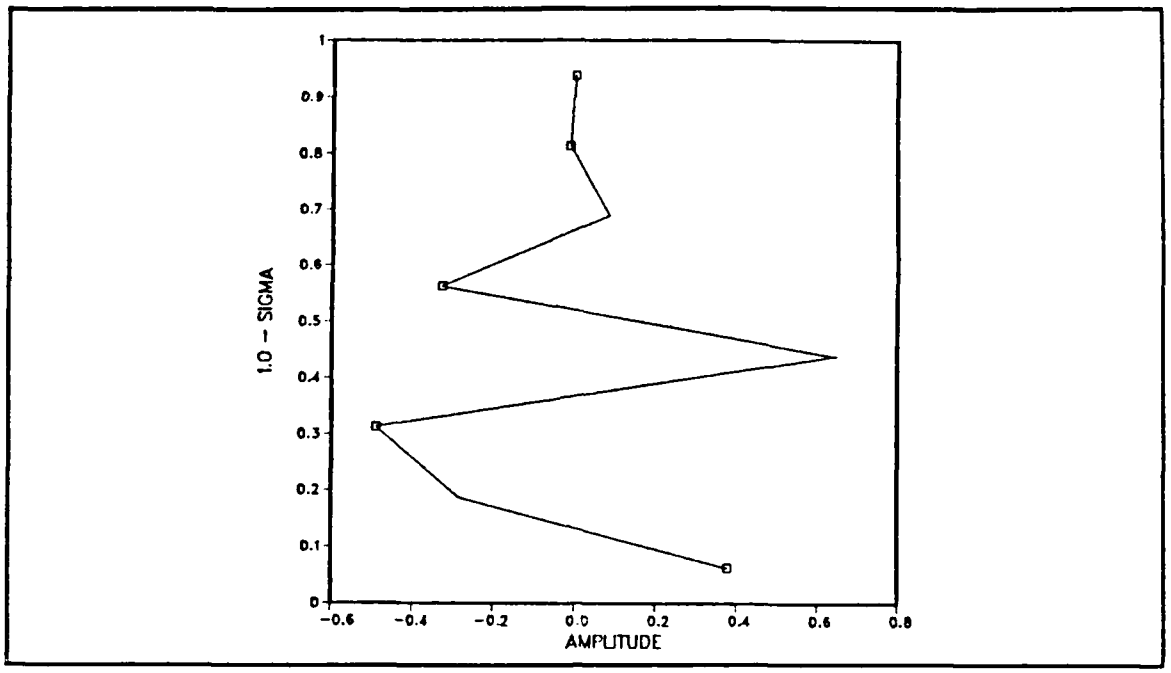

Figure 6.7. Vertical Profile of Normal Mode 7

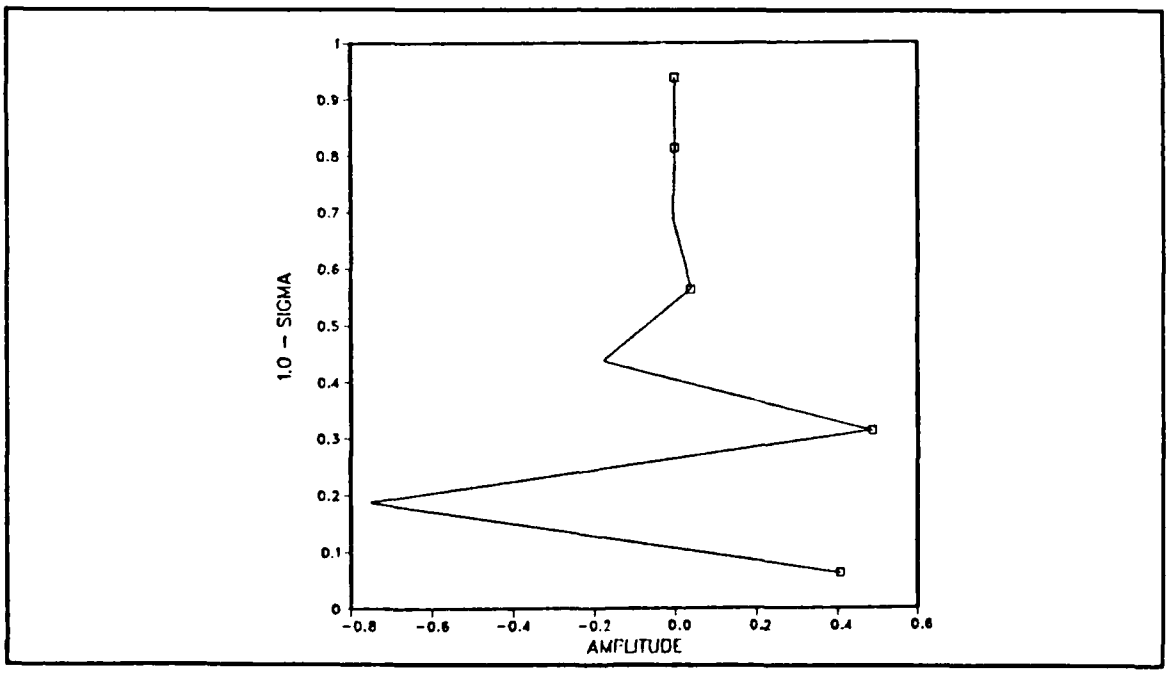

Figure 6.8. Vertical Profile of Normal Mode 8

B. PHASE I RESULTS

The forcing functions of Phase I will use the development of forced Rossby waves from Chapter II. In each experiment the forcing is applied between 24° N and 36° N, and the model is integrated forward in time for 240 hours. The frequency (ω) and corresponding period of the temporal component of the forcing function (Eq. 4.6) are given in Table 6.2. Recall from Chapter II, that the sign of the variable α^2 determines whether the solution to each vertical mode will propagate away from the source region. The variable α^2, as a function of equivalent depth and frequency, is given in Tables 6.3a and 6.3b. The α^2 values are determined by first setting $\alpha = K = 3.797 \times 10^{-7}\ m^{-1}$. This value of K corresponds to wavenumber three at 30° N. The frequency is calculated for each equivalent depth by using this value of K in Eq. 2.12. The variable α^2 is then calculated for each frequency and equivalent depth using Eq. 2.11. Both f_0 and β_0 of Eqs. 2.11 and 2.12 are calculated at 30° N. When $\alpha^2 > 0$, the solution for that specific equivalent depth and frequency will propagate energy away from the source region. According to theory, only the barotropic mode (H = 7083.1 m) will propagate energy away from the source when the frequency (ω) equals $-206.30 \times 10^{-7}\ s^{-1}$. As the frequency ($\omega$) decreases, the higher modes have propagating solutions.

TABLE 6.2. ROSSBY WAVE FREQUENCY AND PERIOD OF VERTICAL MODES

Mode	Frequency (ω), s^{-1} x 10^{-7}	Period, days
1	–206.30	3.5
2	–26.13	27.8
3	–8.04	90.4
4	–3.80	187.4
5	–2.22	327.4
6	–1.36	535.1
7	–0.85	853.2
8	–0.53	1382.0

TABLE 6.3A. ALPHA SQUARED (M^{-1} X 10^{-12}) FOR HIGH FREQUENCY MODES

		Frequency (ω), s^{-1} x 10^{-7}			
		–206.30	–26.13	–8.04	–3.88
	7083.1	0.14	2.60	9.14	19.18
	209.1	–2.37	0.14	6.62	16.66
Equivalent	59.7	–8.85	–6.34	0.14	10.18
Depth	28.4	–18.89	–16.38	–9.90	0.14
(H),	16.1	–33.38	–30.86	–24.38	–14.34
m	9.8	–54.87	–52.36	–45.88	–35.84
	6.1	–87.81	–85.29	–78.81	–68.77
	3.8	–142.50	–140.00	–133.50	–123.50

TABLE 6.3B. ALPHA SQUARED (M^{-1} X 10^{-12}) FOR LOW FREQUENCY MODES

		Frequency (ω), s^{-1} x 10^{-7}				
		–2.22	–1.36	–0.85	–0.53	*206.30
	7083.1	33.67	55.16	88.10	142.80	–0.59
	209.1	31.15	52.65	85.58	140.30	–3.10
Equivalent	59.7	24.67	46.17	79.10	133.80	–9.58
Depth	28.4	14.63	36.13	69.06	123.80	–19.62
(H),	16.1	0.14	21.64	54.57	109.30	–34.11
m	9.8	–21.35	0.14	33.08	87.81	–55.60
	6.1	–54.29	–32.79	0.14	54.87	–88.54
	3.8	–109.00	–87.52	–54.59	0.14	–143.30

* changed the sign of ω associated with mode 1

Phase I consists of seven experiments. Each experiment will help determine how the primitive equation model reacts to the analytical forcings derived in Chapter II. The seven experiments are summarized in Table 6.4. The first three experiments will determine the effects of a thermal forcing with different equivalent heights (H) or frequencies (ω). Experiments 4, 5 and 6 will determine the effects of a vorticity forcing with different frequencies. Since the sign of ω in Experiment 5 is reversed, α^2 is negative, and all Rossby waves should be trapped near the source. The variable α in Experiment 7 is a singular point in Eq. 2.15.

TABLE 6.4. PHASE I EXPERIMENTS

Experiment	Thermal Forcing	Vorticity Forcing	Equivalent Depth
1	X		7083.1 m
2	X		209.1 m
3	X		59.7 m
4		X	7083.1 m
5		X	*7083.1 m
6		X	209.1 m
7		X	**209.1 m

* sign of ω changed

** $\alpha = \pi / W$

1. Experiment 1

In this experiment the forcing function is only added to the thermal equation (Eq. 3.4). The mean or equivalent height (H) in Eq. 2.12 is 7083.1 m, which is exactly equal to the scale height of the first vertical mode (the barotropic mode). The wave frequency (ω) is $-206.30 \times 10^{-7}\ s^{-1}$ and the period is 3.5 days. The wind velocity vectors for the lowest level ($\sigma = .938$) are displayed in Figs. 6.9 to 6.18. The scale of the wind vectors is shown in meters per second at the bottom of each figure.

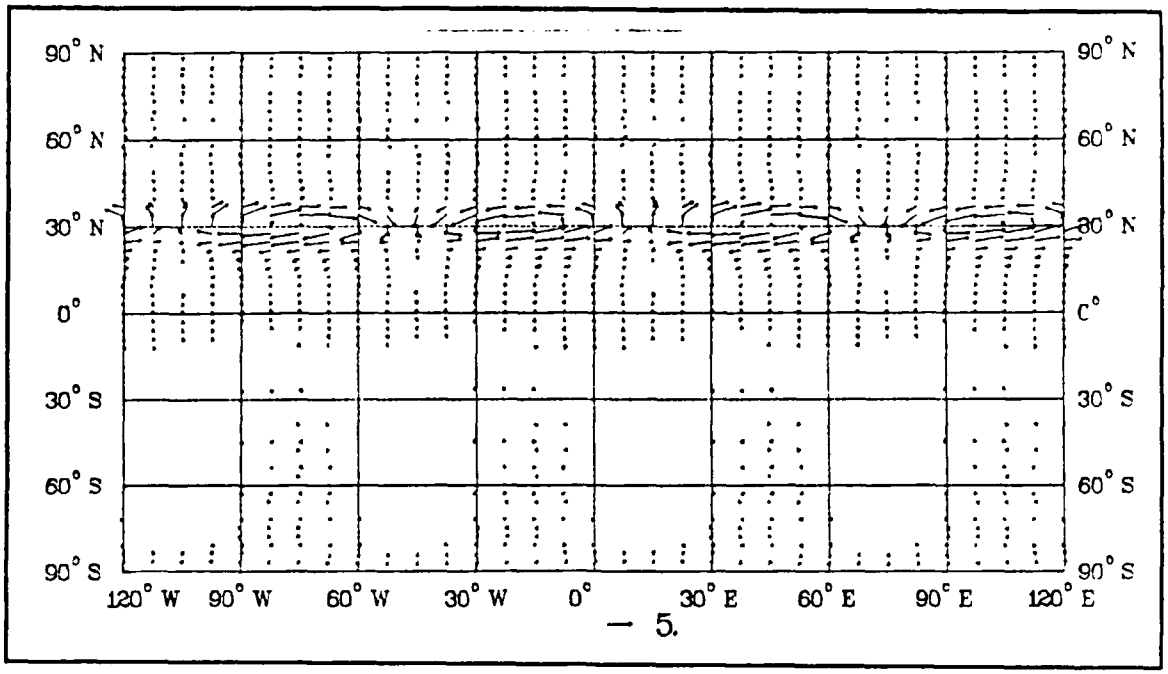

Figure 6.9. Wind Vectors at 24 Hours for Phase I, Experiment 1

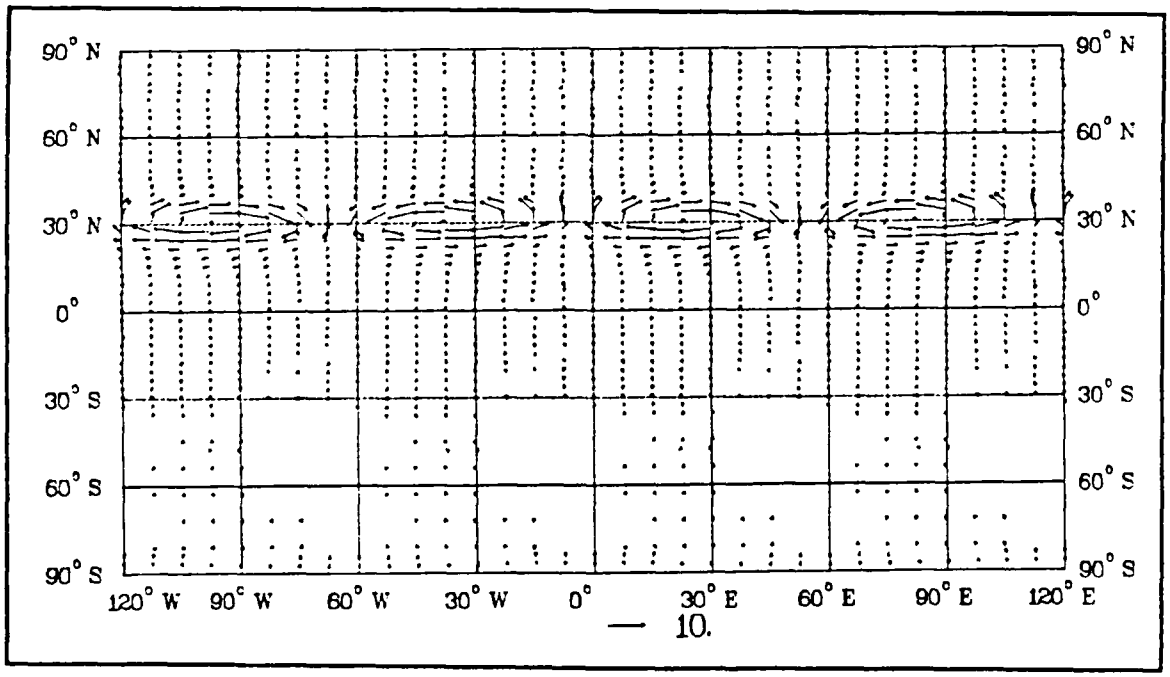

Figure 6.10. Wind Vectors at 48 Hours for Phase I, Experiment 1

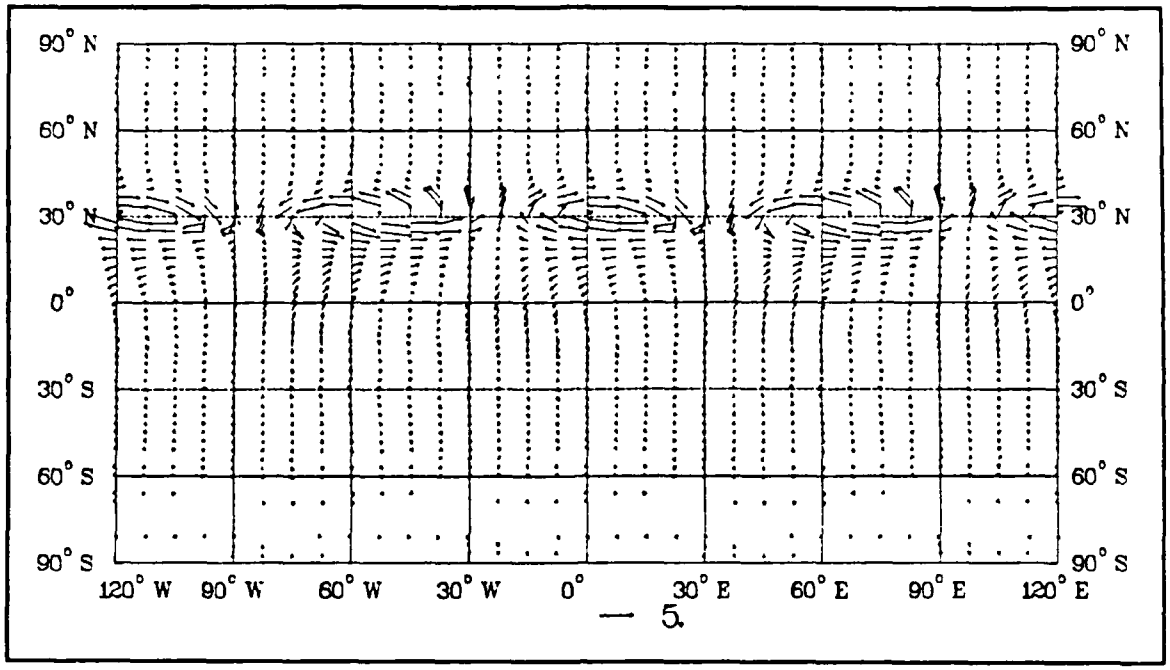

Figure 6.11. Wind Vectors at 72 Hours for Phase I, Experiment 1

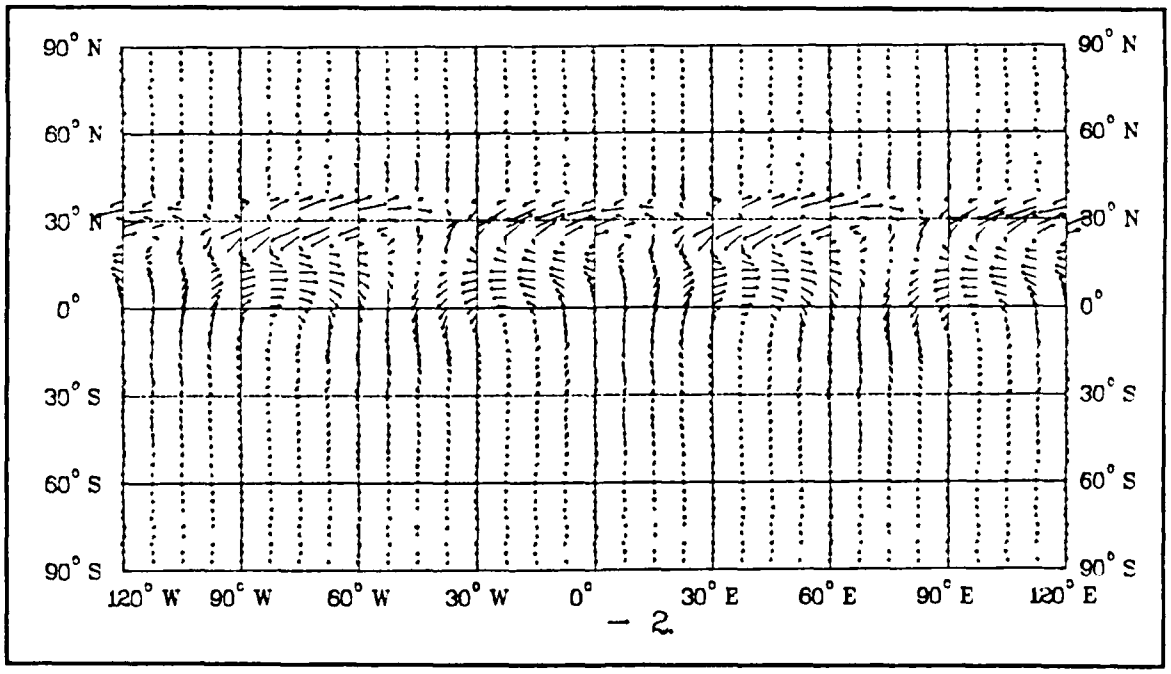

Figure 6.12. Wind Vectors at 96 Hours for Phase I, Experiment 1

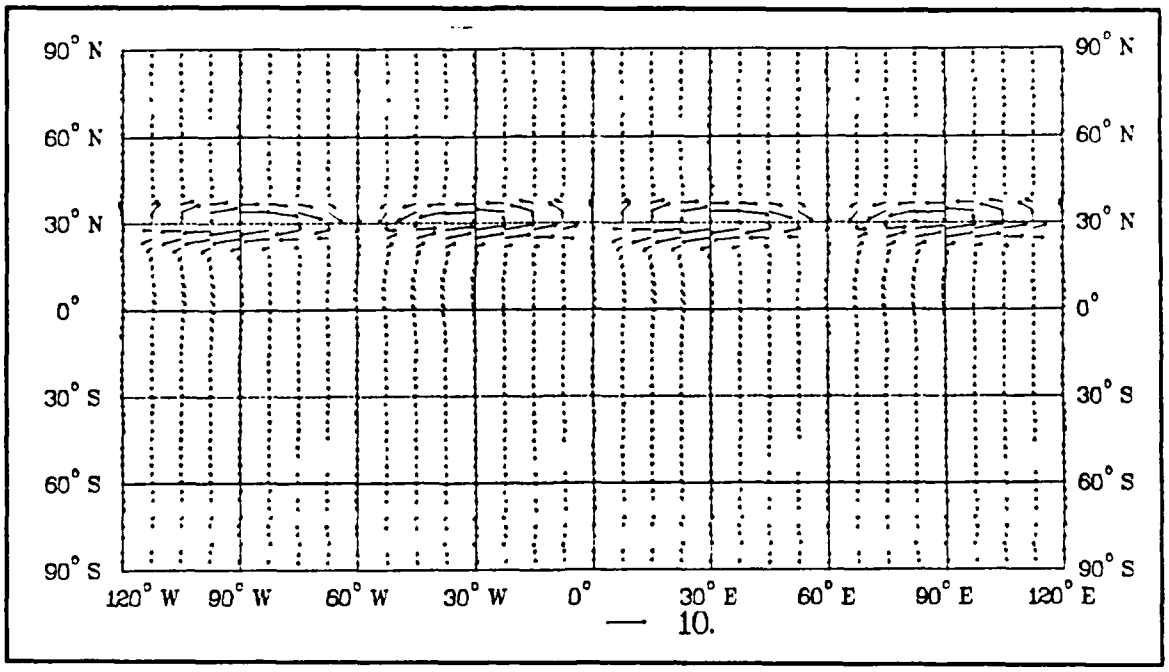

Figure 6.13. Wind Vectors at 120 Hours for Phase I, Experiment 1

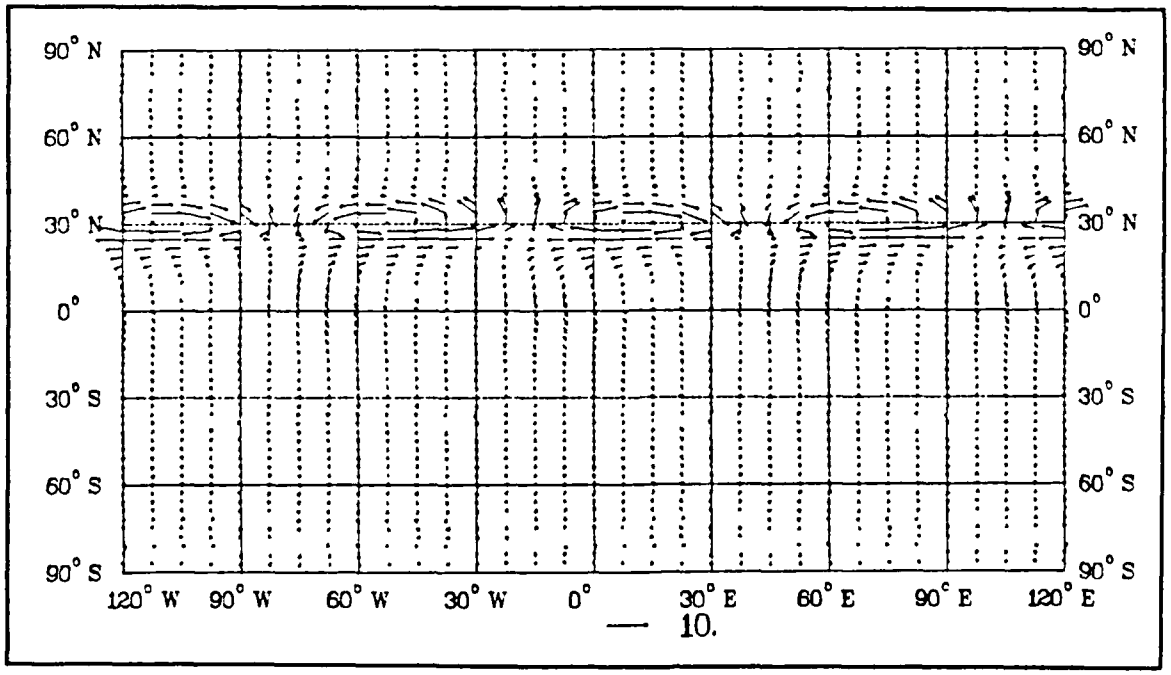

Figure 6.14. Wind Vectors at 144 Hours for Phase I, Experiment 1

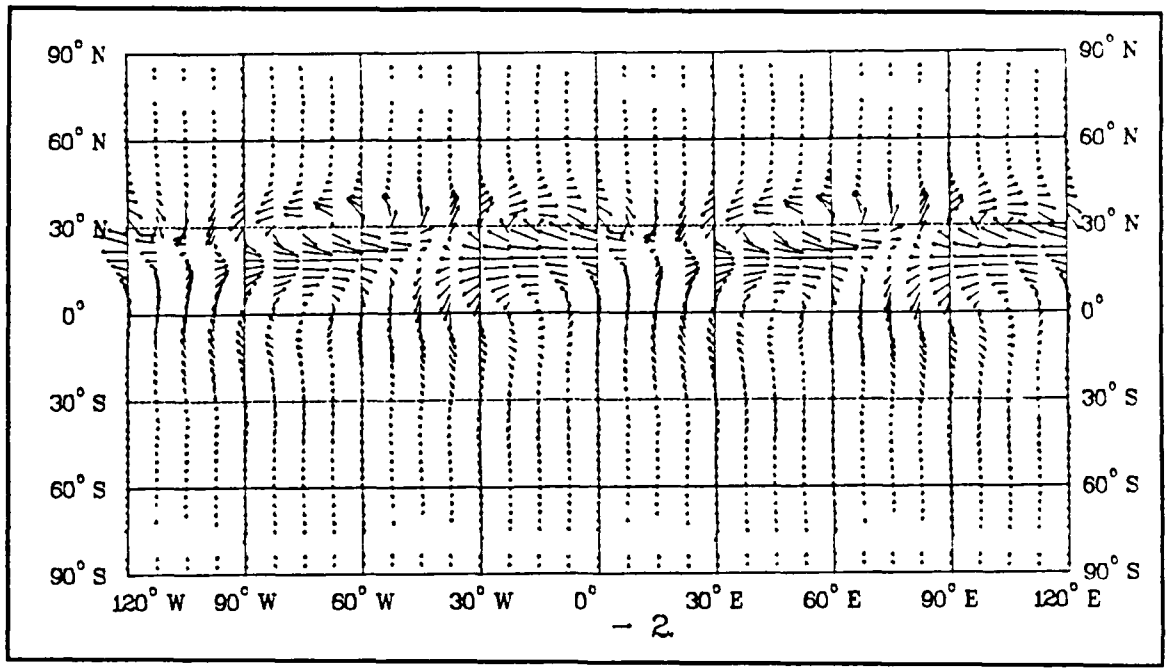

Figure 6.15. Wind Vectors at 168 Hours for Phase I, Experiment 1

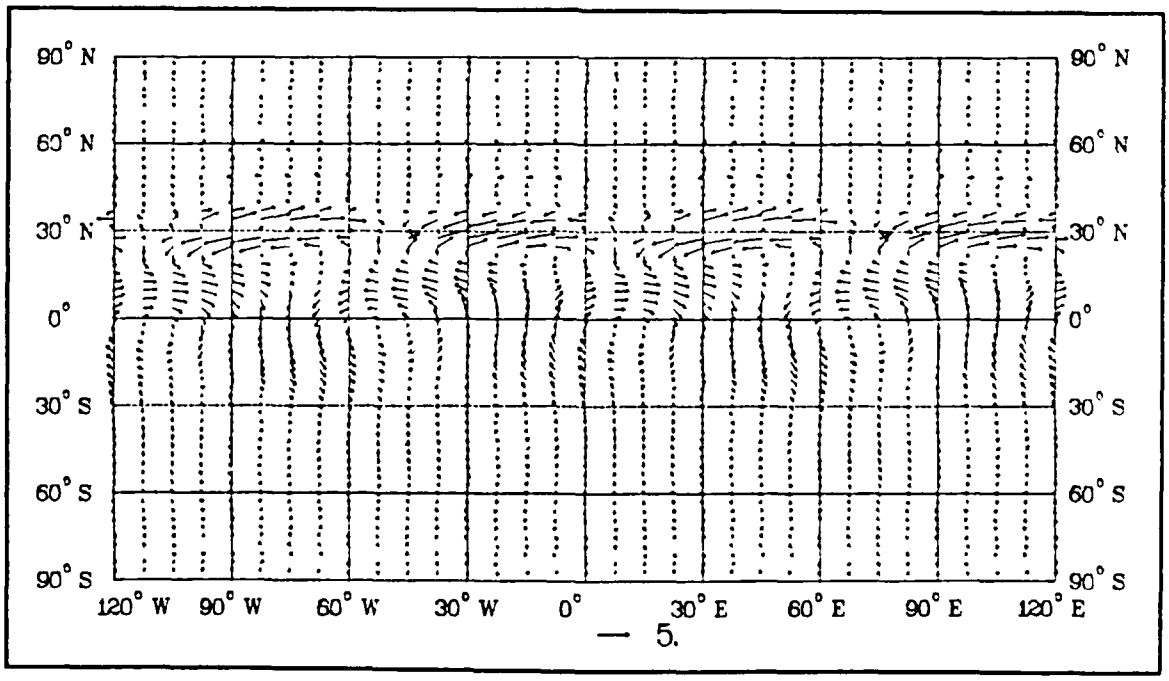

Figure 6.16. Wind Vectors at 192 Hours for Phase I, Experiment 1

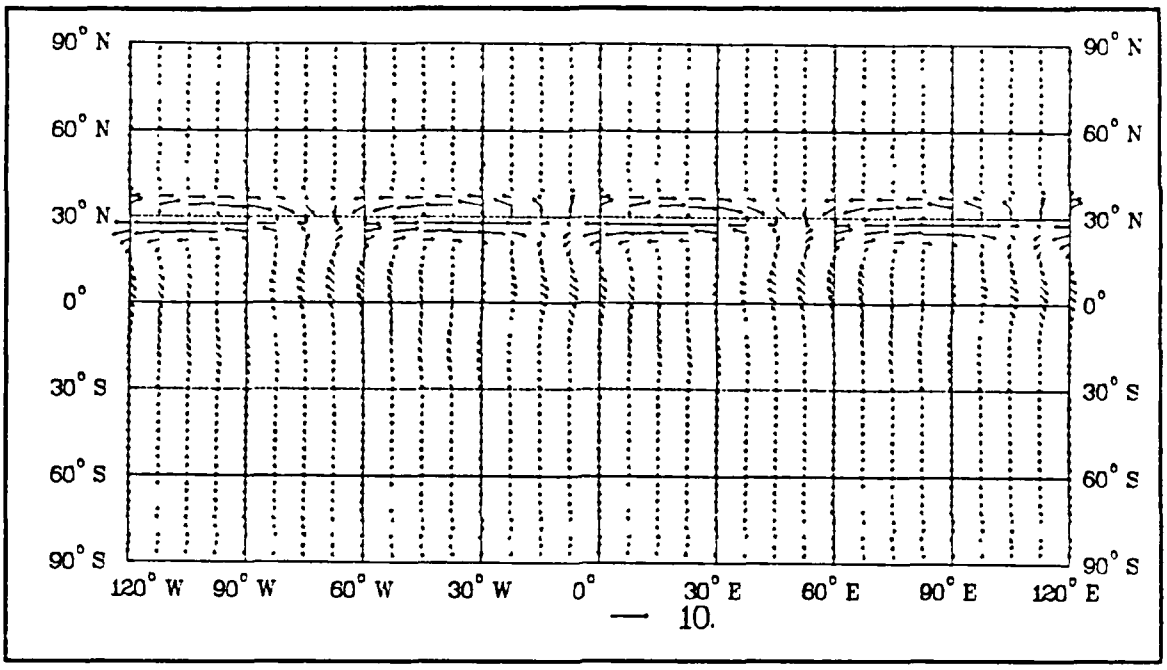

Figure 6.17. Wind Vectors at 216 Hours for Phase I, Experiment 1

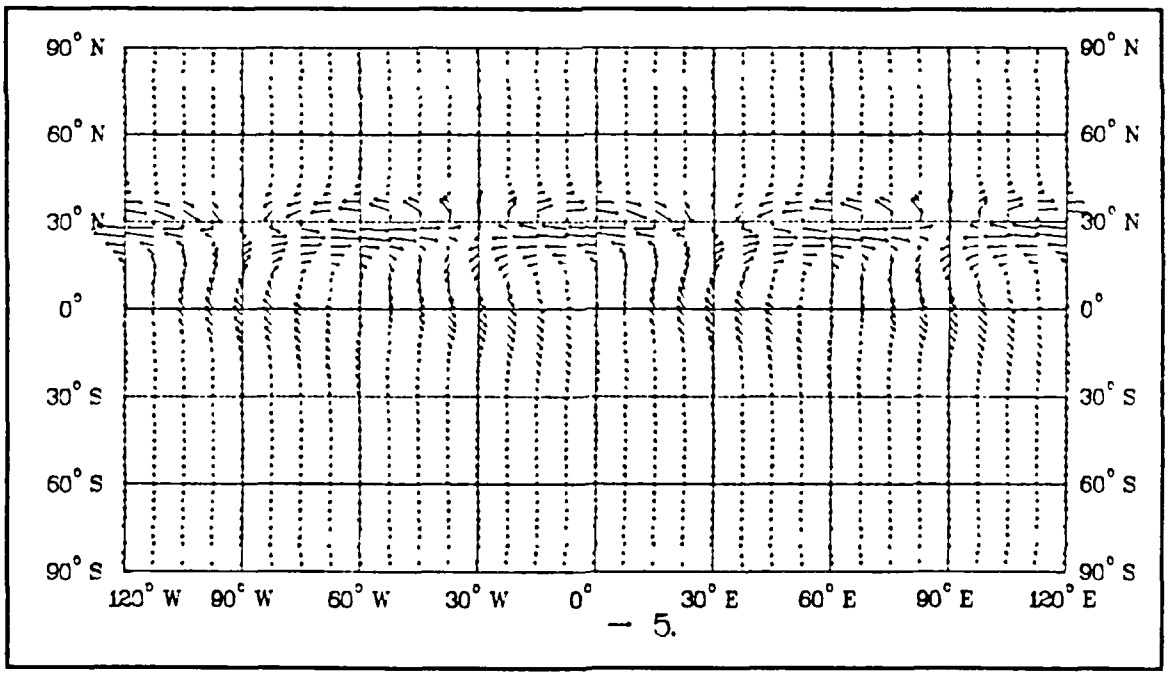

Figure 6.18. Wind Vectors at 240 Hours for Phase I, Experiment 1

In the first 24 hours it is evident that wavenumber three develops, since there is one wave in each 120° sector. The circulation is confined to the latitudes of the forcing. By 48 hours the overall magnitude of the vectors has increased, but there still is not significant propagation into the tropics. At the 72 hour point the magnitude of the wind vectors has decreased, and the circulation has pushed southward toward the equator. The wave patterns move toward the west, but the expected northeast-southwest tilt of Rossby waves is not present. By 96 hours the overall magnitude of the wind vectors is at the minimum, and there is weak circulation extending into the Southern Hemisphere. After 120 hours the overall magnitude of the wind vectors has increased to the value at 24 hours, and the weak circulation in the tropics is not evident.

A similar pattern of changes occur at 144, 168, 192, 216 and 240 hours. The three-and-a-half day oscillation, or beat, of the overall velocity vector magnitude is consistent with the three-and-a-half day period corresponding to the frequency of the waves in this experiment; however, the beat frequency is not consistent with the beta-plane theory. The oscillation in magnitude indicates the wave pattern has not stabilized, and the time variation is not purely sinusoidal, as assumed in the theory.

The circulation patterns in Figs. 6.9 to 6.18 do not propagate very far north. The trapping of waves to the north may be due to an increase in the Coriolis parameter on the beta-plane. As the Coriolis parameter (f) increases in Eq. 2.11, α^2 becomes more negative; consequently, the waves are trapped near the source latitudes.

The wind vectors for the first vertical mode at 24 and 240 hours are displayed in Figs. 6.19 and 6.20. At the 24-hour point, there is significant

circulation in the tropics, but the magnitude is only one meter per second (one fifth of the complete field shown in Fig. 6.9). This observation is consistent with theory, in that it is difficult for a heating or mass source to force the barotropic mode (Lim and Chang, 1987). After 240 hours, the overall magnitude of the wind vectors has doubled. There is significant circulation south of the equator, but the desired northeast-southwest tilt of propagating Rossby waves is not evident.

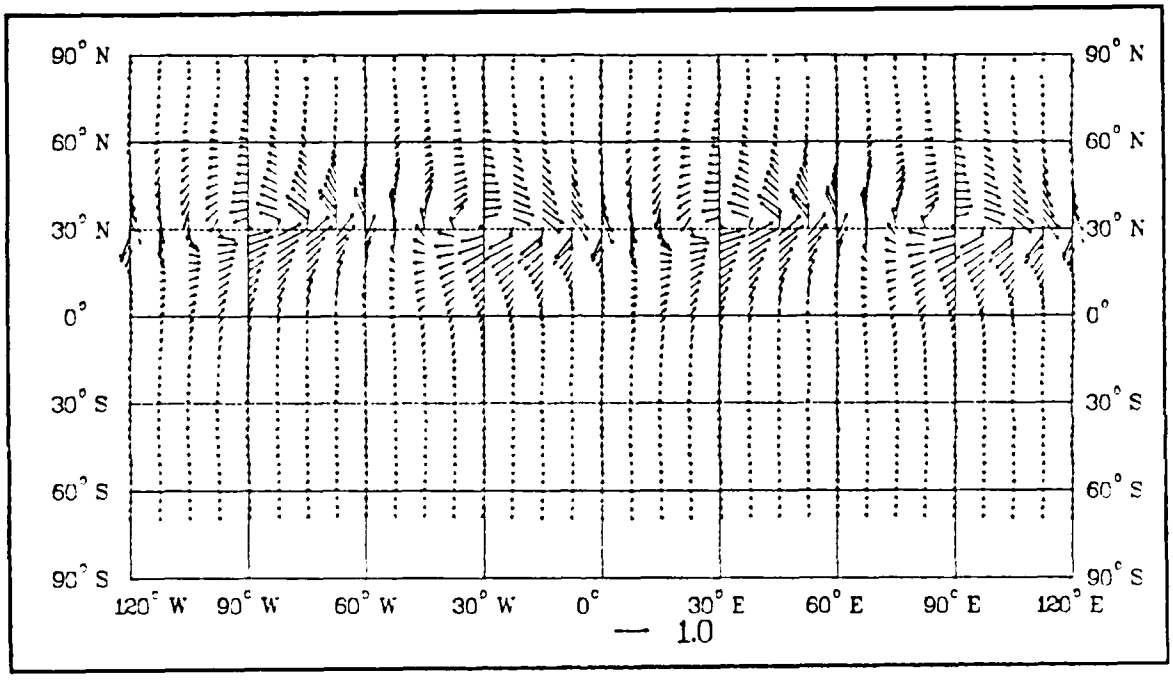

Figure 6.19. Wind Vectors at 24 Hours for Phase I, Experiment 1, Mode 1

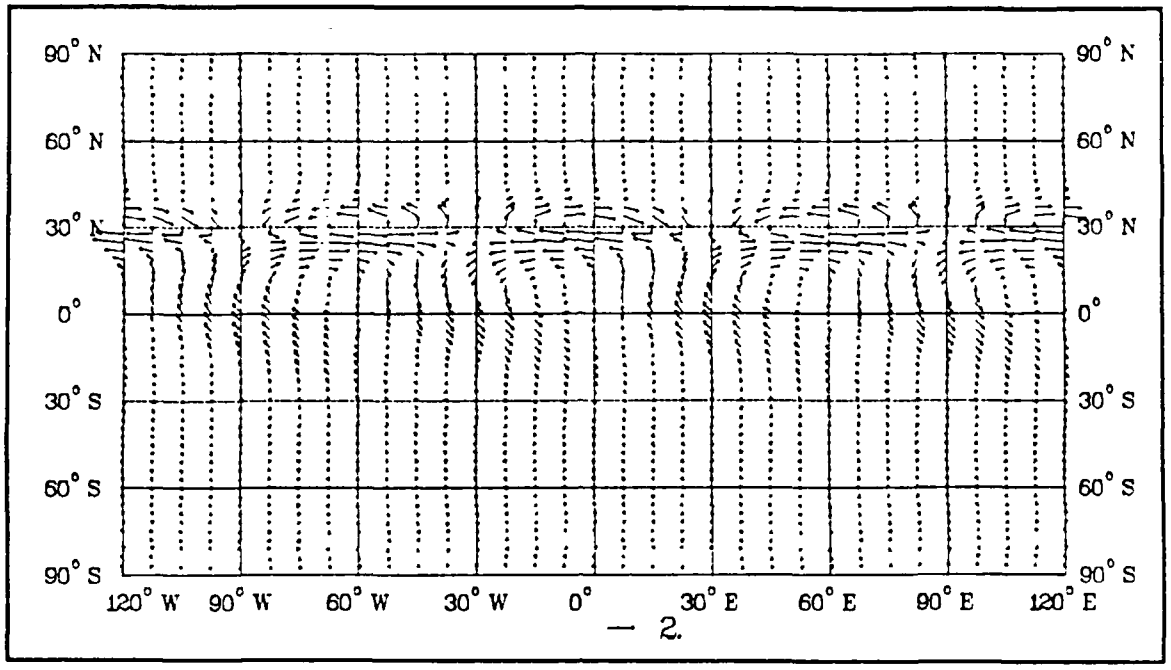

Figure 6.20. Wind Vectors at 240 Hours for Phase I, Experiment 1, Mode 1

The pattern of the first baroclinic mode at 24 hours (Fig. 6.21) is similar to the barotropic mode at 24 hours, but the overall magnitude of the wind vectors is larger. This result is similar to Lim and Chang (1987). Lim and Chang found that a heating source is more effective at forcing the higher order modes. The circulation pattern and overall magnitude of the wind vectors of the first baroclinic mode, after 240 hours (Fig. 6.22), is similar to the barotropic mode at 240 hours, except the modes are 180° out of phase. The overall magnitude of the wind vectors of the higher modes (not shown) are less than or equal to the magnitude of the barotropic mode at 24 hours. According to theory, the barotropic mode is the only mode with a propagating solution (when H = 7083.1 m). The results of this experiment indicate all modes can propagate to some extent.

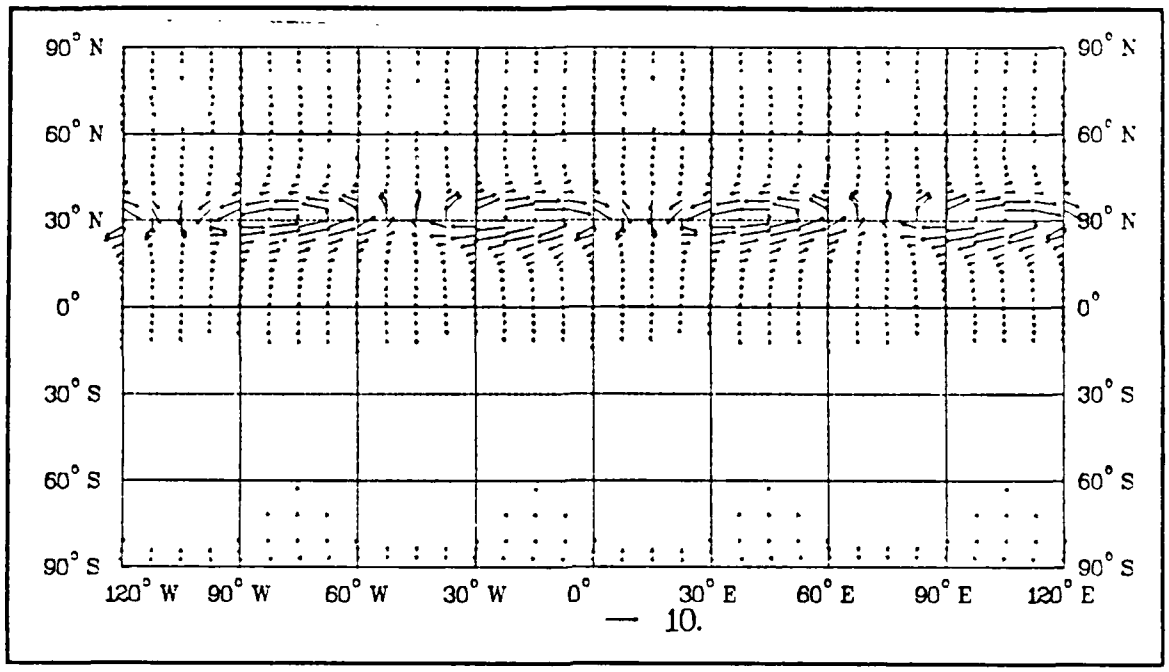

Figure 6.21. Wind Vectors at 24 Hours for Phase I, Experiment 1, Mode 2

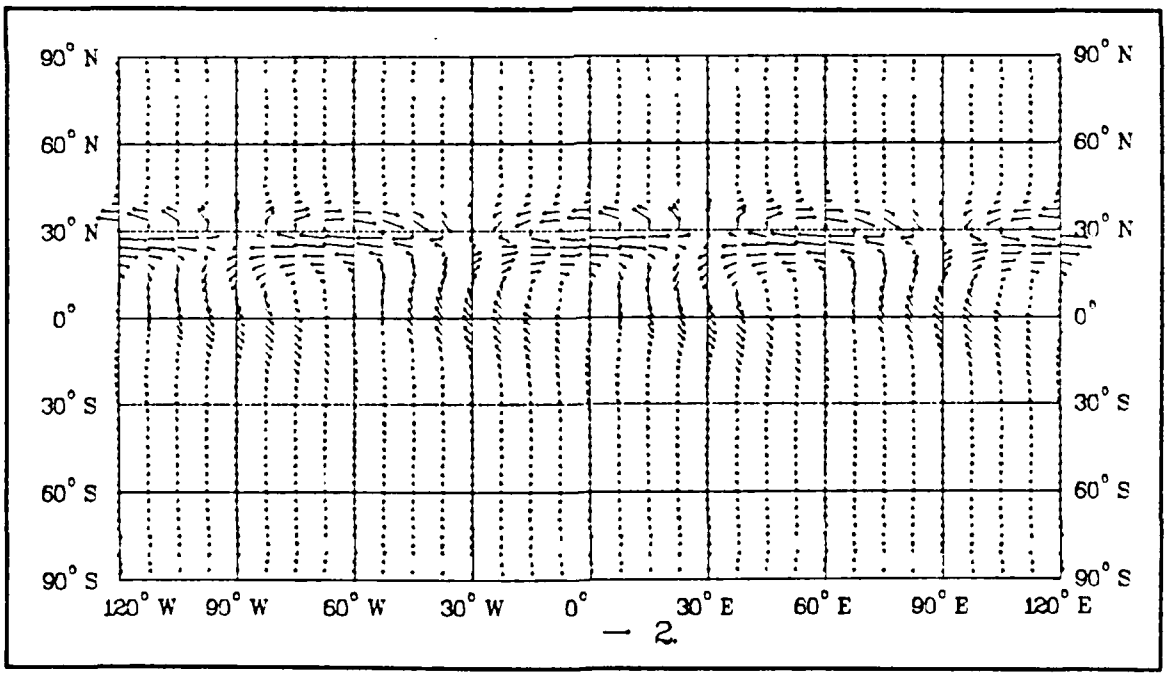

Figure 6.22. Wind Vectors at 240 Hours for Phase I, Experiment 1, Mode 2

2. Experiment 2

In this experiment the forcing function is again added to the thermal equation, (Eq. 3.4) but the equivalent depth (H) is 209.09 m. This value of H corresponds to the first baroclinic mode, which is mode two. The wave frequency (ω) is $26.13 \times 10^{-7}\ s^{-1}$ and the period is 27.8 days. The wind vector fields for the lowest level ($\sigma = .938$) at 24 and 240 hours are displayed in Figs. 6.23 and 6.24. The patterns are not significantly different than Experiment 1. The overall amplitude of the wind vectors is much larger than for Experiment 1. The beat oscillation of the overall vector magnitude is not present, since the period is 27.8 days. The westward propagation is slower than in Experiment 1, also due to the longer period. The overall magnitude of the wind vectors of the barotropic mode at 24 hours (not shown) is one meter per second, whereas the overall magnitude of the baroclinic wind vectors (not shown) is ten meters per second. The magnitudes of the wind vectors of the higher modes are also on the order of the barotropic mode at 24 hours. All the modes at later times show similar patterns and magnitudes.

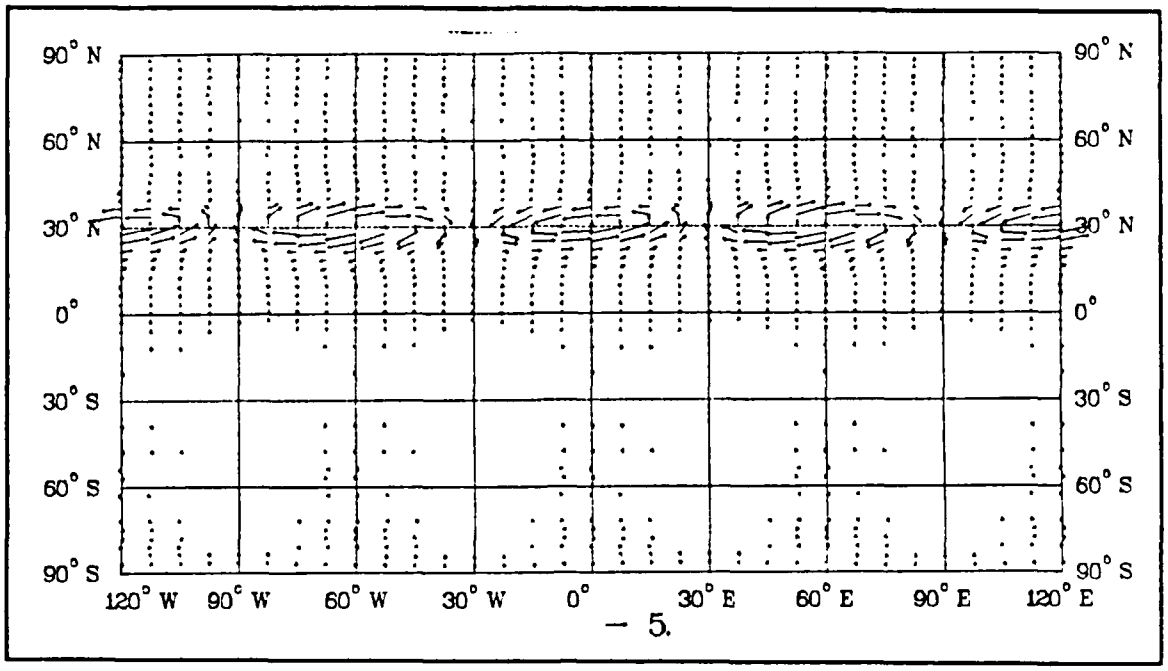

Figure 6.23. Wind Vectors at 24 Hours for Phase I, Experiment 2

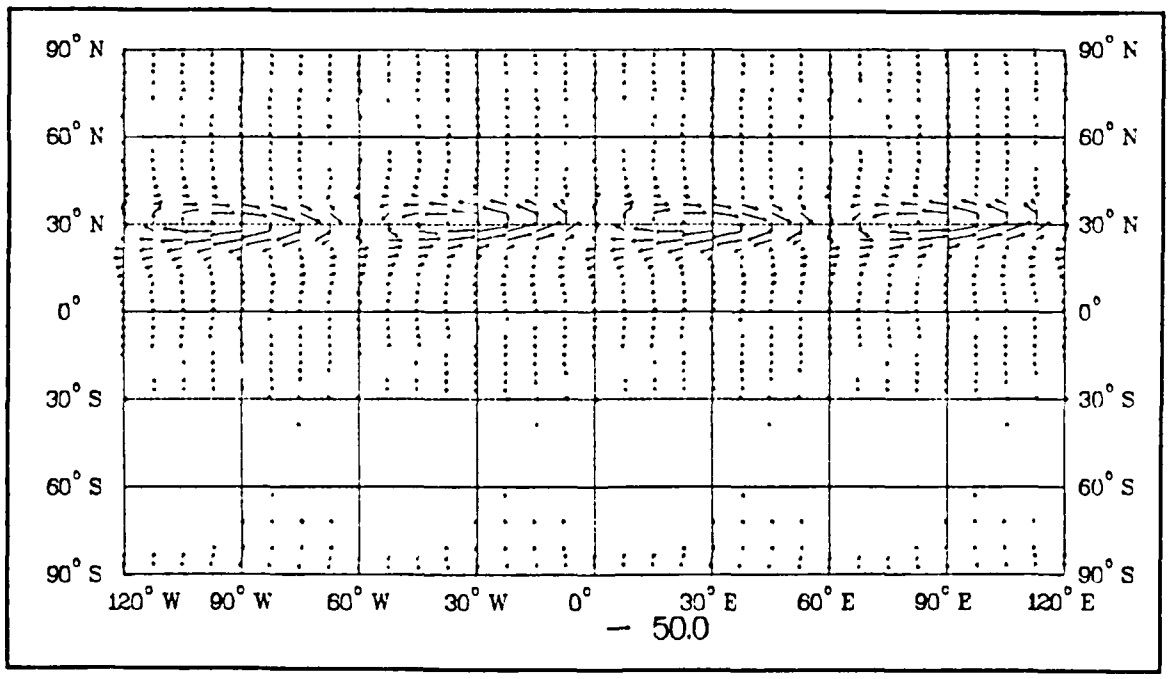

Figure 6.24. Wind Vectors at 240 Hours for Phase I, Experiment 2

3. Experiment 3

The forcing function of this experiment is added to the thermal equation (Eq. 3.4), and uses an equivalent depth (H) of 59.748 m. The frequency (ω) is $-8.04 \times 10^{-7}\ s^{-1}$ and the period is 90.4 days. The results are similar to Experiments 1 and 2, except the overall magnitude of the velocity vectors is greater and the westward propagation of the circulation patterns is slower. The magnitude of the wind vectors of the barotropic mode is again much less than the baroclinic mode.

4. Experiment 4

In this experiment the forcing function is only added to the vorticity equation (Eq. 3.1). The equivalent height (H) in Eq. 2.12 is 7083.1 m, which is the height of the barotropic mode. The frequency (ω) is $-206.30 \times 10^{-7}\ s^{-1}$ and the period is 3.5 days. The wind vector fields for the lowest level (σ = .938) are displayed in Figs. 6.25 to 6.34. The circulation patterns are substantially different than when the source is added to the thermal equations in Experiments 1 through 3. After 24 hours there is significant circulation moving toward the tropics. By 48 hours the flow has crossed the equator and has the northeast-southwest tilt consistent with propagating Rossby waves. The 72 through 240 hour solutions show the circulation continues to move toward the south. Notice again, that the circulation does not move too far north. The overall magnitude of the vectors is unrealistic at the end of the time period. The large magnitude is caused by the arbitrary amplitude factor used in the forcing function. The results of this experiment are more consistent with the midlatitude beta-plane theory than the results of Experiments 1 through 3.

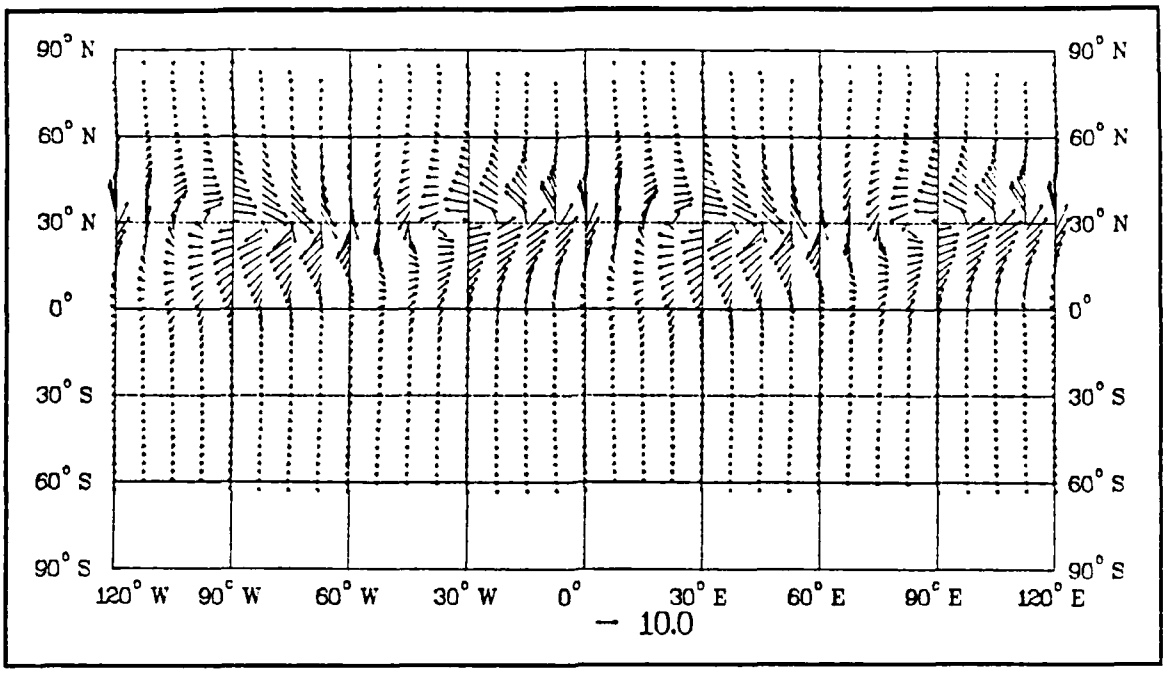

Figure 6.25. Wind Vectors at 24 Hours for Phase I, Experiment 4

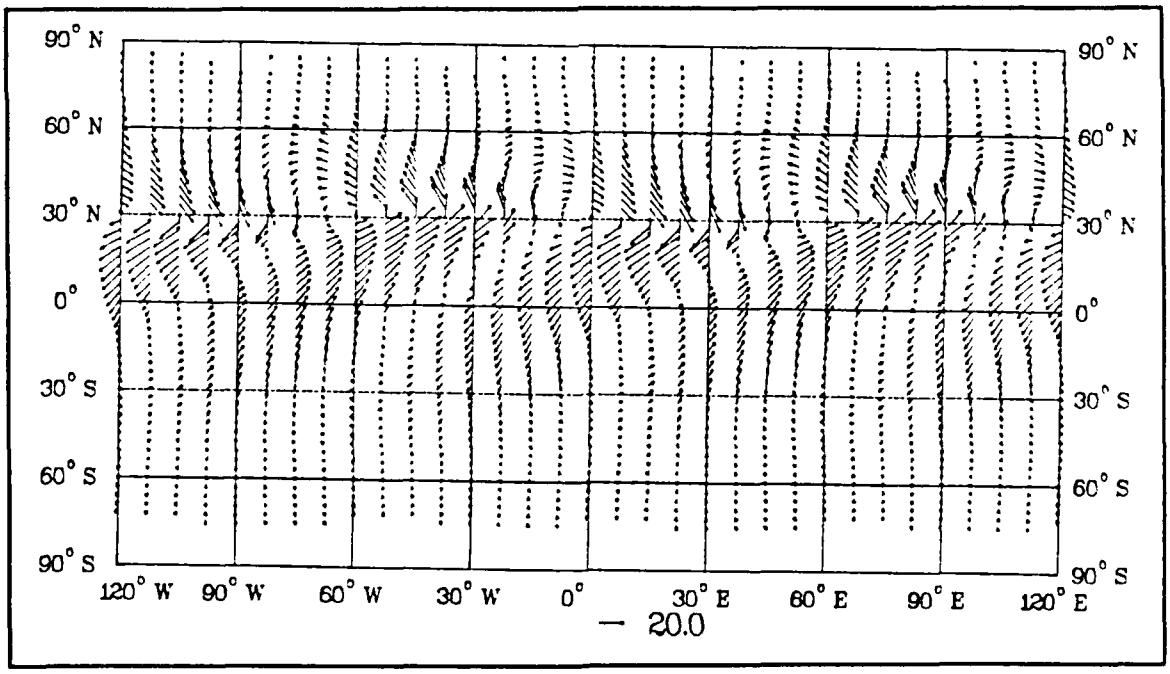

Figure 6.26. Wind Vectors at 48 Hours for Phase I, Experiment 4

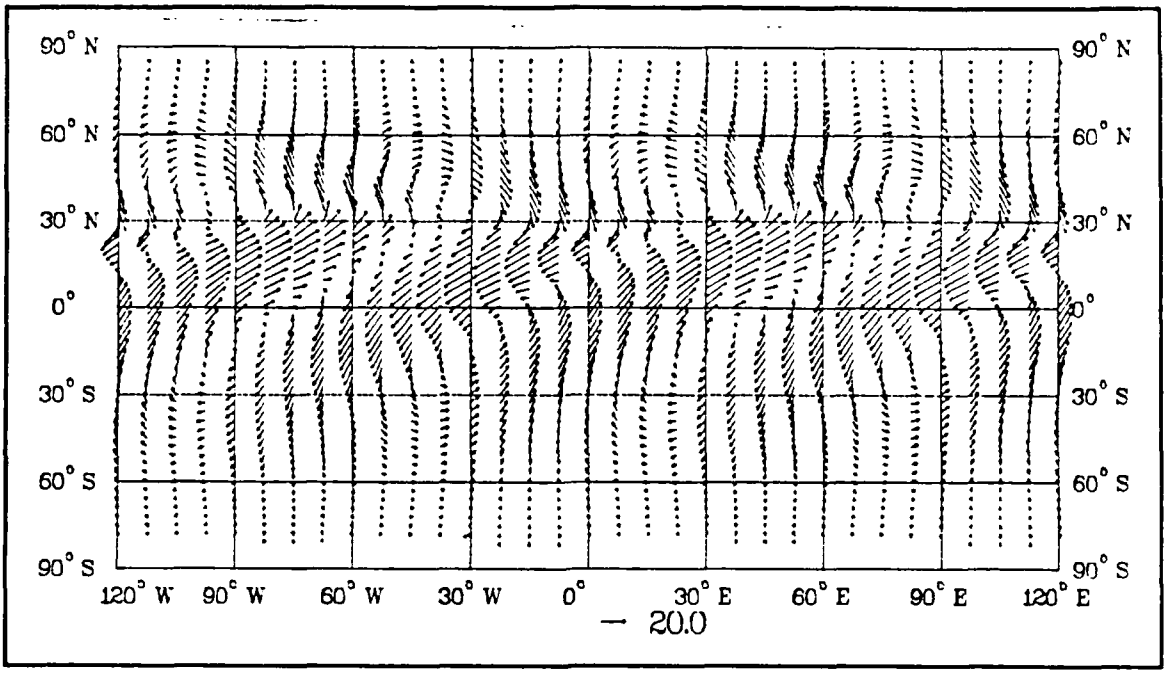

Figure 6.27. Wind Vectors at 72 Hours for Phase I, Experiment 4

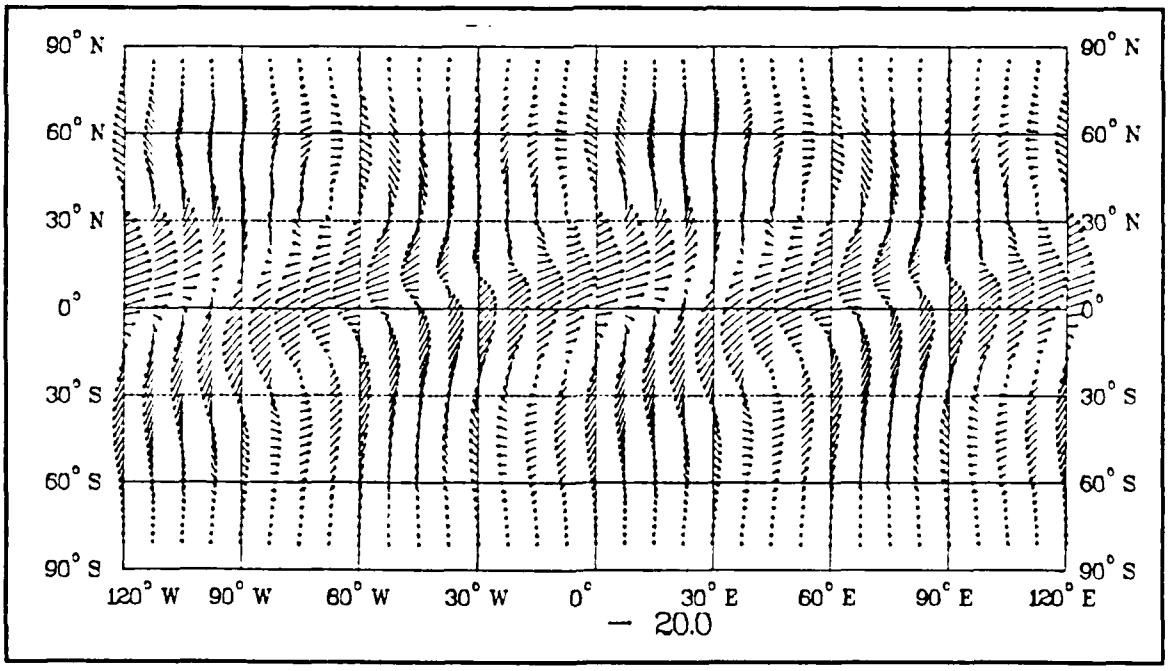

Figure 6.28. Wind Vectors at 96 Hours for Phase I, Experiment 4

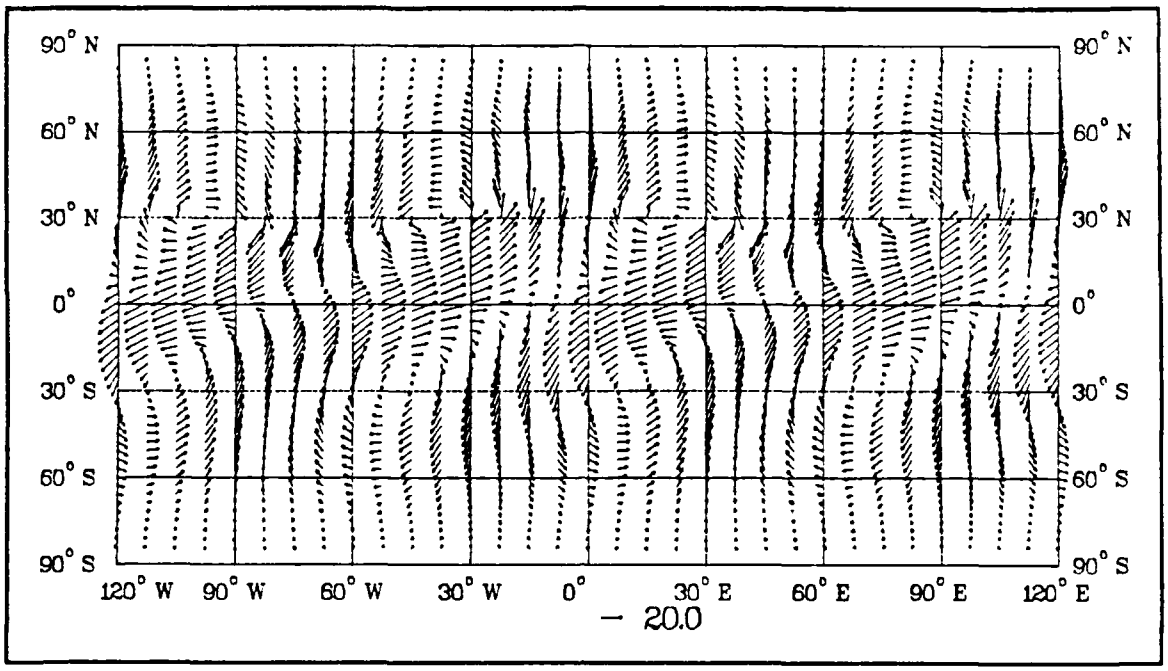

Figure 6.29. Wind Vectors at 120 Hours for Phase I, Experiment 4

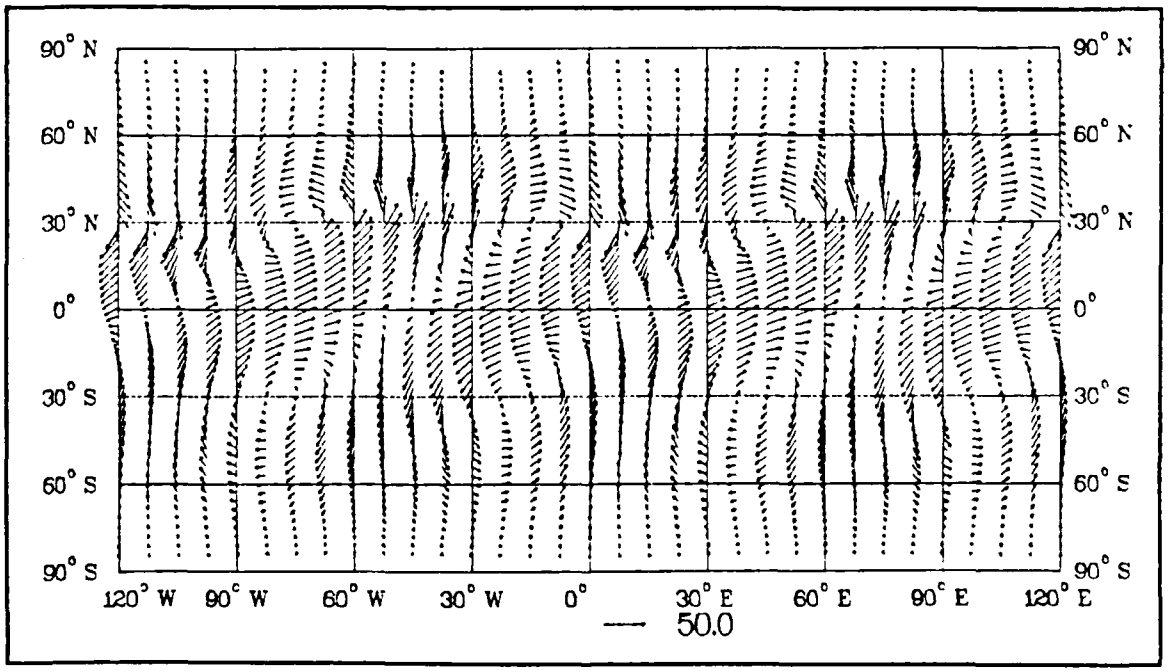

Figure 6.30. Wind Vectors at 144 Hours for Phase I, Experiment 4

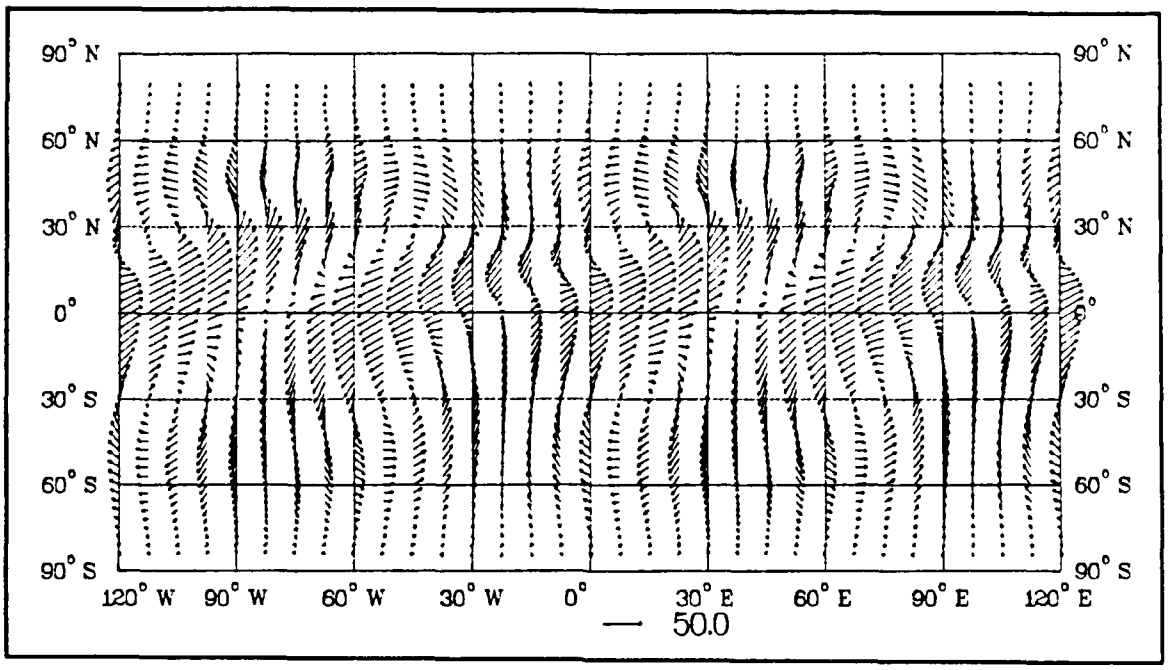

Figure 6.31. Wind Vectors at 168 Hours for Phase I, Experiment 4

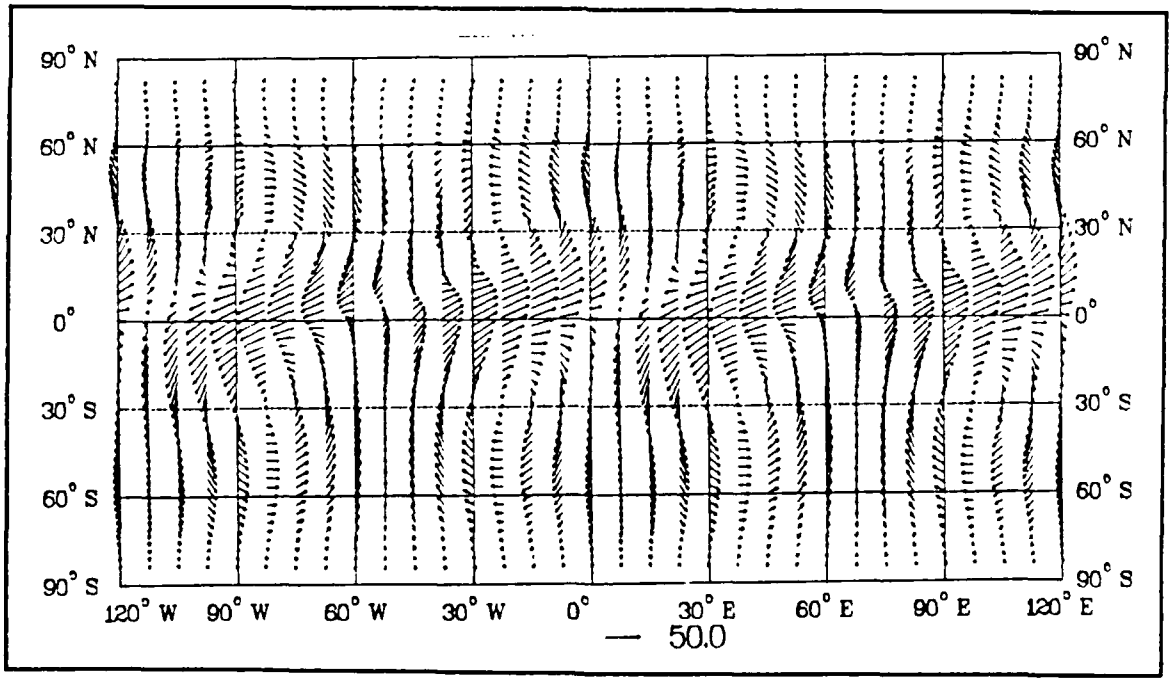

Figure 6.32. Wind Vectors at 192 Hours for Phase I, Experiment 4

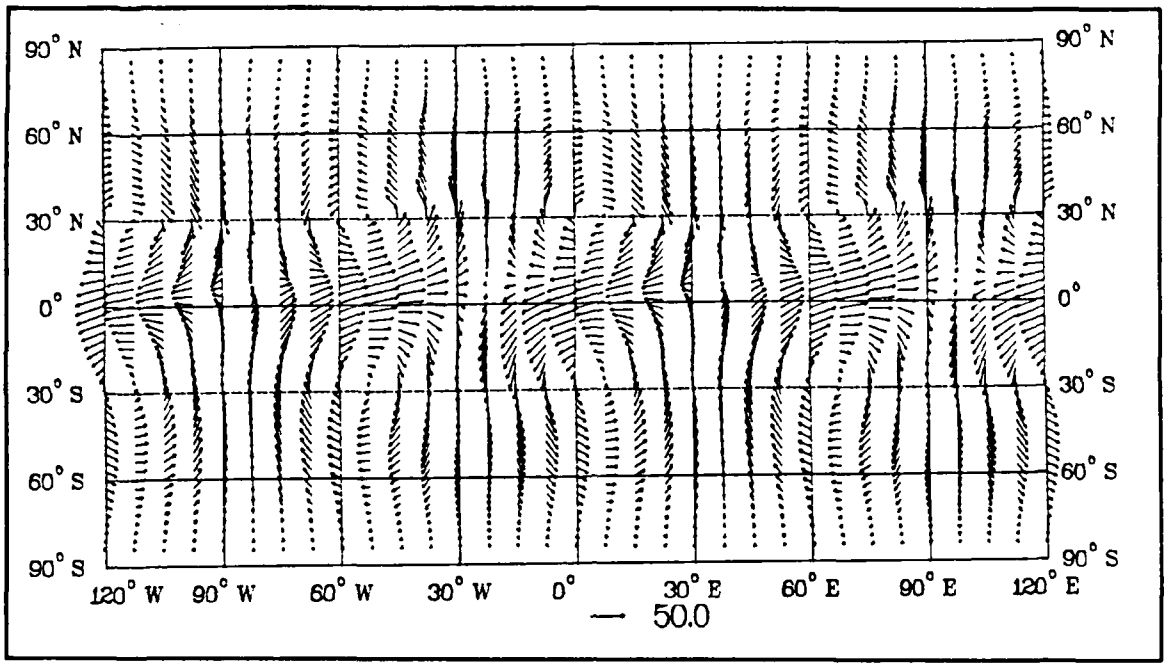

Figure 6.33. Wind Vectors at 216 Hours for Phase I, Experiment 4

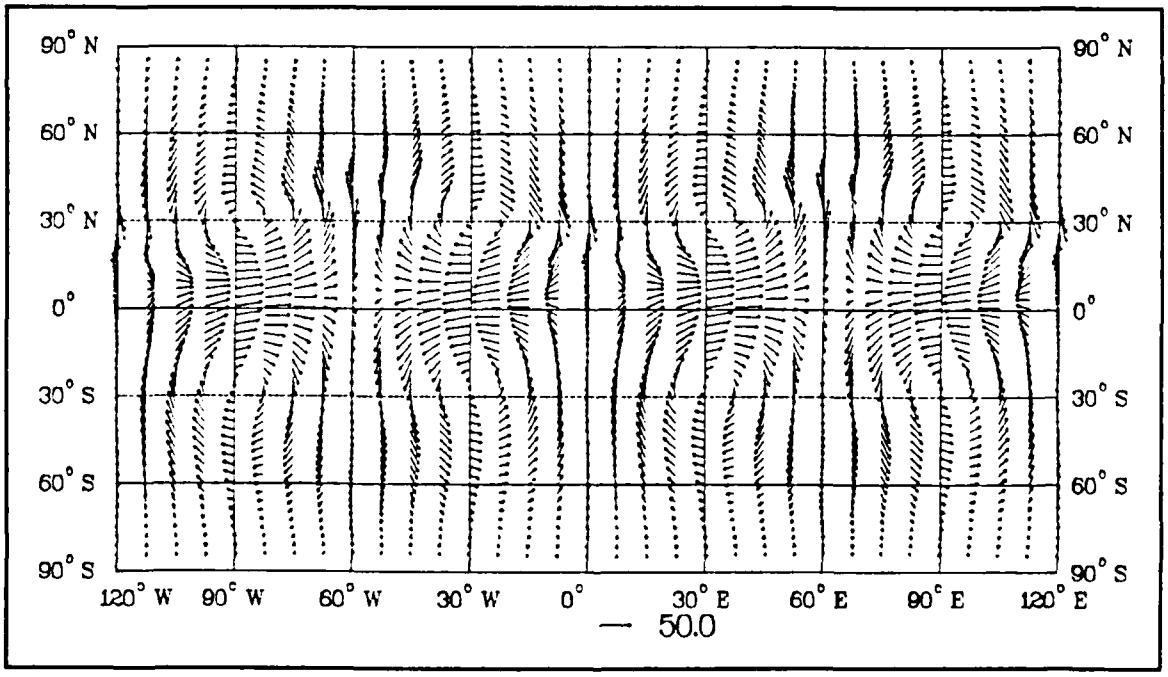

Figure 6.34. Wind Vectors at 240 Hours for Phase I, Experiment 4

The overall magnitude of the wind vectors of the barotropic mode at 24 hours (Fig. 6.35) is five times larger than the magnitude of the wind vectors of the baroclinic mode at the same time (Fig. 6.36). The vorticity source is much more efficient at forcing the barotropic mode.

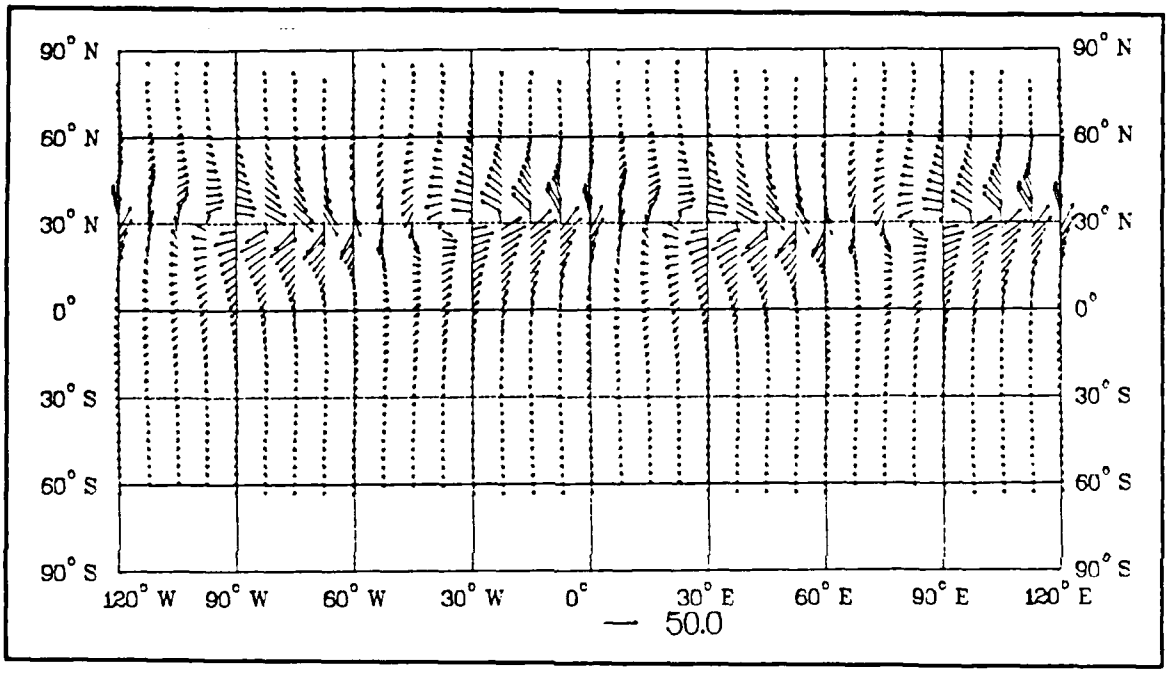

Figure 6.35. Wind Vectors at 24 Hours for Phase I, Experiment 4, Mode 1

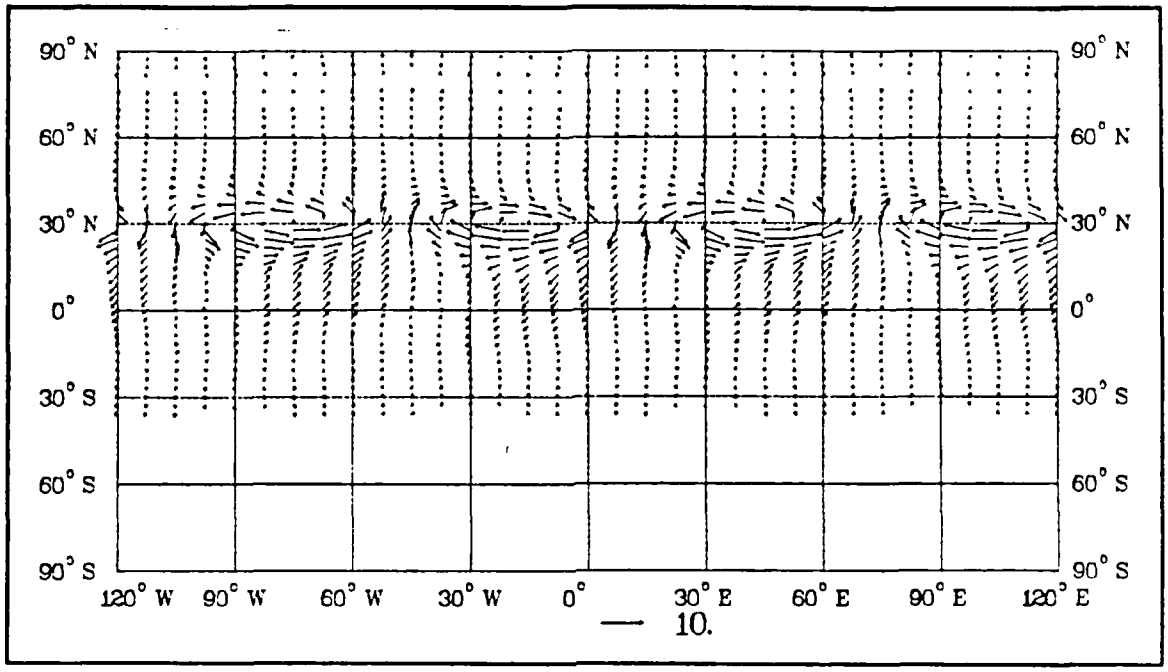

Figure 6.36. Wind Vectors at 24 Hours for Phase I, Experiment 4, Mode 2

5. Experiment 5

This experiment is exactly the same as Experiment 4, except the sign of the frequency (ω) in Eq. 2.12 is changed. With a positive frequency (ω), $\mu > 0$ in Eq. 2.26 and the circulation should be trapped near the source. The wind velocity vectors for the lowest level (σ = .938) at 24 and 240 hours are displayed in Figs. 6.37 and 6.38. The overall magnitude of the vectors is significantly smaller than those of Experiment 4. However, the circulation did propagate past the equator, but to a much less extent. The propagation is most likely due to fast moving gravity waves. The modal analysis is consistent with the complete solution, and the results of Experiment 4.

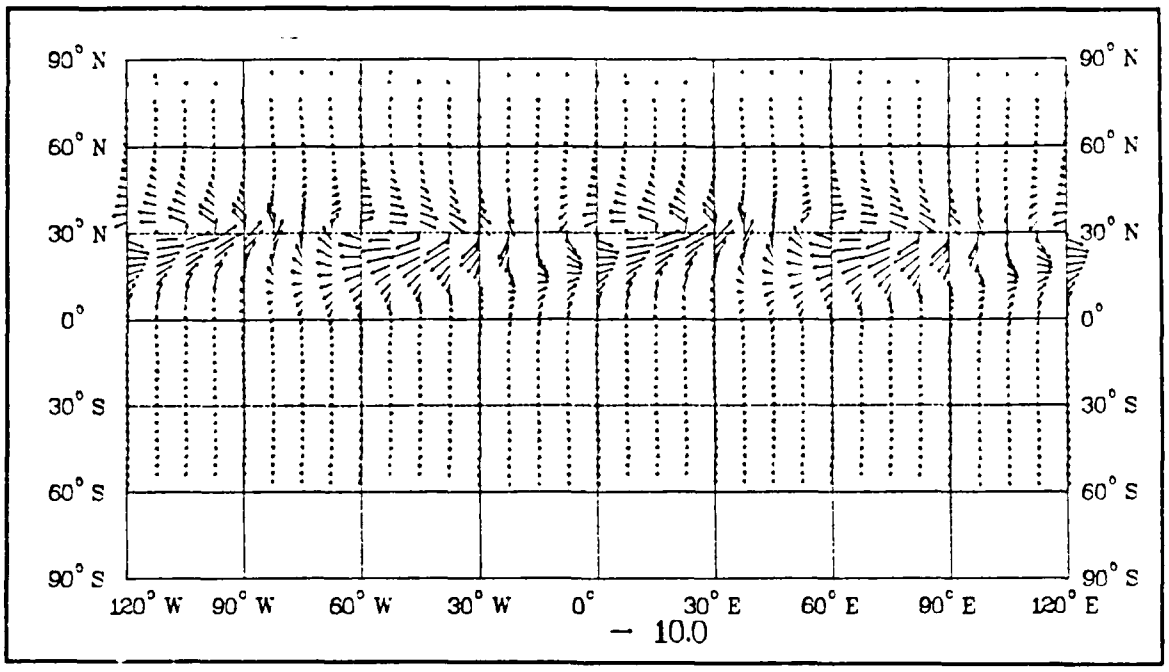

Figure 6.37. Wind Vectors at 24 Hours for Phase I, Experiment 5

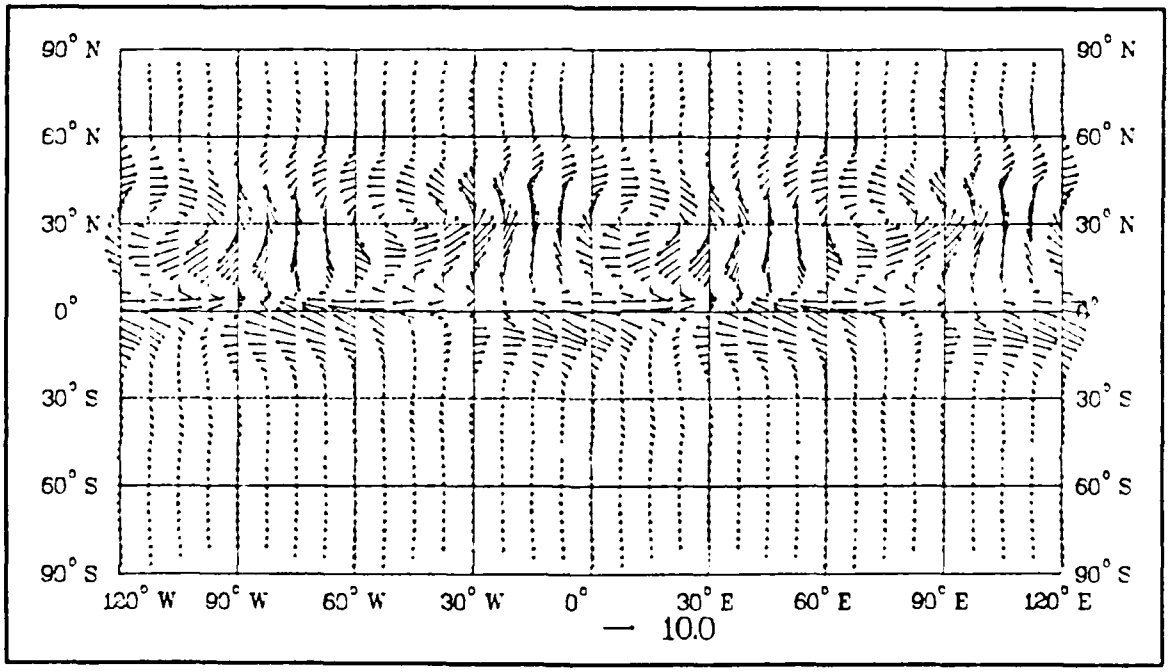

Figure 6.38. Wind Vectors at 240 Hours for Phase I, Experiment 5

6. Experiment 6

In this experiment the forcing is only added to the vorticity equation (Eq. 3.1). The equivalent height (H) is 209.09 m, which is the height of the first baroclinic mode. The frequency (ω) is 26.13 x 10^{-7} s^{-1} and the period is 27.8 days. The wind velocity vectors for the lowest level (σ = .938) at 24 and 240 hours are displayed in Figs. 6.39 and 6.40. The circulation patterns show a significant tilt toward the southwest, but the circulation does not propagate significantly into the Southern Hemisphere. The overall magnitude of the barotropic mode vectors (not shown) is again much larger than the baroclinic mode vectors (not shown) at the 24-hour point.

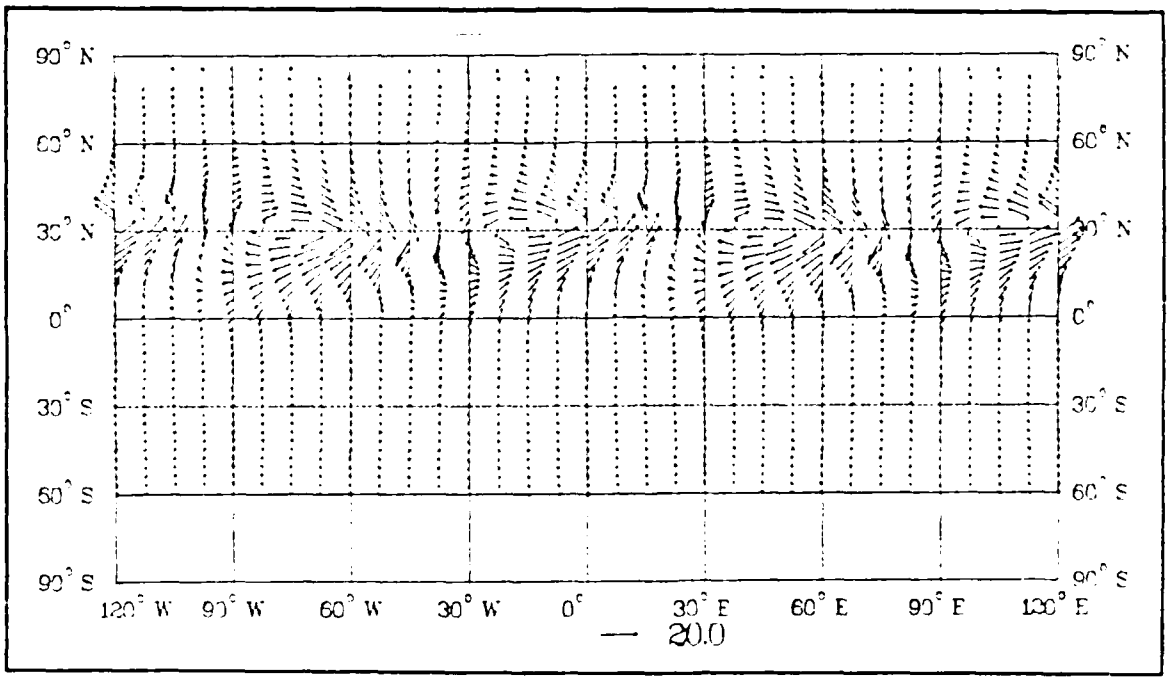

Figure 6.39. Wind Vectors at 24 Hours for Phase I, Experiment 6

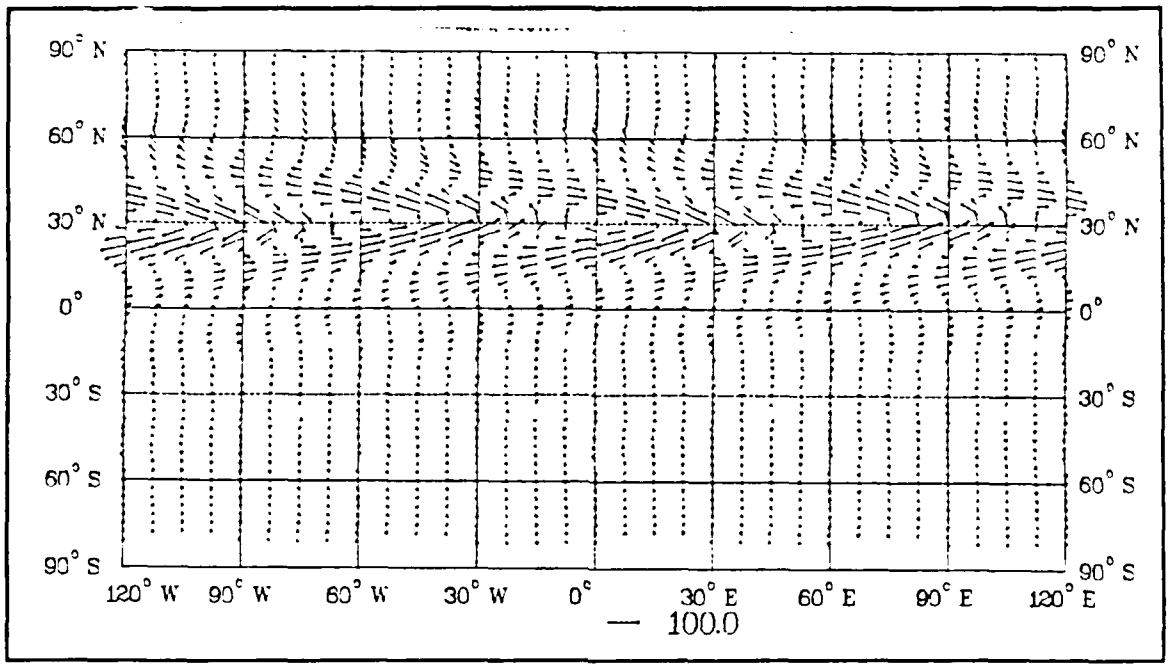

Figure 6.40. Wind Vectors at 240 Hours for Phase I, Experiment 6

7. Experiment 7

In this experiment the forcing function is added to the vorticity equation (Eq. 3.1). The equivalent height (H) in Eq. 2.12 is 209.09 m, which is exactly equal to the first baroclinic mode. The variable α equals π / W, where W is half the width of the forcing function in degrees latitude. This value of α is a singular point in the complete propagating solution (Eqs. 2.17 and 2.18). The wind velocity vectors for the lowest level (σ = .938) are displayed in Figs. 6.41 to 6.50.

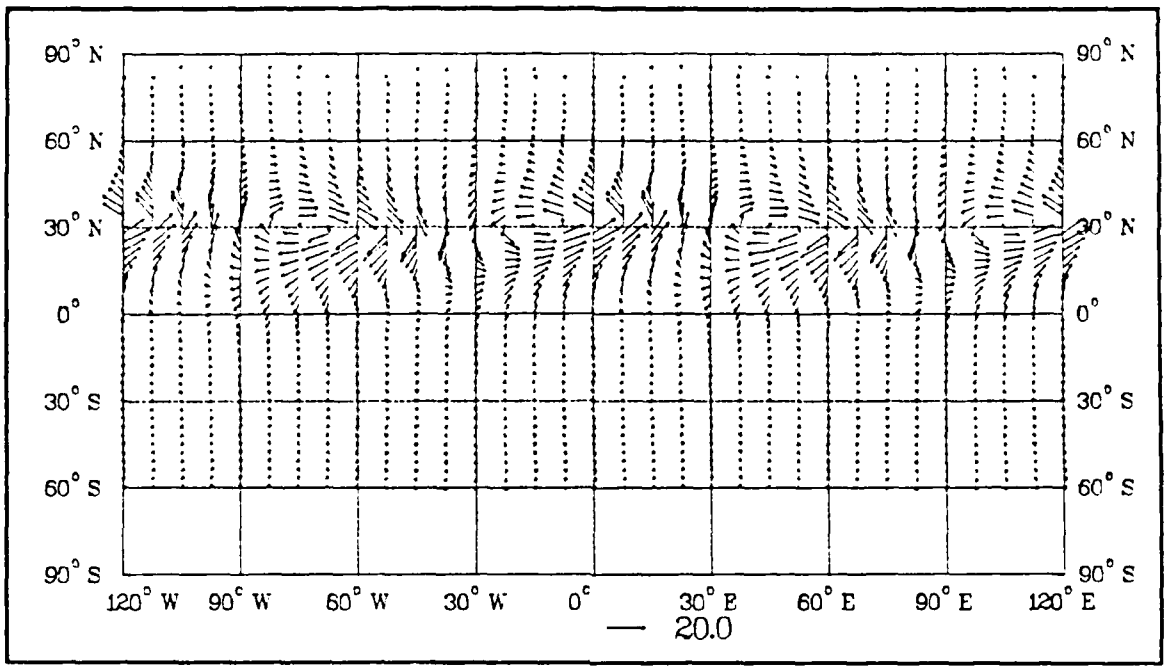

Figure 6.41. Wind Vectors at 24 Hours for Phase I, Experiment 7

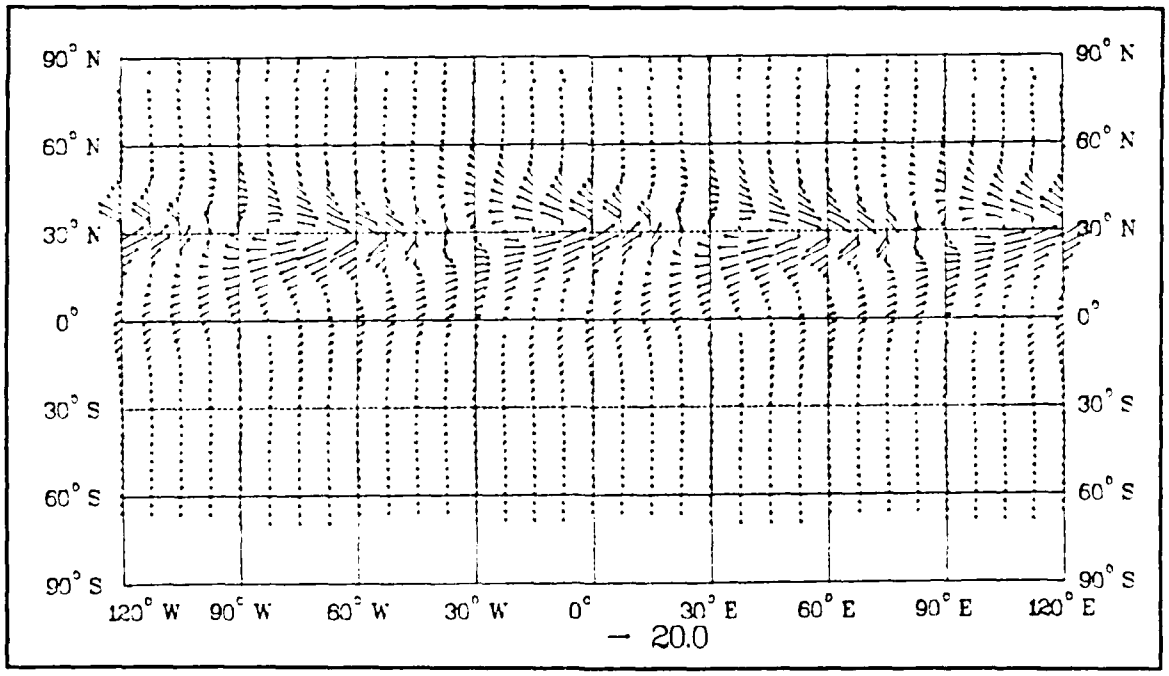

Figure 6.42. Wind Vectors at 48 Hours for Phase I, Experiment 7

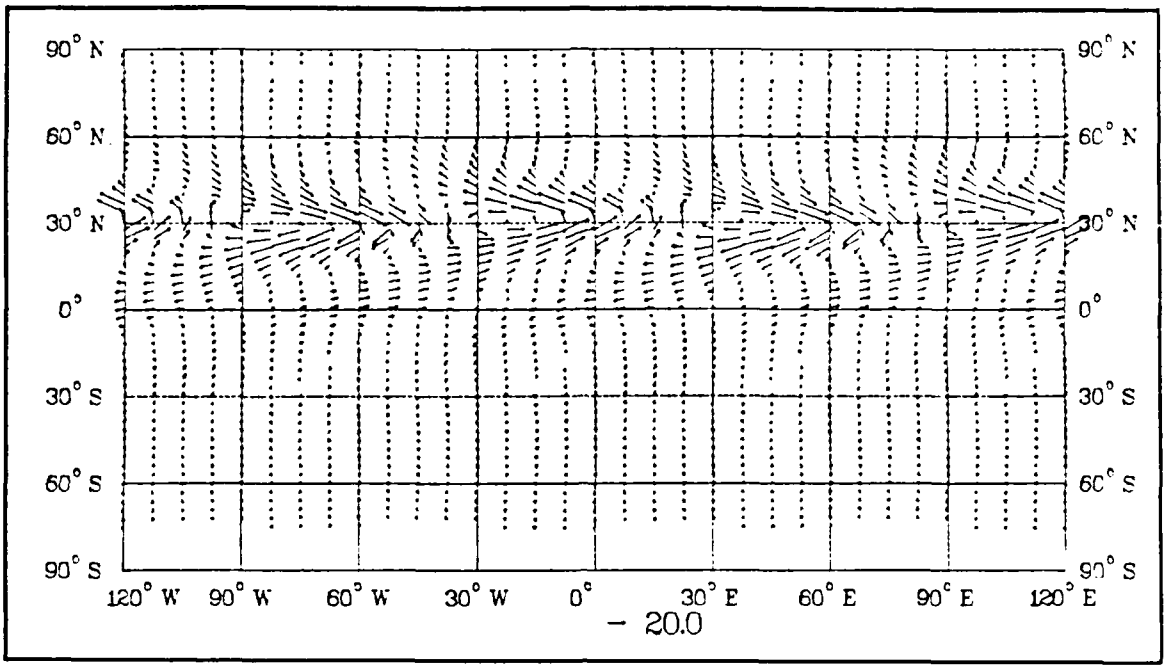

Figure 6.43. Wind Vectors at 72 Hours for Phase I, Experiment 7

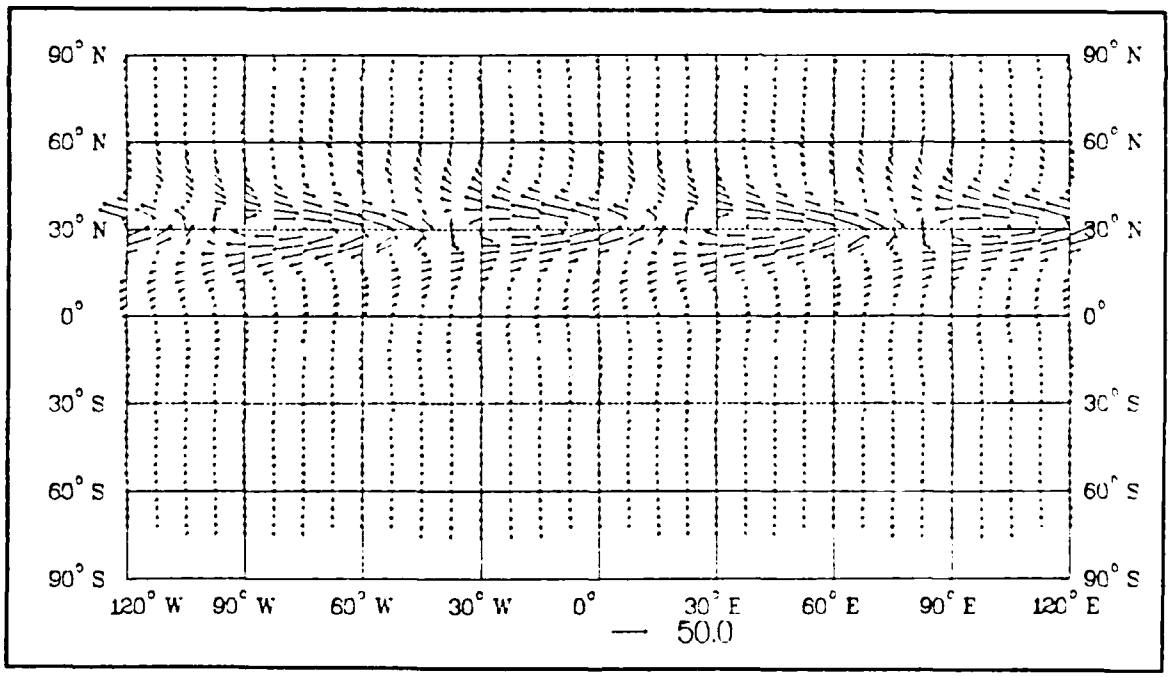

Figure 6.44. Wind Vectors at 96 Hours for Phase I, Experiment 7

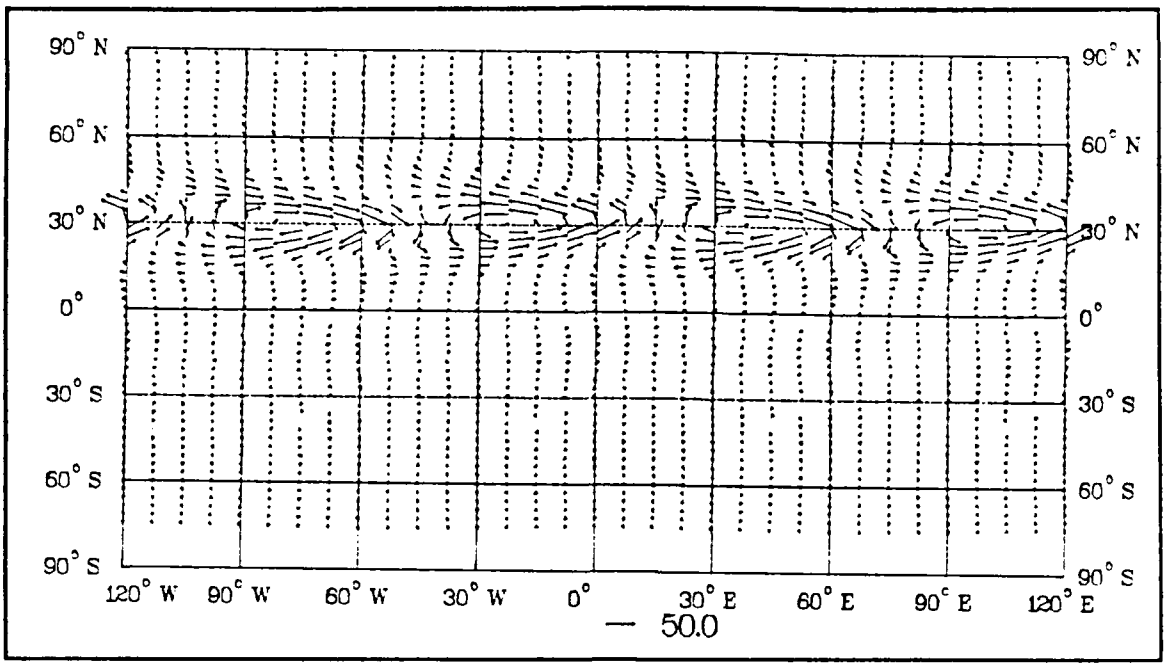

Figure 6.45. Wind Vectors at 120 Hours for Phase I, Experiment 7

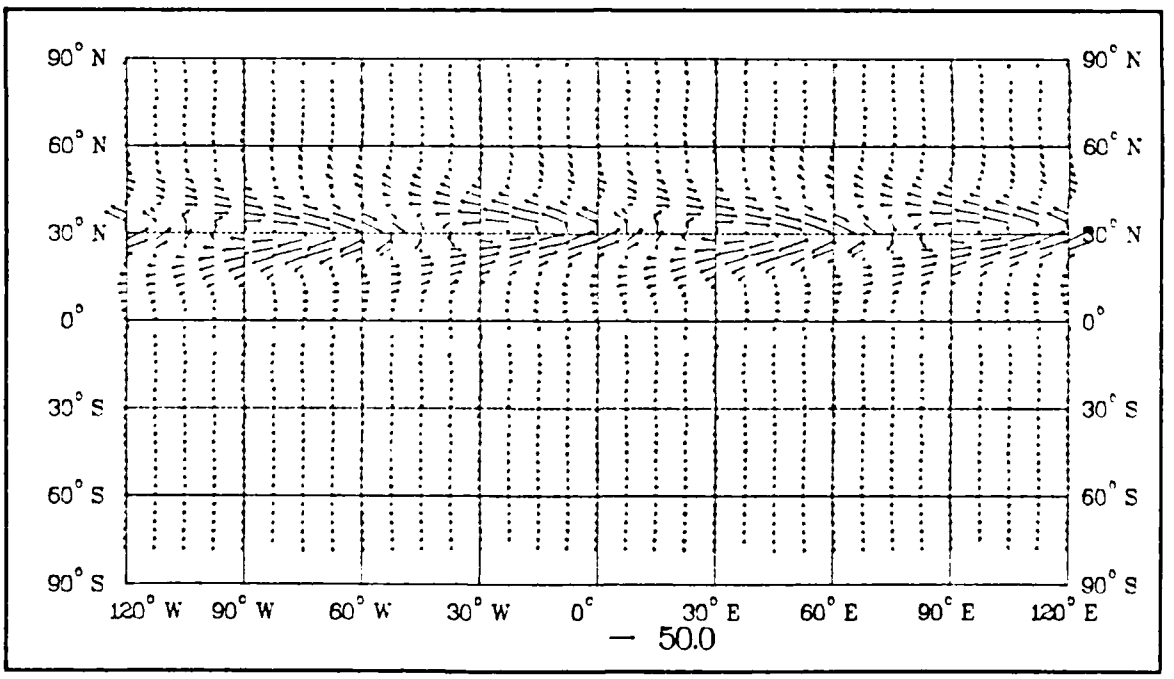

Figure 6.46. Wind Vectors at 144 Hours for Phase I, Experiment 7

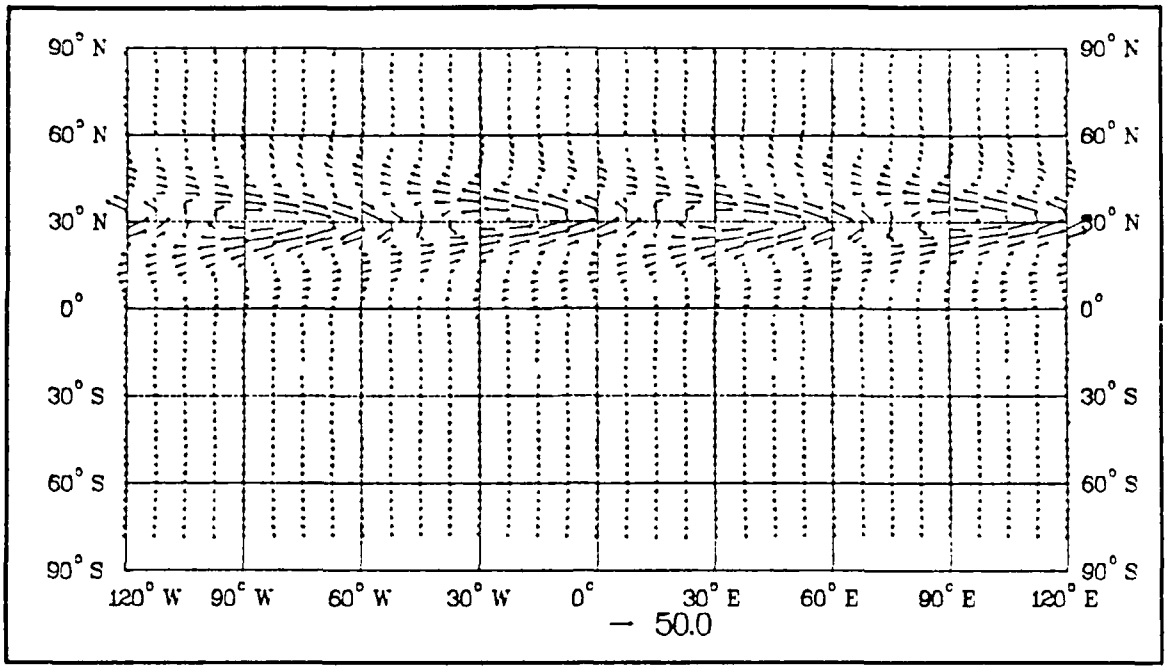

Figure 6.47. Wind Vectors at 168 Hours for Phase I, Experiment 7

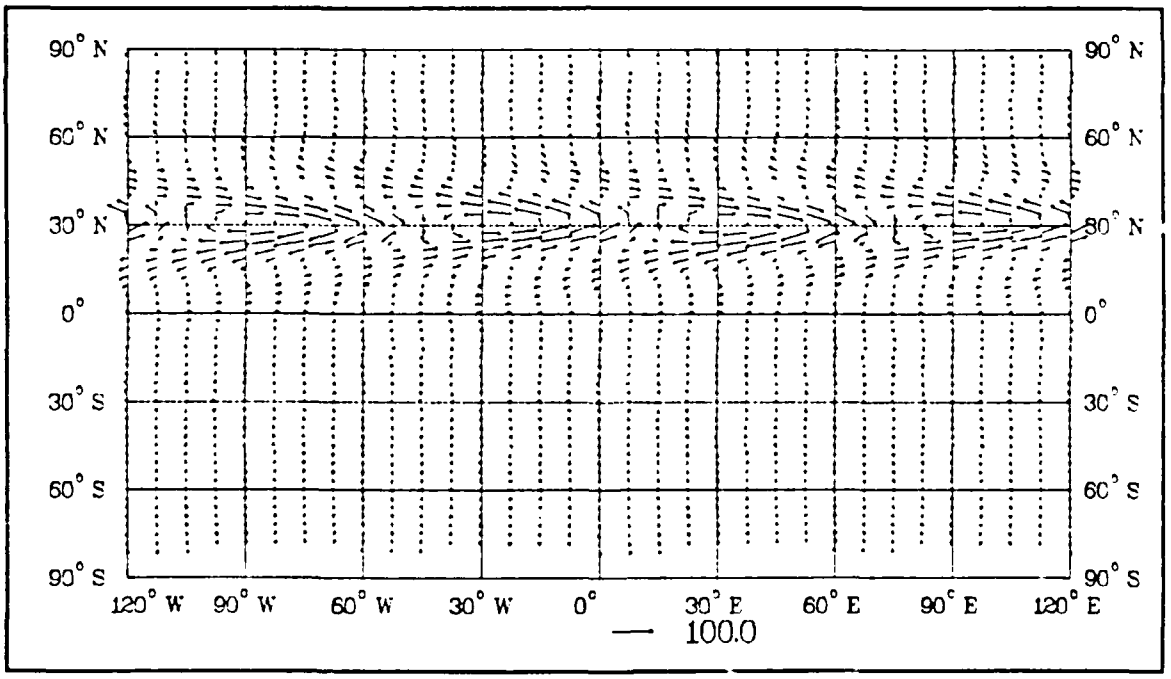

Figure 6.48. Wind Vectors at 192 Hours for Phase I, Experiment 7

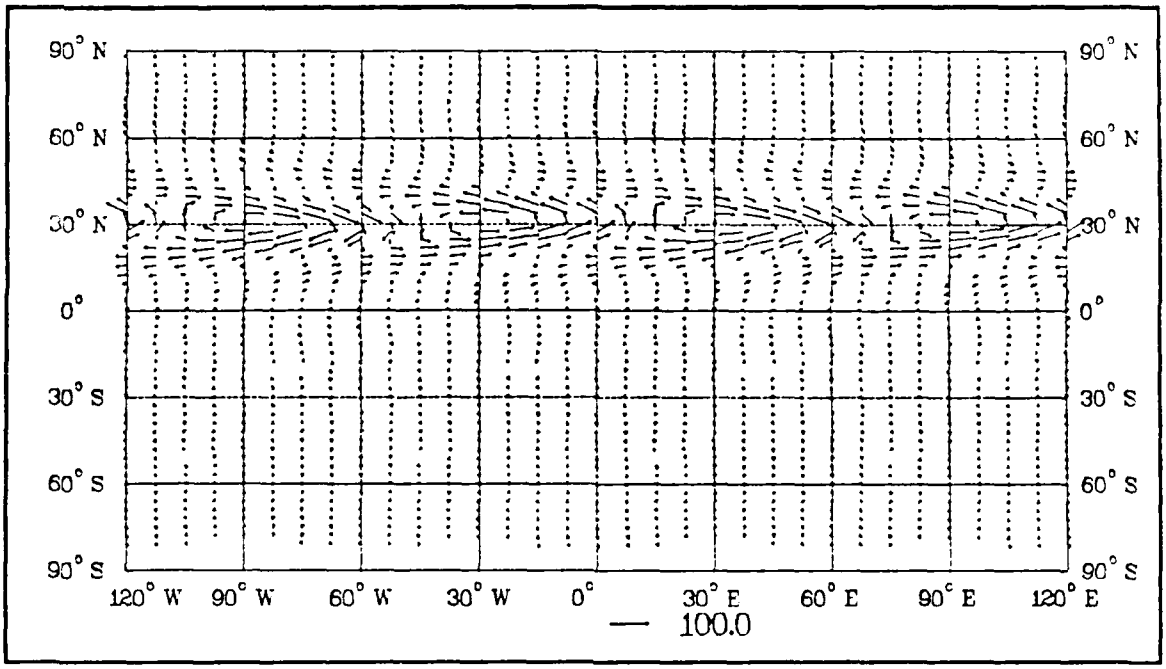

Figure 6.49. Wind Vectors at 216 Hours for Phase I, Experiment 7

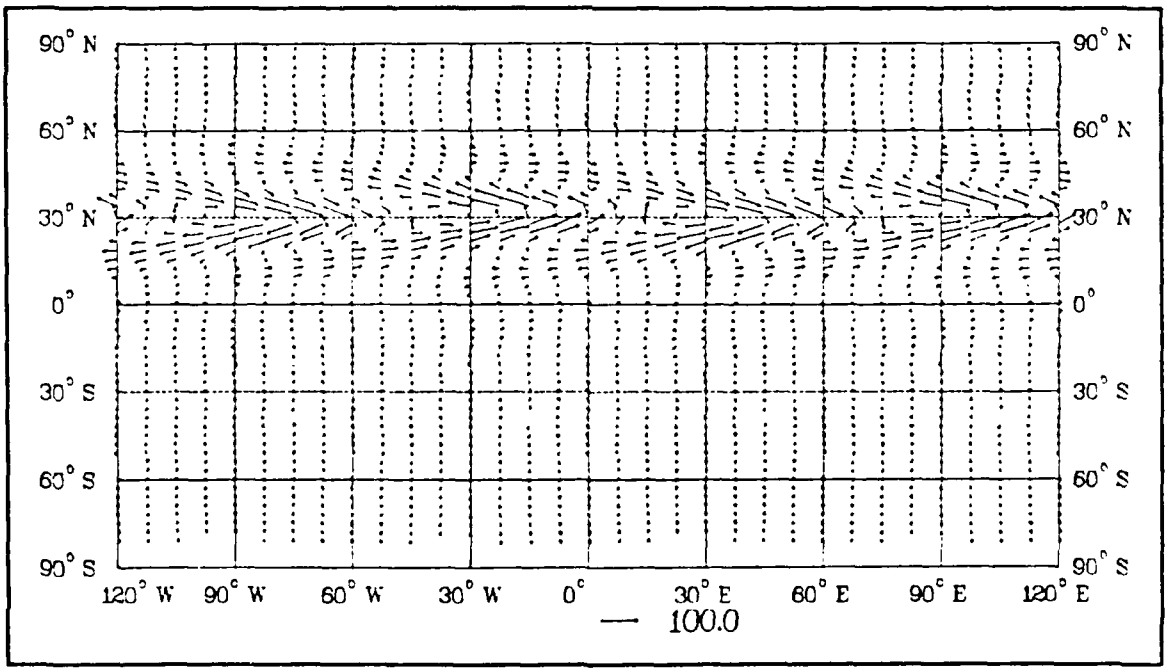

Figure 6.50. Wind Vectors at 240 Hours for Phase I, Experiment 7

The overall magnitude of the wind vectors is approximately the same as in Experiment 6, but the circulation pattern has more of a northeast-southwest tilt. The frequency (ω) of this forcing function is $-3.05 \times 10^{-7}\ s^{-1}$ and the period is 238.6 days. The westward movement of the circulation pattern is much slower than in Experiment 6, due to the longer period. The modal analysis is consistent with the analyses of Experiments 4 through 6.

8. Phase I Summary

The results of Phase I indicate that forced Rossby wave forcings applied to the thermal equation do not produce significant Rossby-type cold surge responses. However, when the same forcings are applied to the vorticity equation, the responses are consistent with Rossby-beta-plane theory. Forcing the thermal equation consistently produces a stronger response in the baroclinic mode, and forcing the vorticity equation produces a stronger barotropic response. When the sign of the frequency (ω) is changed, the solution does propagate southward. The southward propagating solution is not consistent with Rossby wave theory. The propagating waves in this case could be gravity waves since the overall magnitude of the velocity vectors is small.

C. PHASE II RESULTS

The forcing functions of Phase II use the impulse function described in Chapter V. The maximum amplitude of the forcing is at 24 hours and $\sigma = .375$. In each experiment the forcing is applied between 24° N and 36° N, and the model is again integrated forward in time for 240 hours. The maximum amplitude of the forcing occurs at 24 hours (as shown in Fig. 4.3). The two experiments of Phase II are summarized in Table 6.5. Experiments 8 and 9 will compare the effects of the impulse forcing in either the thermal or vorticity equations.

TABLE 6.5. PHASE II EXPERIMENTS

Experiment	Thermal Forcing	Vorticity Forcing
8	X	
9		X

1. Experiment 8

In this experiment the impulse source is only added to the thermal equation (Eq. 3.4). The wind velocity vector fields for the lowest level (σ = .938) are displayed in Figs. 6.51 through 6.60. After 24 hours a wavenumber three circulation develops near the source latitudes. The overall magnitude of the velocity vectors is relatively small and the circulation does not propagate very far south. At 48 hours the magnitude increases and the circulation pattern moves toward the west, but the circulation is still confined to the source latitudes. By 144 hours there is a slight northeasterly flow toward the equator. The magnitude of the northeasterly flow does not significantly increase after 240 hours.

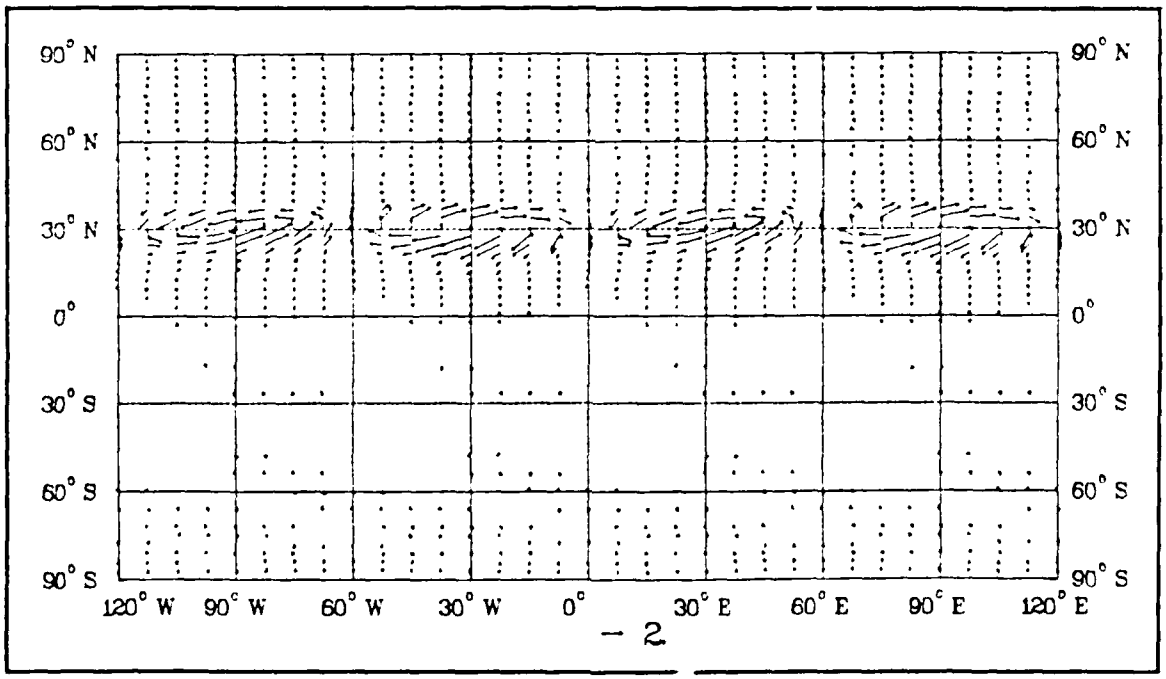

Figure 6.51. Wind Vectors at 24 Hour for Phase II, Experiment 8

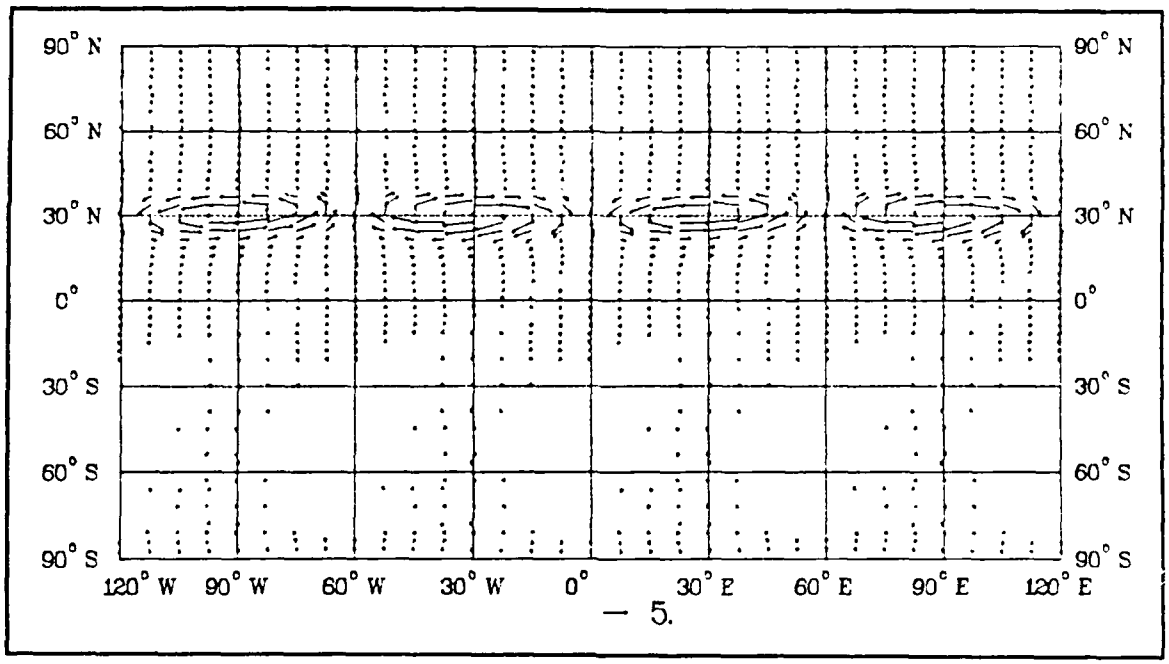

Figure 6.52. Wind Vectors at 48 Hours for Phase II, Experiment 8

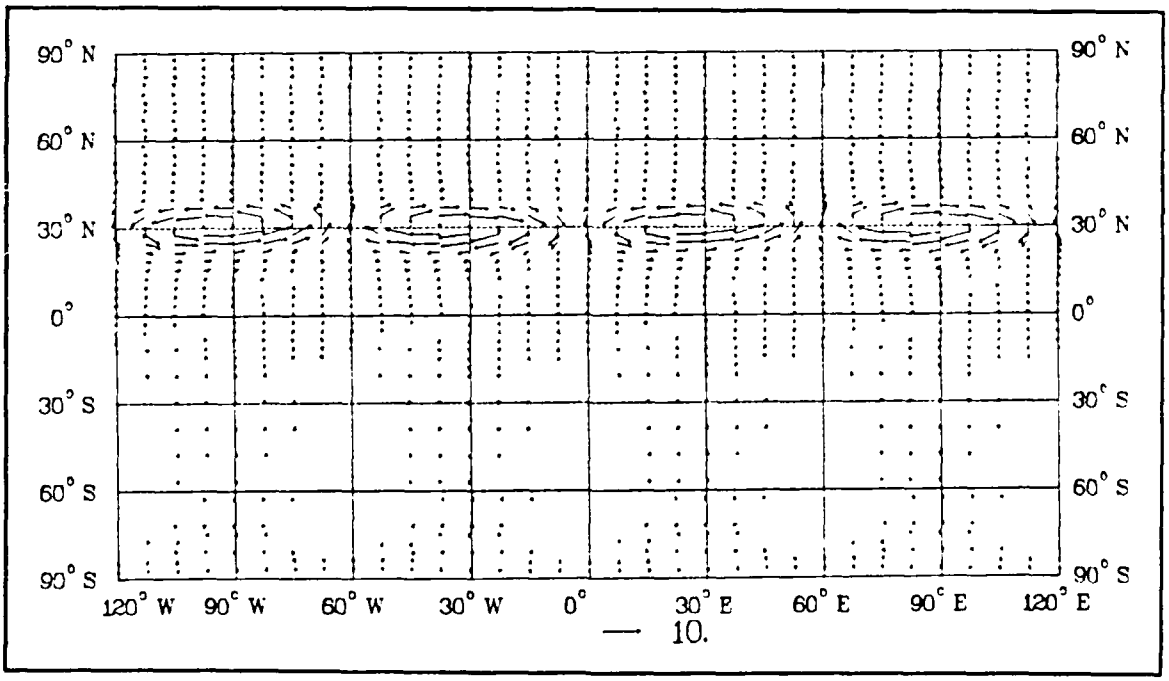

Figure 6.53. Wind Vectors at 72 Hours for Phase II, Experiment 8

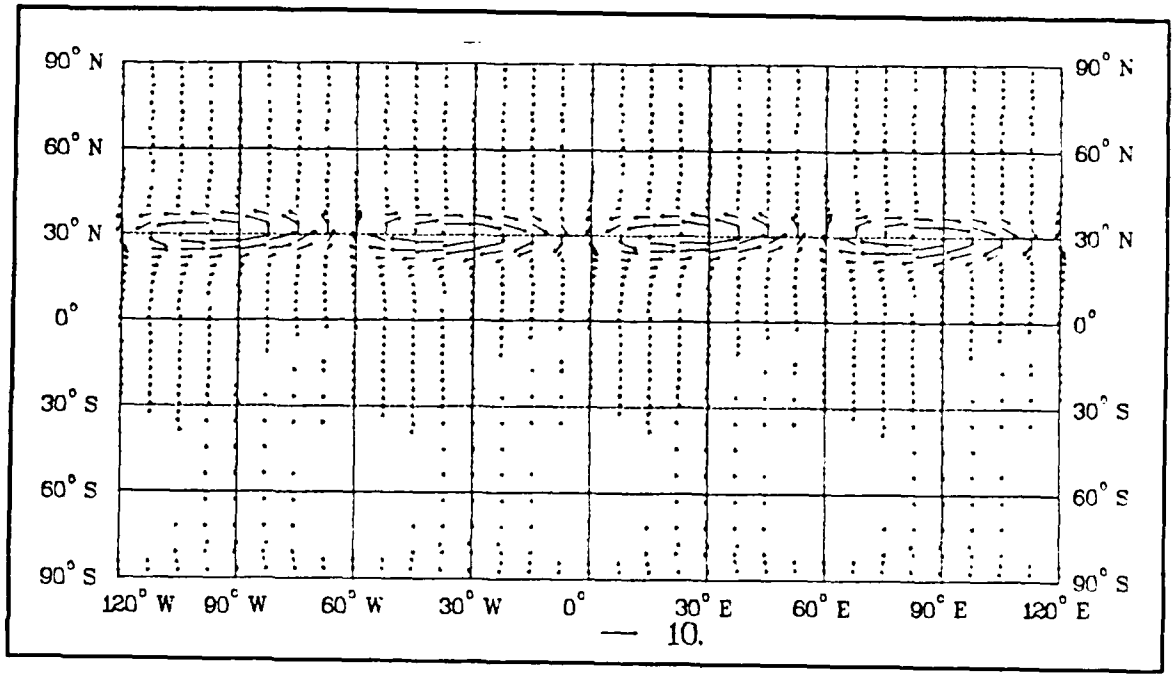

Figure 6.54. Wind Vectors at 96 Hours for Phase II, Experiment 8

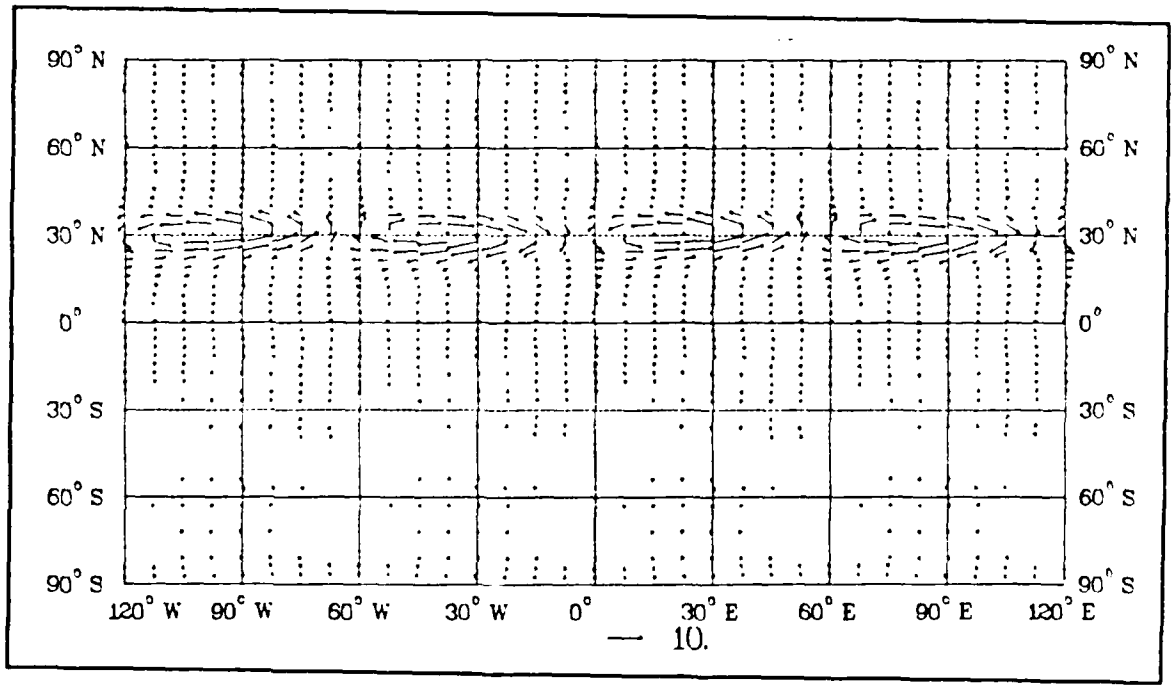

Figure 6.55. Wind Vectors at 120 Hours for Phase II, Experiment 8

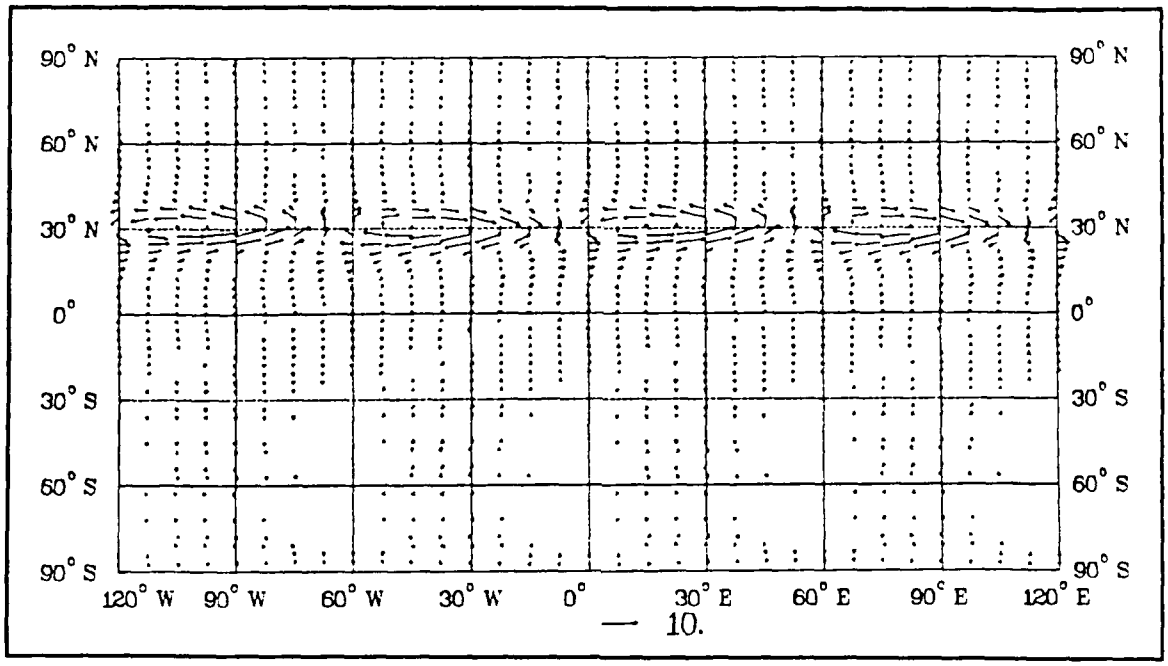

Figure 6.56. Wind Vectors at 144 Hours for Phase II, Experiment 8

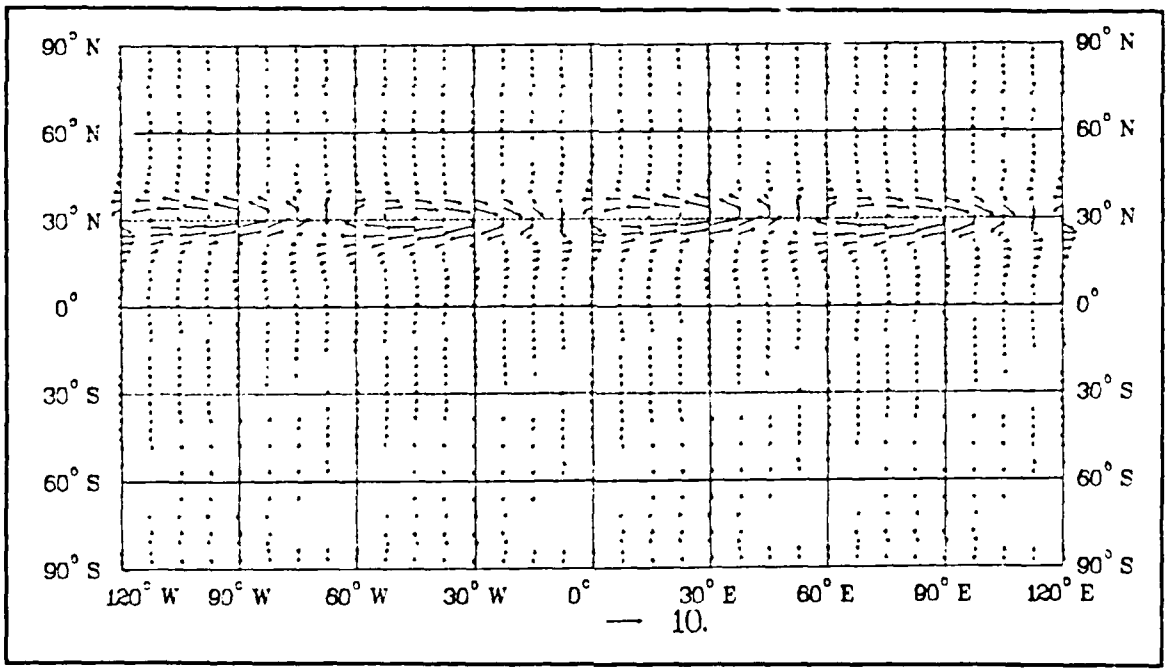

Figure 6.57. Wind Vectors at 168 Hours for Phase II, Experiment 8

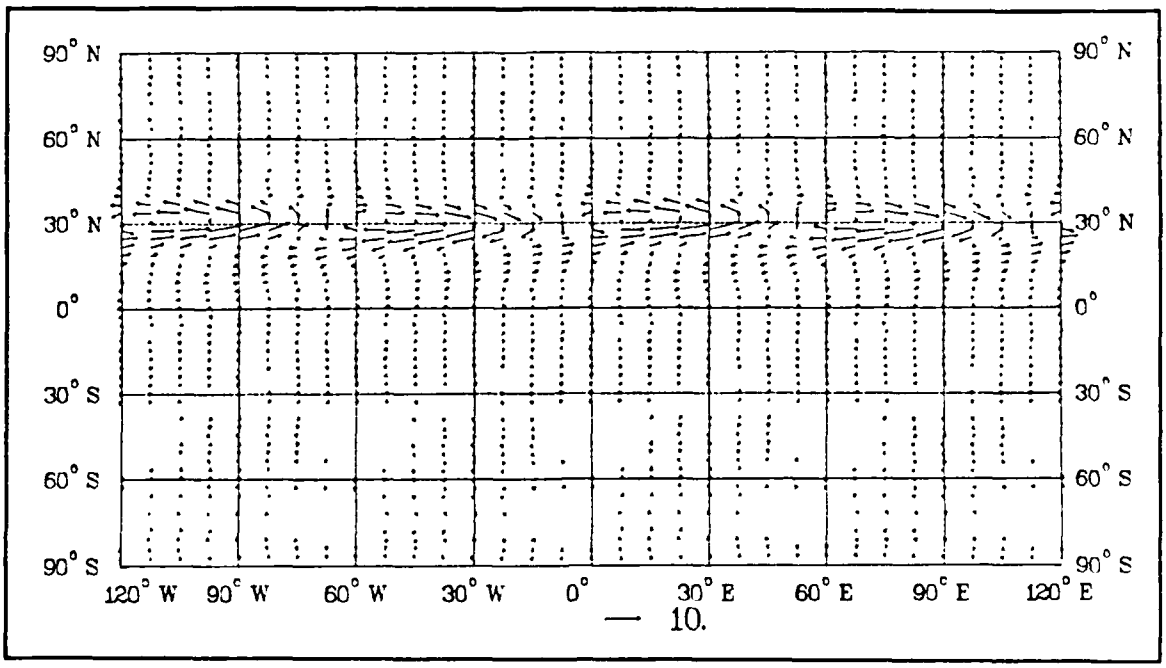

Figure 6.58. Wind Vectors at 192 Hours for Phase II, Experiment 8

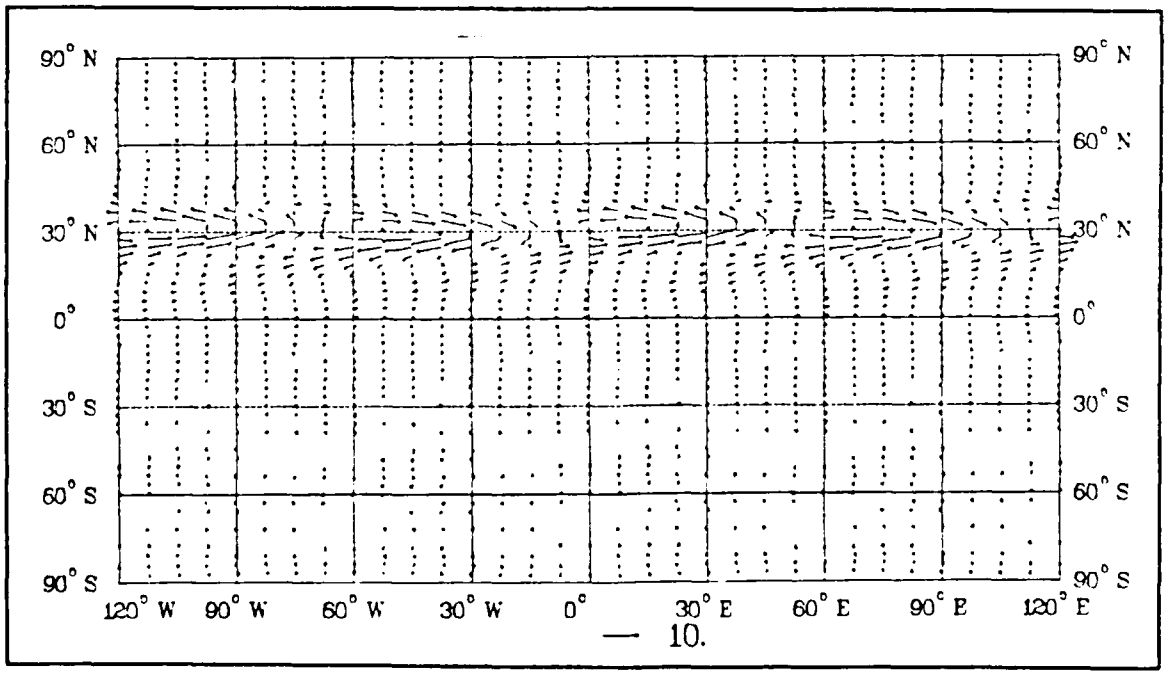

Figure 6.59. Wind Vectors at 216 Hours for Phase II, Experiment 8

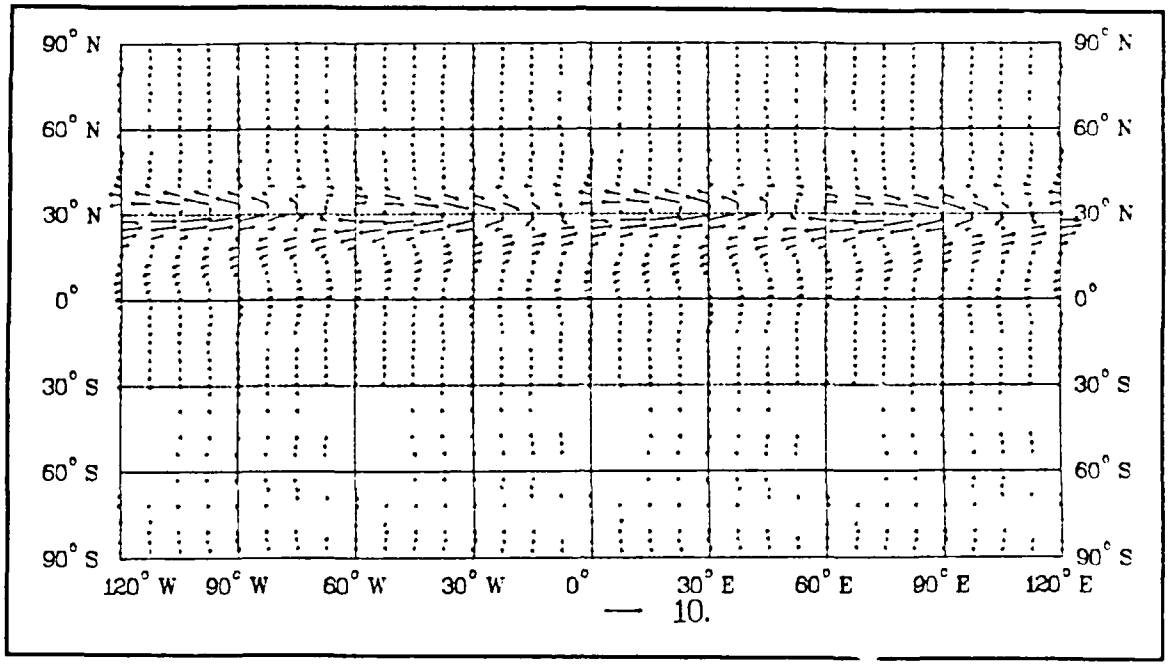

Figure 6.60. Wind Vectors at 240 Hours for Phase II, Experiment 8

The overall magnitude of the velocity vectors of the barotropic mode (not shown) is on the order of 0.5 $m \cdot s^{-1}$. The overall magnitude of the first baroclinic mode velocity vectors (not shown) is ten times greater. The larger baroclinic response is consistent with Phase I. The circulation patterns of the modal analyses are not significantly different than the total patterns shown in Figs. 6.51 through 6.60.

2. Experiment 9

In this experiment the impulse function is only added to the vorticity equation (Eq. 3.1). The wind velocity vector fields for the lowest level ($\sigma = .938$) are displayed in Figs. 6.61 through 6.70. After 24 hours a wavenumber three circulation develops and significant circulation patterns propagate toward the equator. By 48 hours the magnitude doubles and the northeasterly flow intensifies. By 72 hours there is significant flow past the equator. A definite northeast-

southwest tilt in the circulation pattern is evident at 96 hours. This tilt is much more pronounced than in Experiment 8. By 192 hours there are closed circulation cells in the tropics. It is interesting to note that the circulation patterns of this experiment also propagate north of the forcing region.

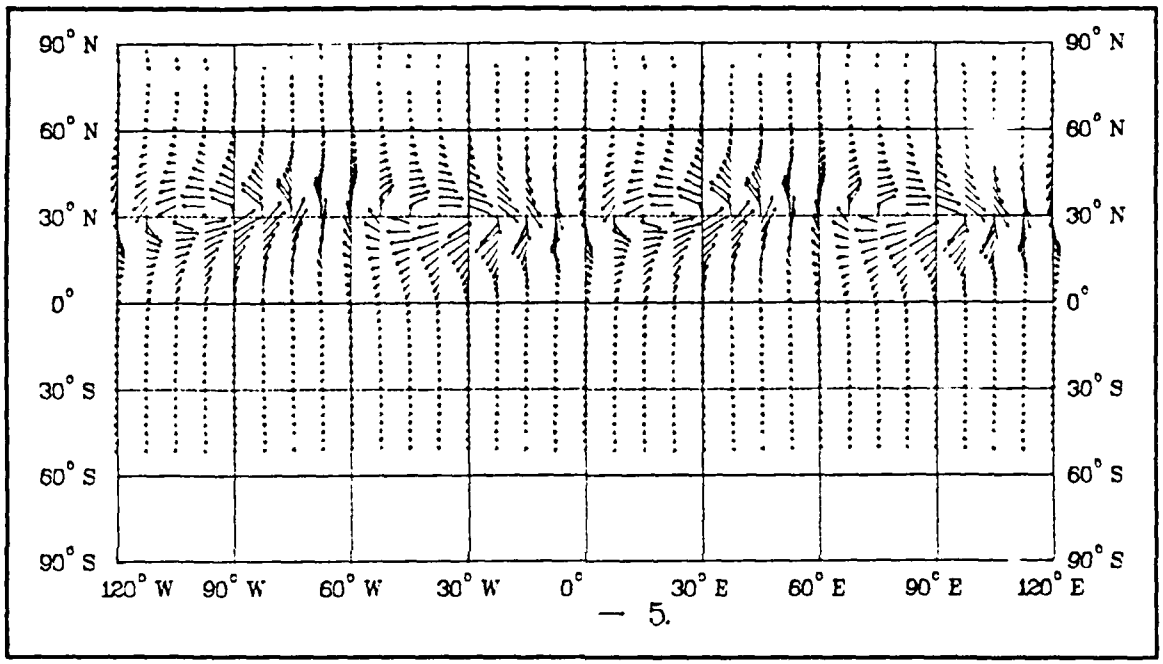

Figure 6.61. Wind Vectors at 24 Hours for Phase II, Experiment 9

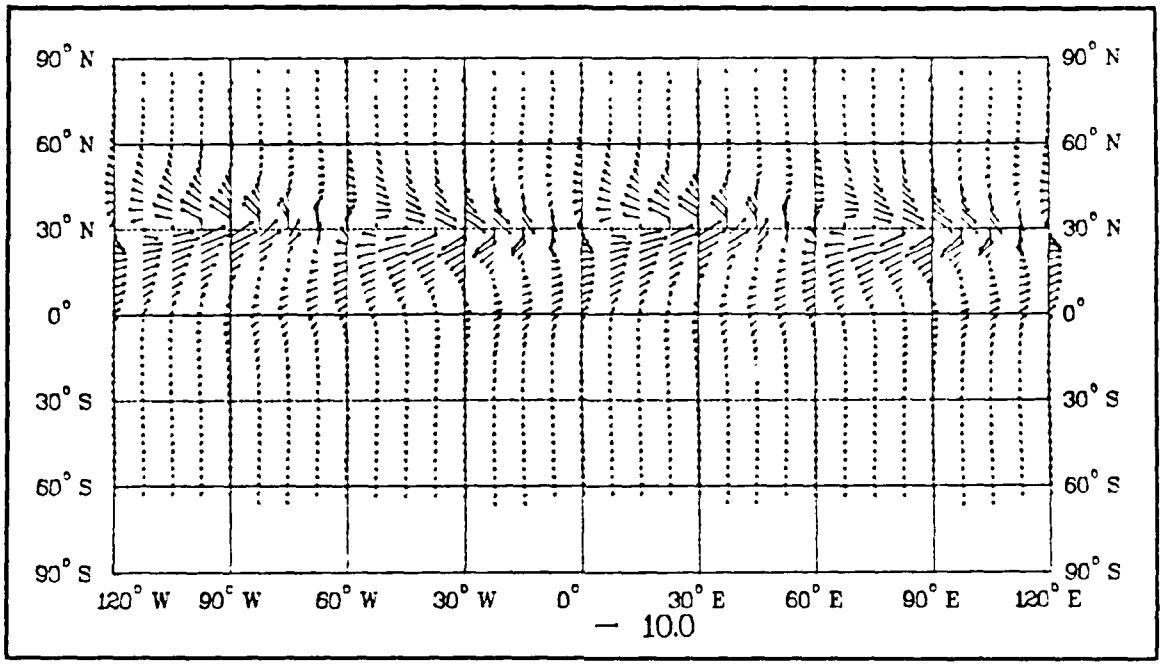

Figure 6.62. Wind Vectors at 48 Hours for Phase II, Experiment 9

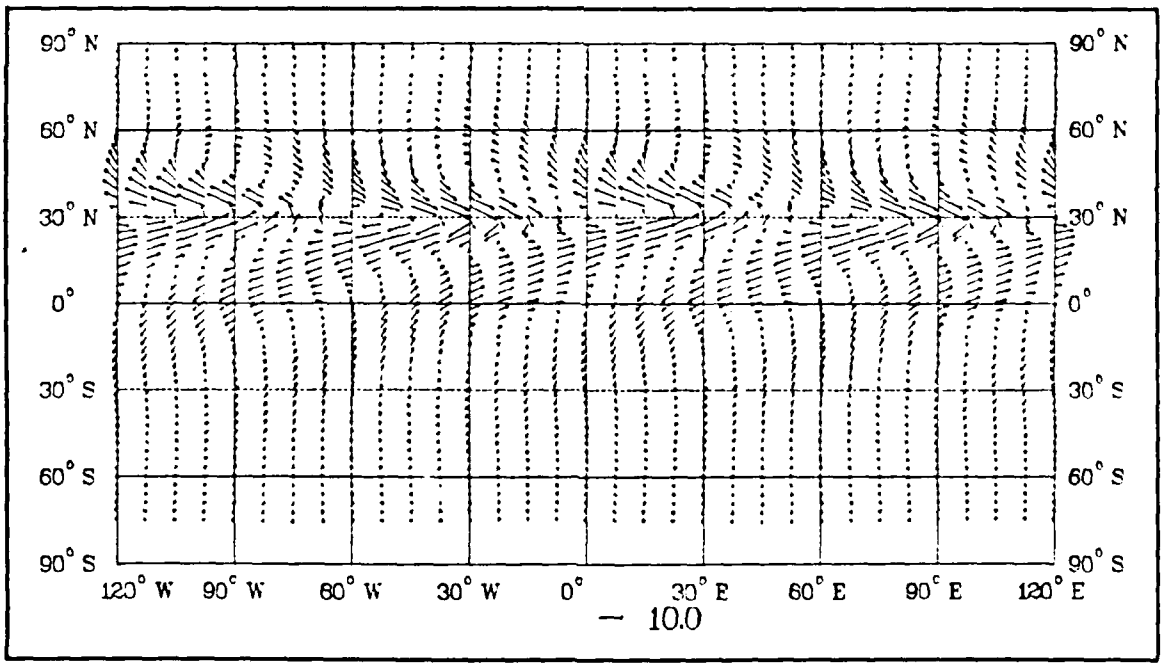

Figure 6.63. Wind Vectors at 72 Hours for Phase II, Experiment 9

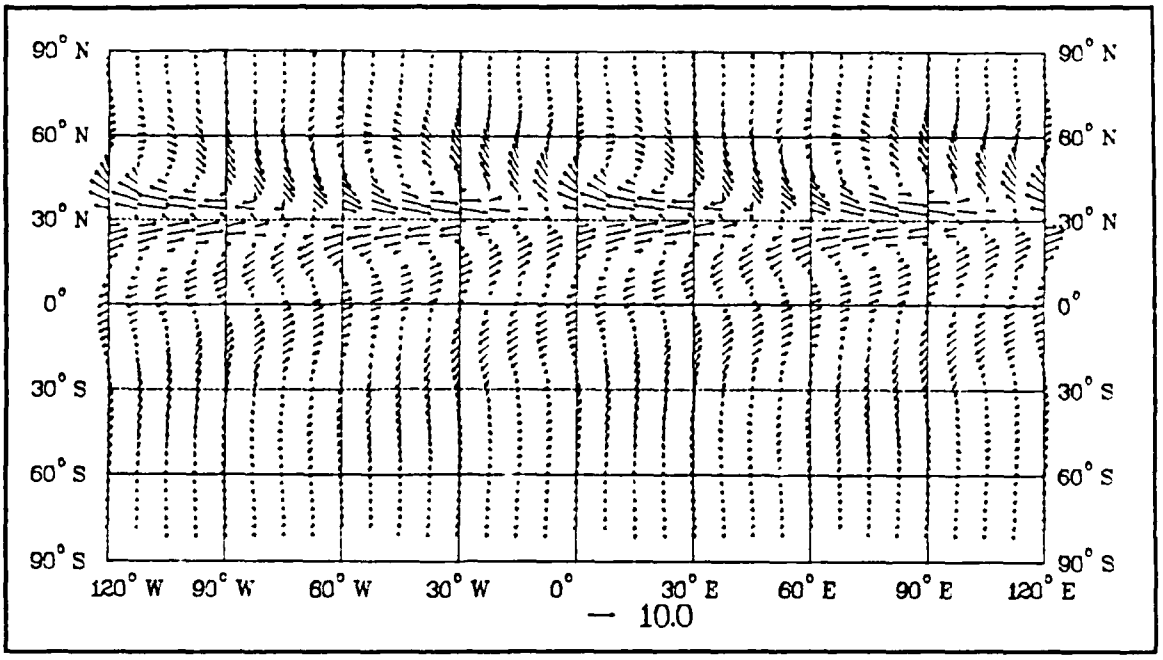

Figure 6.64. Wind Vectors at 96 Hours for Phase II, Experiment 9

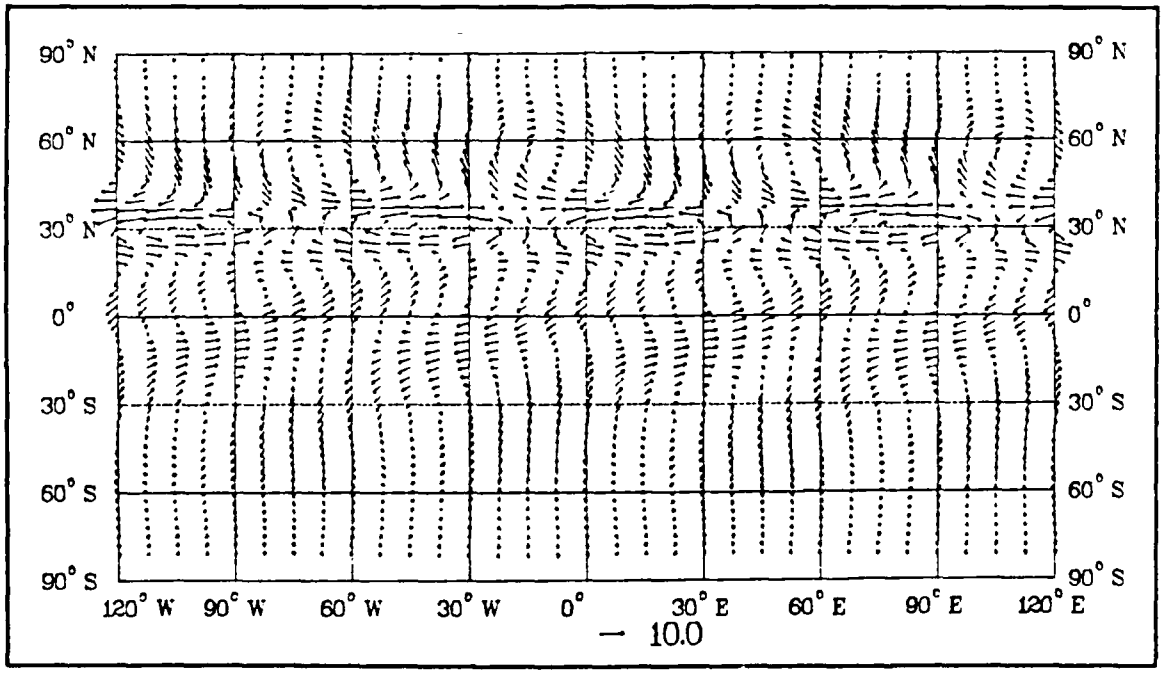

Figure 6.65. Wind Vectors at 120 Hours for Phase II, Experiment 9

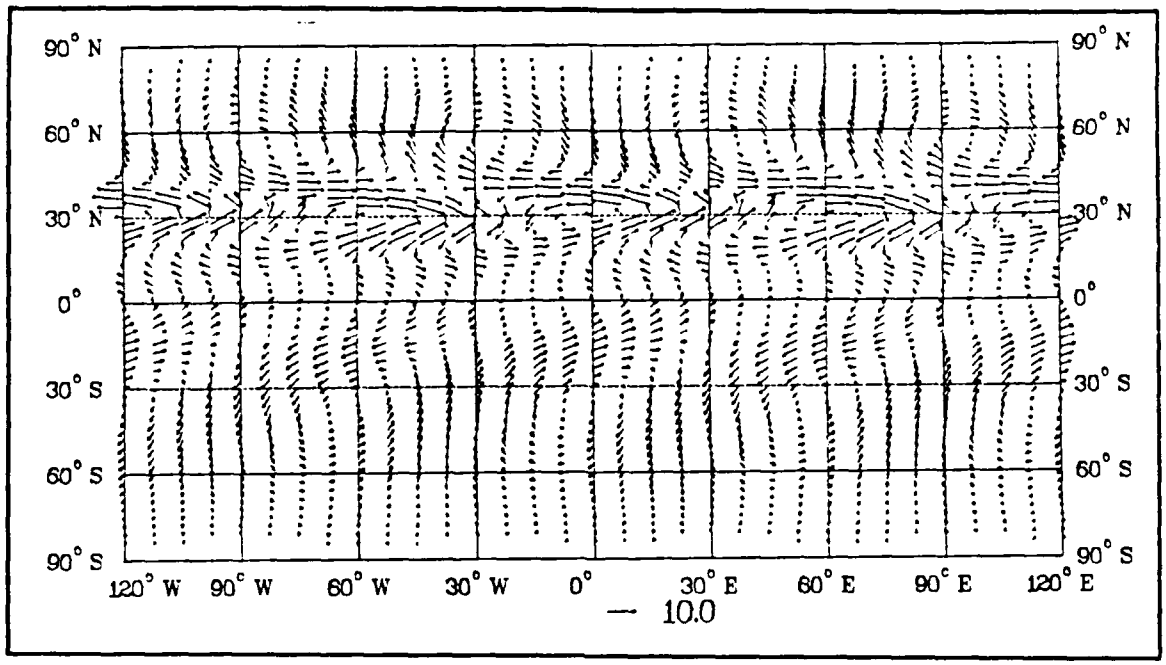

Figure 6.66. Wind Vectors at 144 Hours for Phase II, Experiment 9

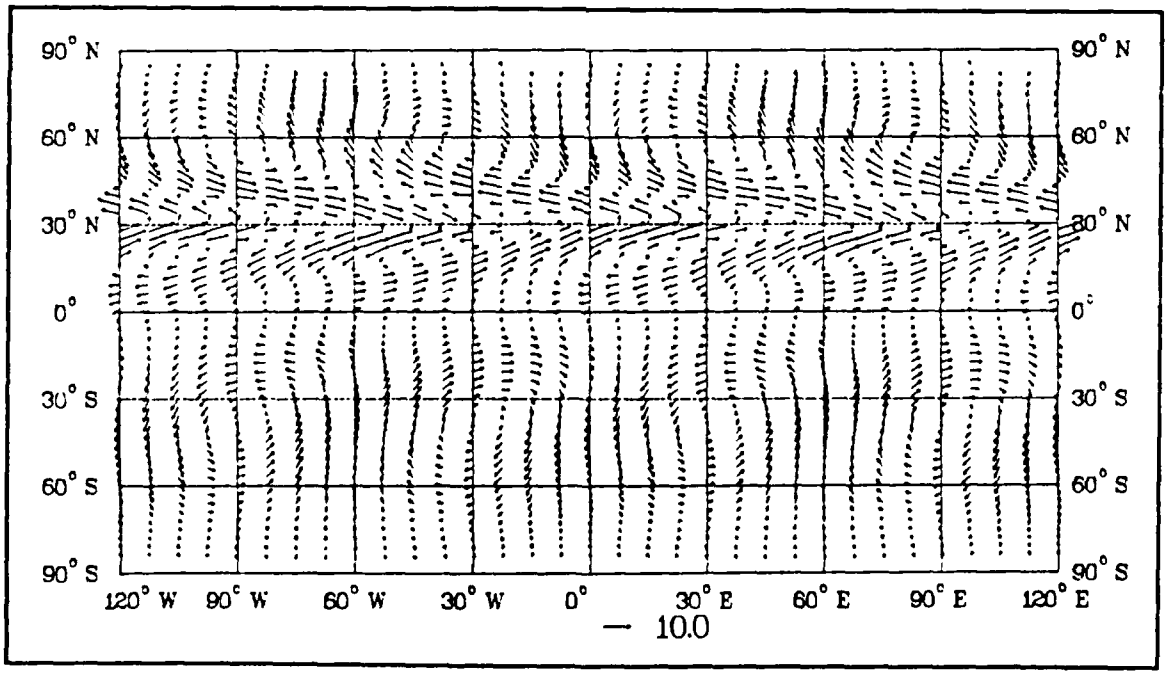

Figure 6.67. Wind Vectors at 168 Hours for Phase II, Experiment 9

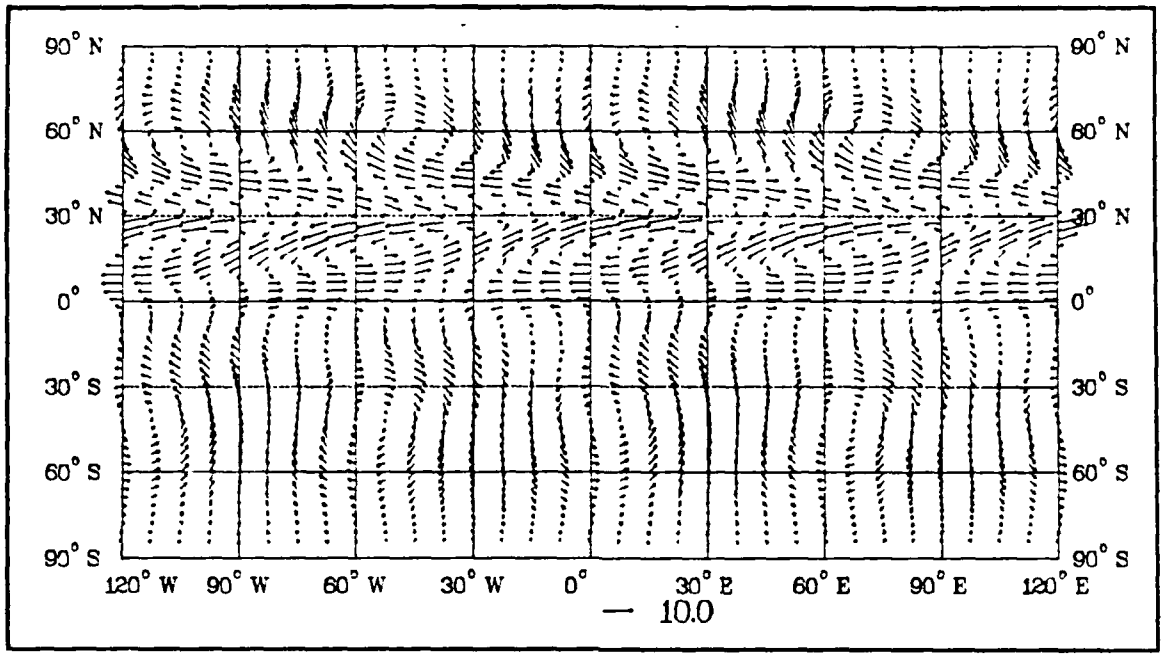

Figure 6.68. Wind Vectors at 192 Hours for Phase II, Experiment 9

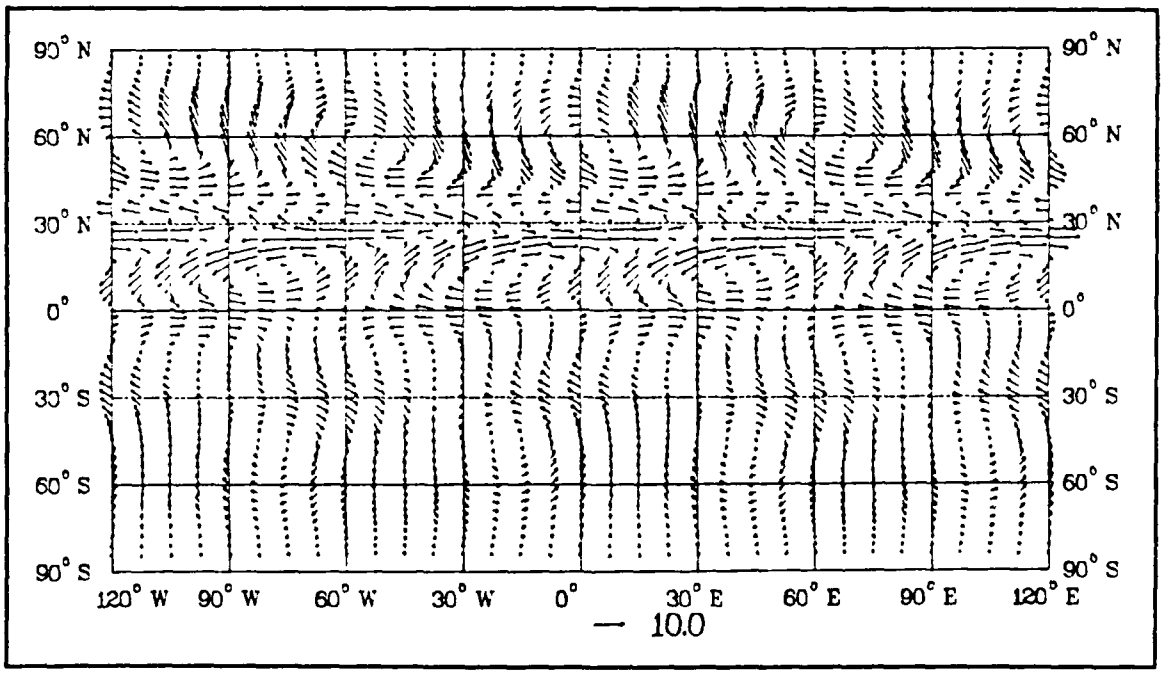

Figure 6.69. Wind Vectors at 216 Hours for Phase II, Experiment 9

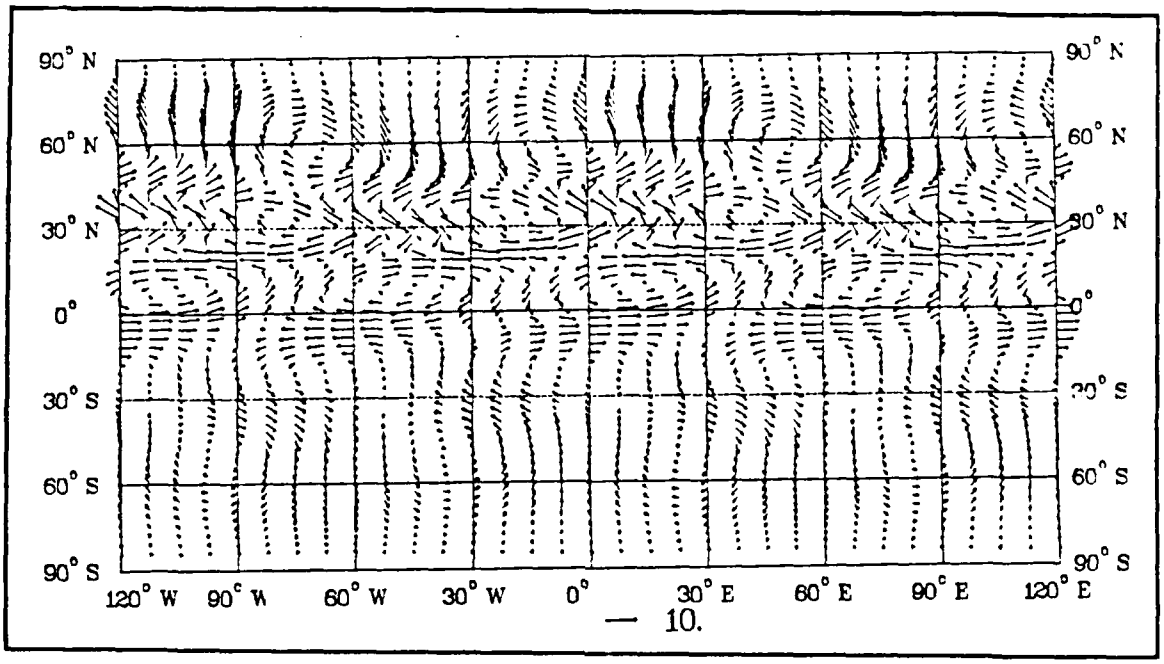

Figure 6.70. Wind Vectors at 240 Hours for Phase II, Experiment 9

The velocity vector patterns of the first and second modes are similar to the complete vector patterns. The overall magnitude of the barotropic mode vectors is ten times greater than the baroclinic mode vectors at 24 hours. The larger response of the barotropic mode is consistent with the results of Phase I.

3. Phase II Summary

The results of Phase II indicate that the thermal impulse forcing is not an efficient method of producing a cold surge response. After 240 hours a small but significant northeasterly flow develops, and circulation patterns are evident near the equator; however, ten days is too slow to be realistic. The impulse forcing applied to the vorticity equation does produce a significant, timely response. The northeast-southwest tilt in the circulation patterns is similar to Bashford (1985) and Lim and Chang (1981). The results are consistent with Phase I, in that the vorticity

forcing is more efficient in exciting a barotropic response, and the thermal forcing a baroclinic response.

D. PHASE III RESULTS

The forcing functions of Phase III use the generic cyclone described in Chapter V. In each experiment the baroclinic zone is applied between 30° N and 60° N. This latitudinal range is representative of a synoptic wave moving through the planetary wave over East Asia. The latitudinal structure of both the thermal and vorticity forcing functions are shown in Fig. 6.71. The magnitude of each forcing equals zero in the Southern Hemisphere and outside the source region. The model is integrated forward in time for 240 hours. The maximum amplitude of the forcings occur at the 24-hour and 216-hour points (Fig. 6.72). In the vertical, the maximum amplitude of both thermal (Fig. 6.73) and vorticity forcings (Fig. 6.74) occur at the surface. The three experiments in Phase III will determine which forcing is dominant in the generation of cold surges. The experiments are summarized in Table 6.6.

TABLE 6.6. PHASE III EXPERIMENTS

Experiment	Thermal Forcing	Vorticity Forcing
10	X	X
11	X	
12		X

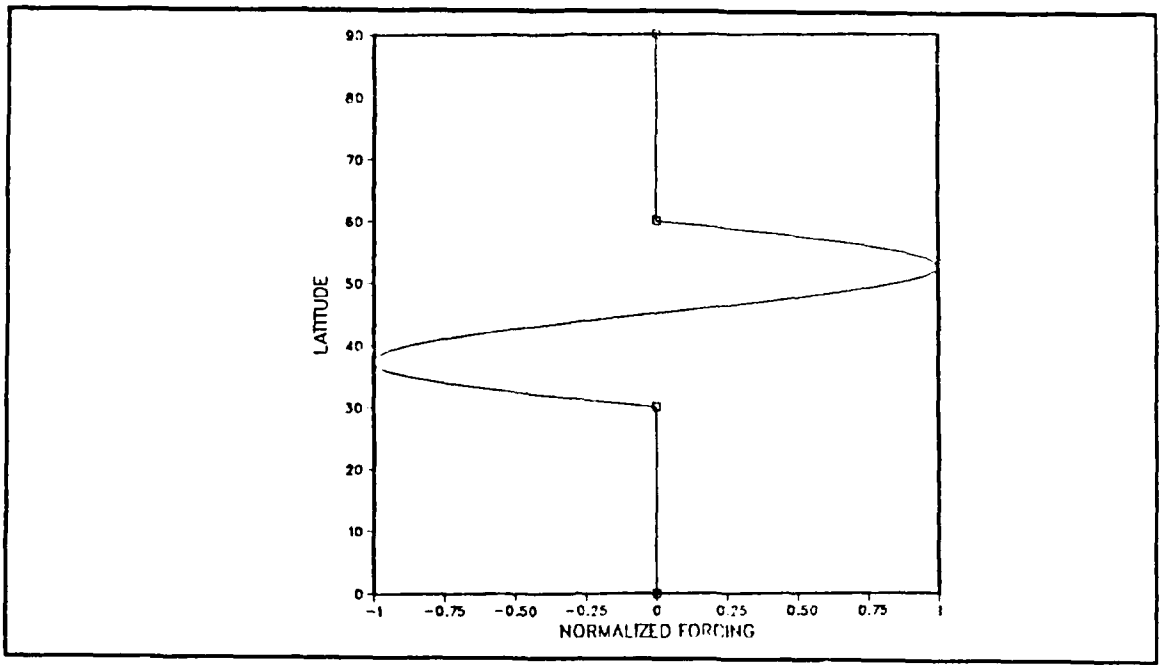

Figure 6.71. Latitudinal Structure of Phase III Forcings

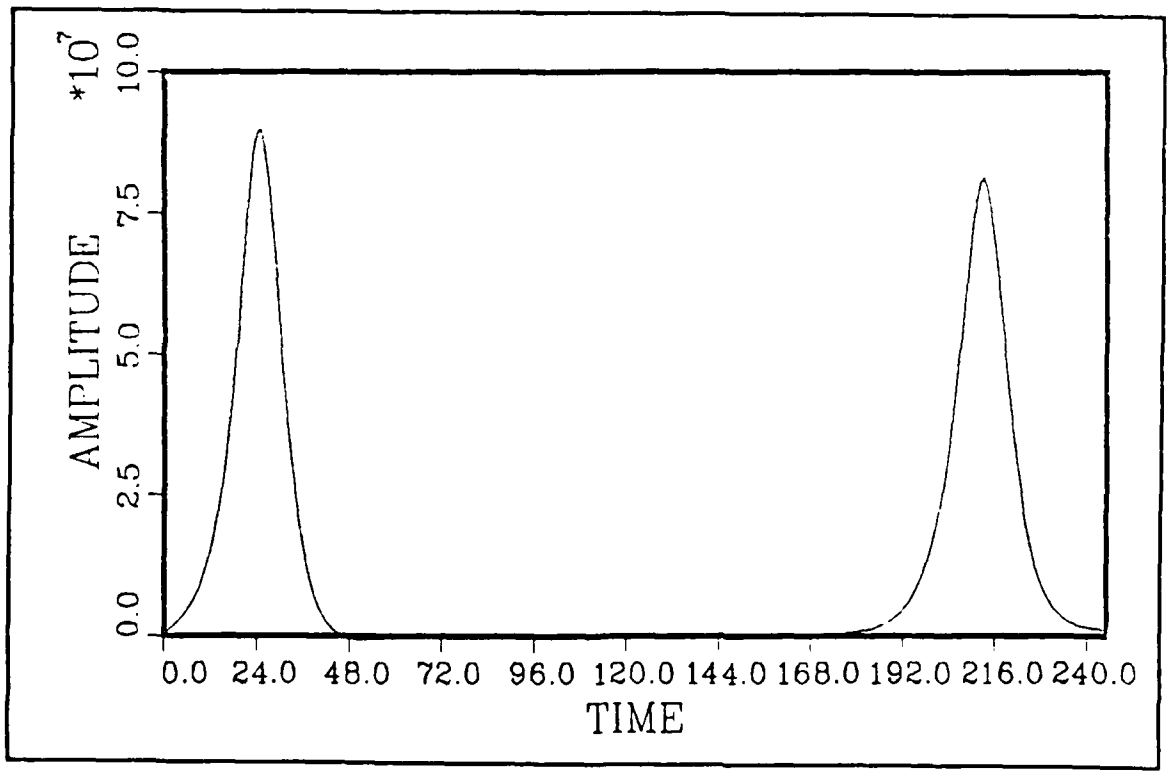

Figure 6.72. Temporal Structure of Phase III Forcings

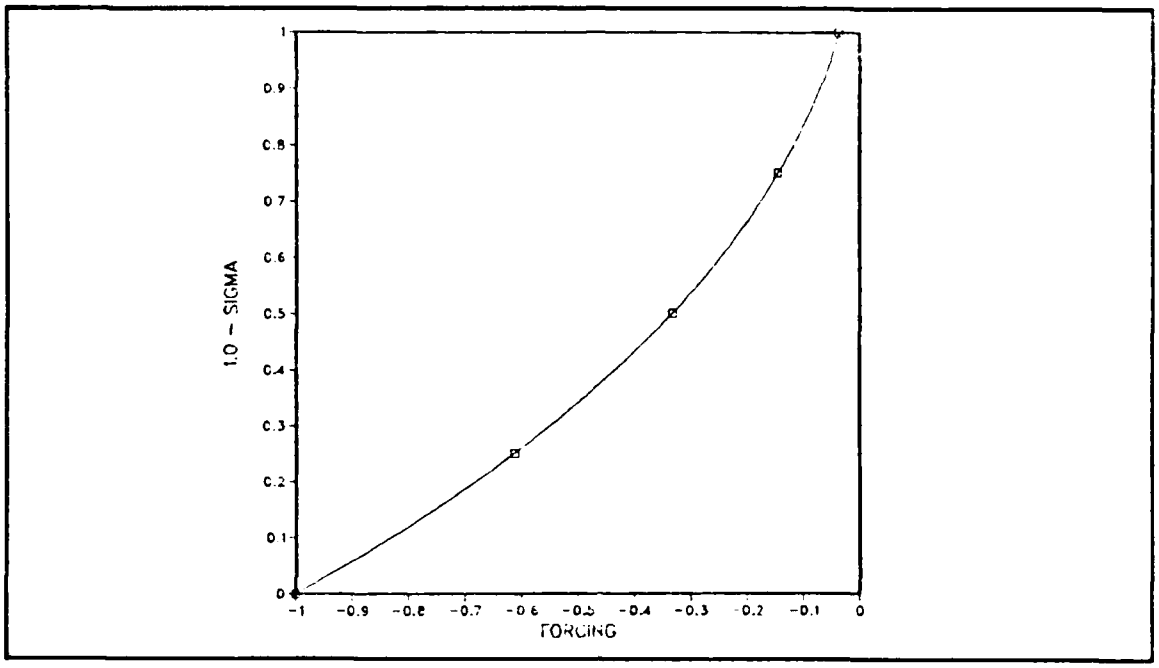

Figure 6.73. Normalized Vertical Structure of Thermal Forcing of Phase III

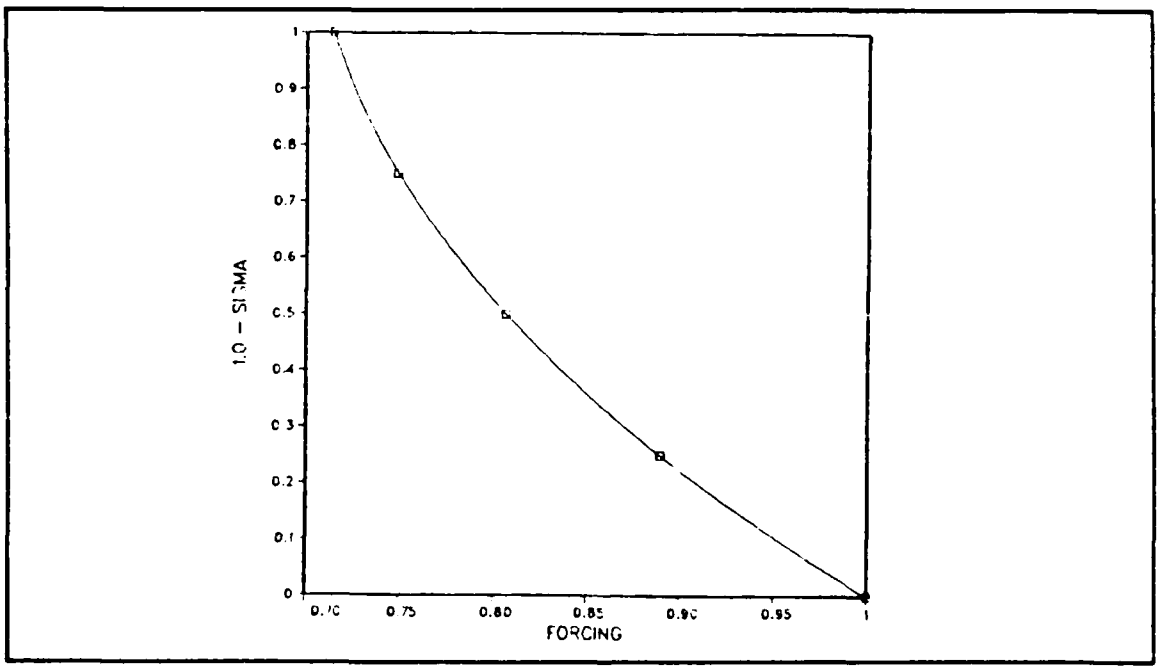

Figure 6.74. Normalized Vertical Structure of Vorticity Forcing of Phase III

1. Experiment 10

In this experiment the forcing is applied to both the thermal (Eq. 3.4) and vorticity (Eq. 3.1) equations. The wind velocity vector fields for the lowest level ($\sigma = .938$) are displayed in Figs. 6.75 through 6.84. After 24 hours a wavenumber three circulation develops near the source latitudes and there is some propagation toward the south. By 48 hours a five meters per second northeasterly wind, typical of an East Asian cold surge, is evident to approximately 10° N. After 72 hours the northeasterly flow extends past the equator into the Southern Hemisphere. The northeast-southwest tilt in the circulation south of the source latitudes, and northwest-southeast tilt north of the source is evident at this time. The tilted circulation pattern is characteristic of propagating Rossby waves. The propagating wave continues in this manner, and at 240 hours there is identifiable circulation at 30° S.

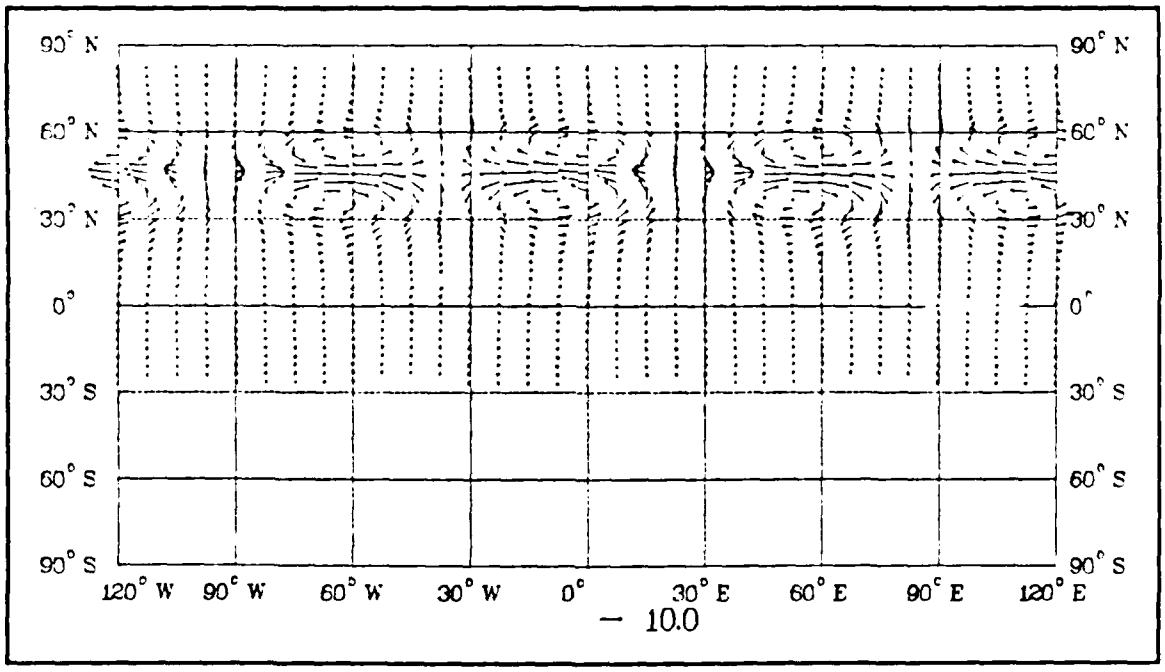

Figure 6.75. Wind Vectors at 24 Hours for Phase III, Experiment 10

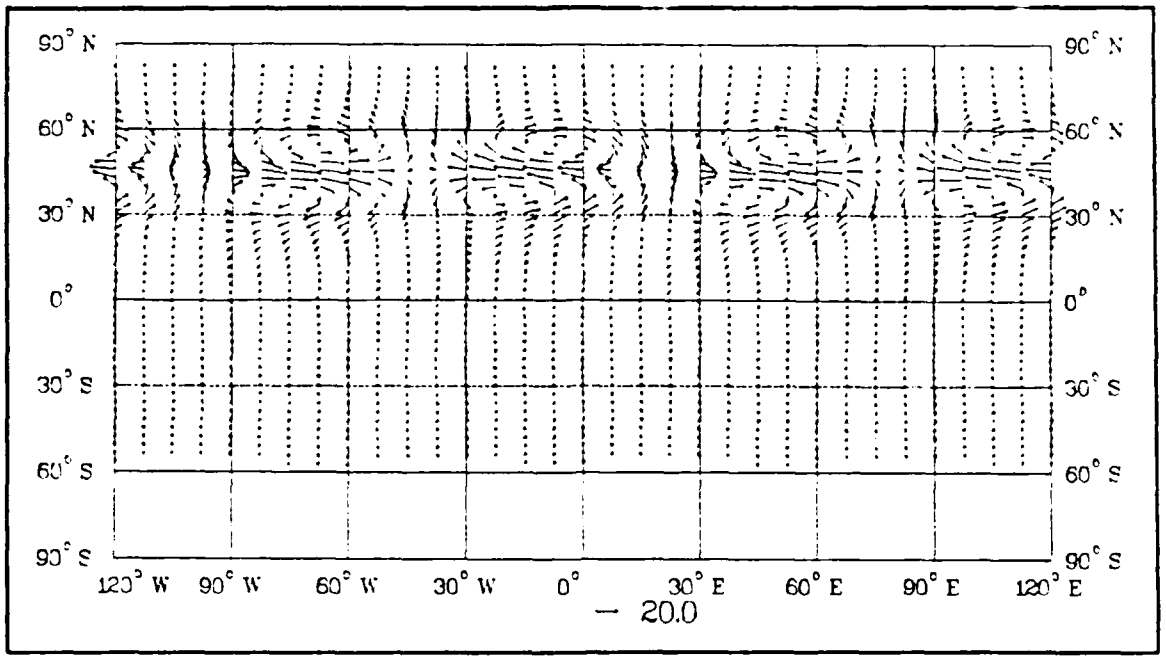

Figure 6.76. Wind Vectors at 48 Hours for Phase III, Experiment 10

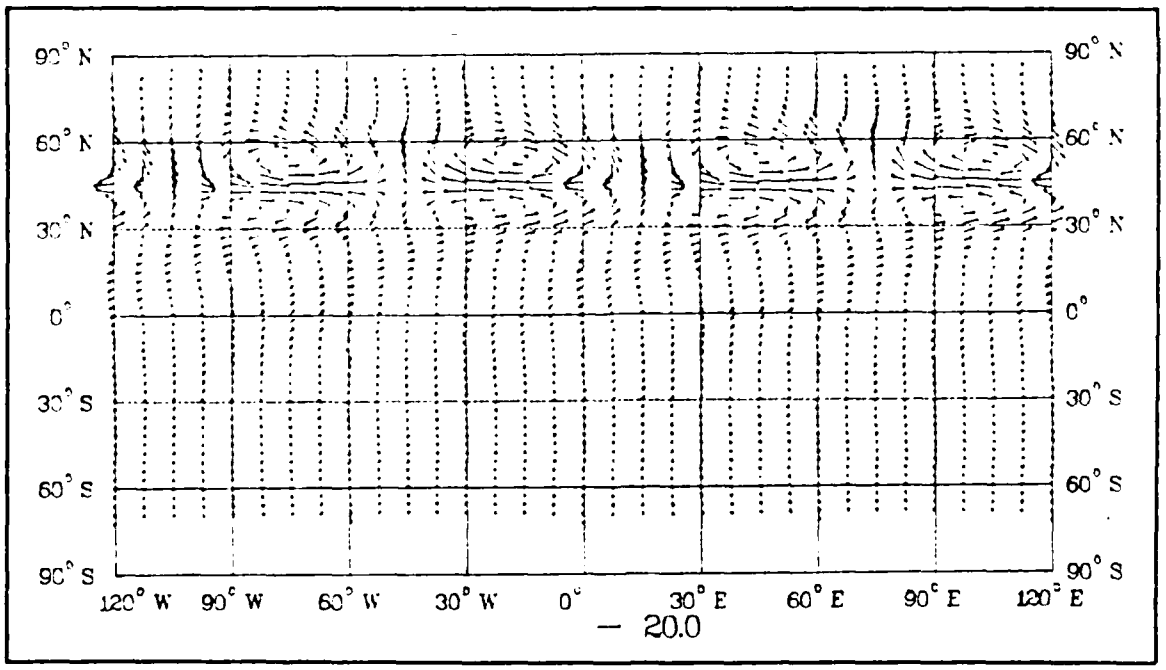

Figure 6.77. Wind Vectors at 72 Hours for Phase III, Experiment 10

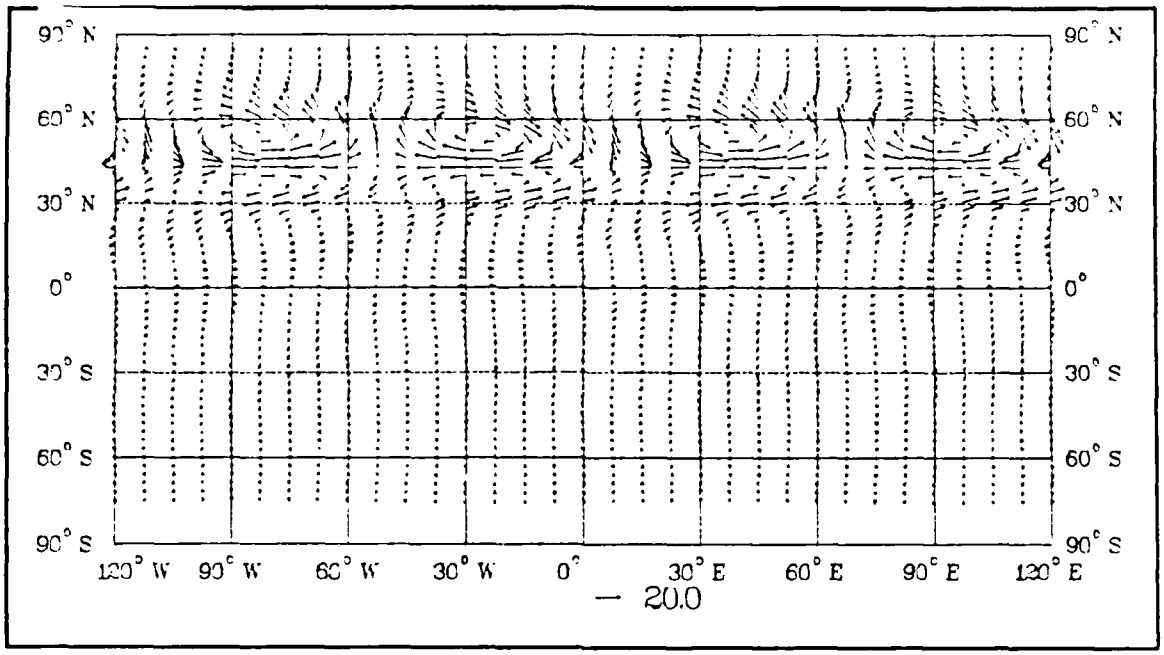

Figure 6.78. Wind Vectors at 96 Hours for Phase III, Experiment 10

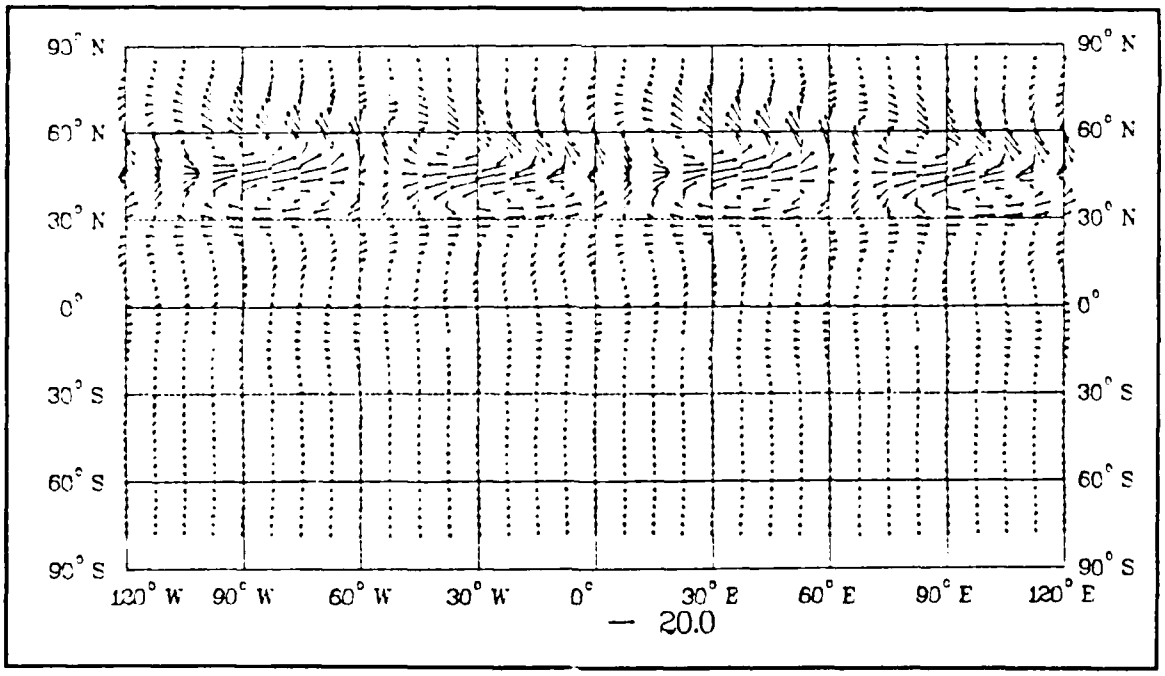

Figure 6.79. Wind Vectors at 120 Hours for Phase III, Experiment 10

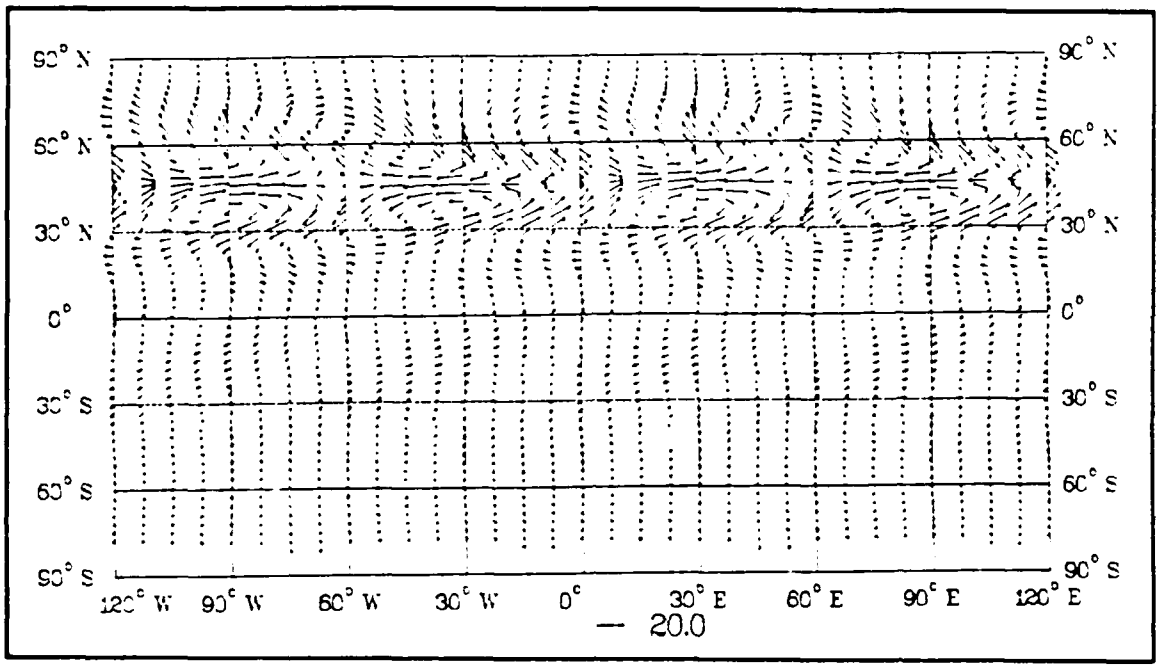

Figure 6.80. Wind Vectors at 144 Hours for Phase III, Experiment 10

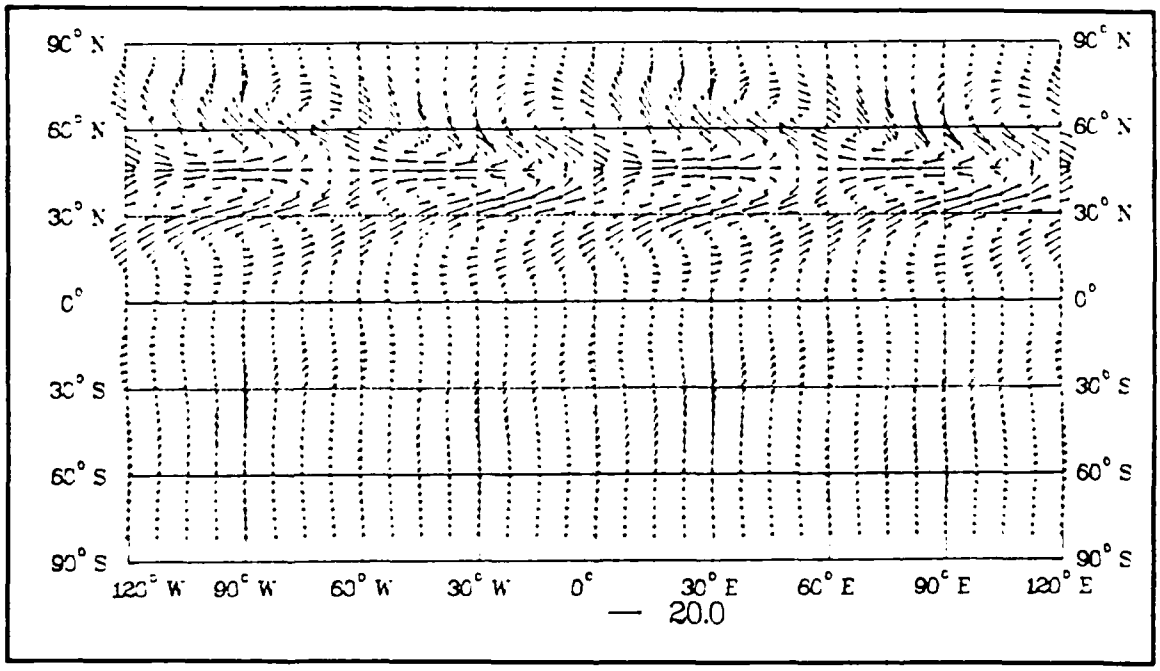

Figure 6.81. Wind Vectors at 168 Hours for Phase III, Experiment 10

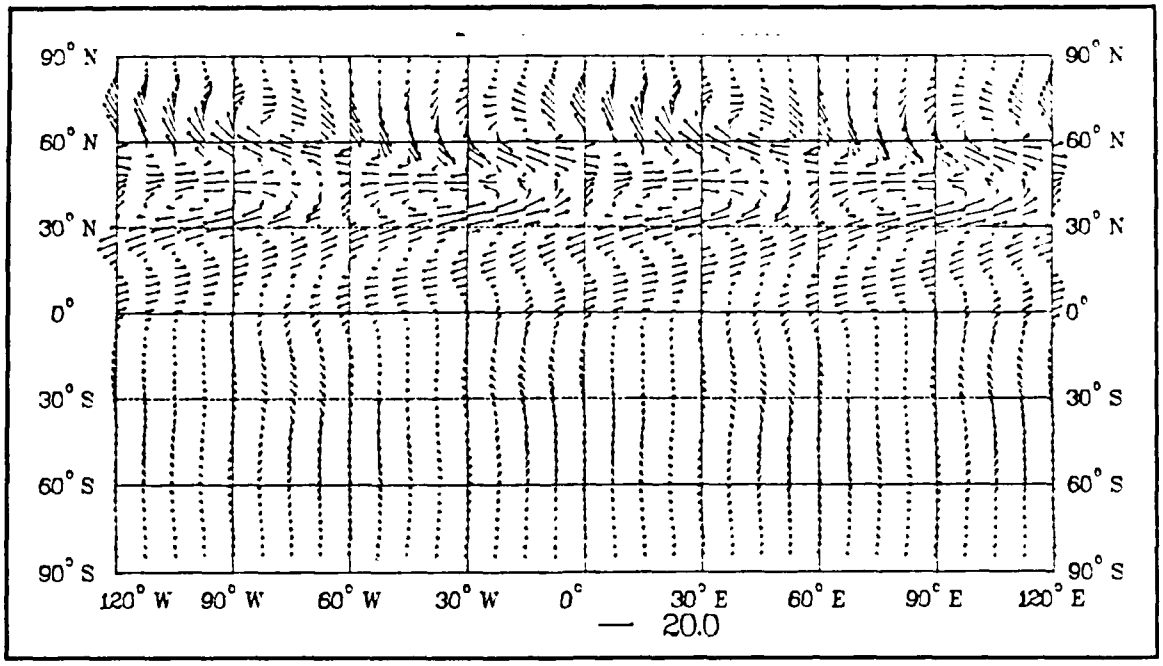

Figure 6.82. Wind Vectors at 192 Hours for Phase III, Experiment 10

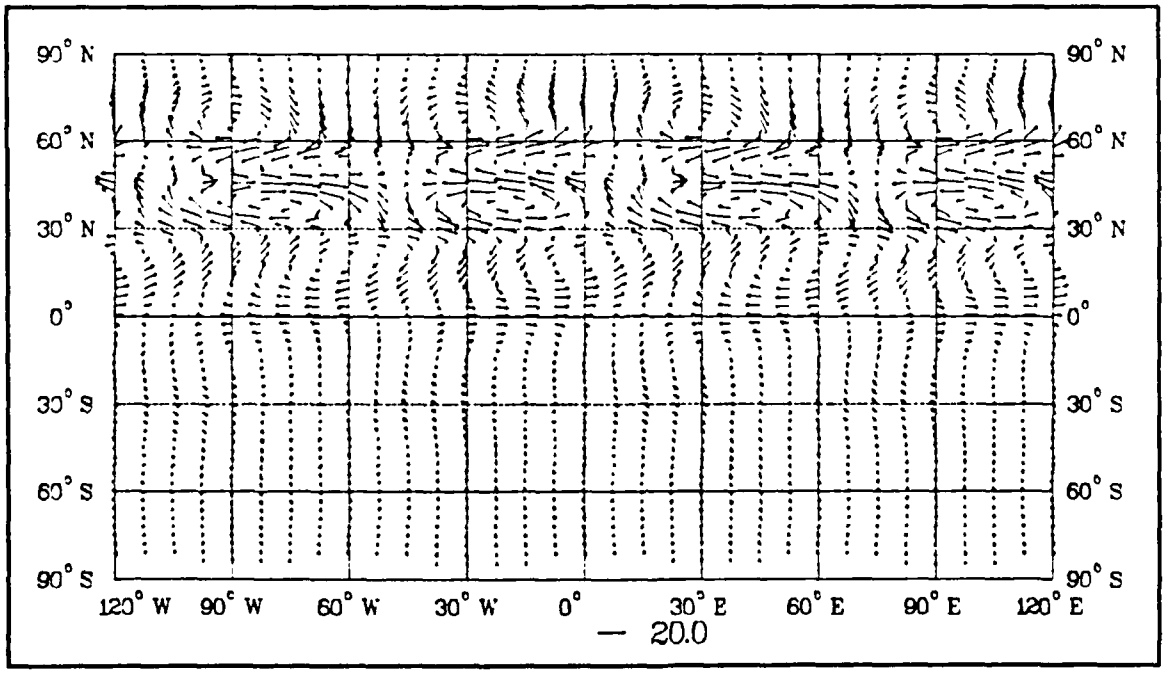

Figure 6.83. Wind Vectors at 216 Hours for Phase III, Experiment 10

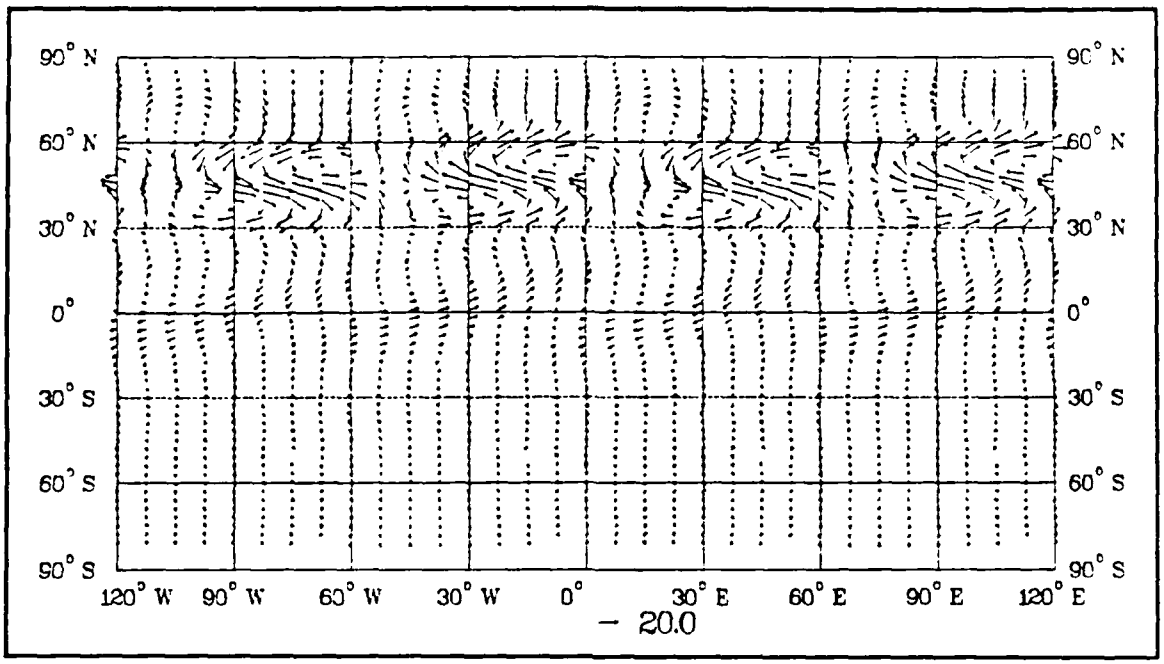

Figure 6.84. Wind Vectors at 240 Hours for Phase III, Experiment 10

The barotropic (Fig. 6.85) and baroclinic (Fig. 6.86) mode analyses at 24 hours show similar circulation patterns as the complete solution at 24 hours. The overall magnitude of the barotropic mode vector field is five times larger than the baroclinic vector field. The larger barotropic response suggests the vorticity forcing is dominant in the generic cyclone. The higher modes have similar circulation patterns, but the overall magnitude of the vector field is much smaller.

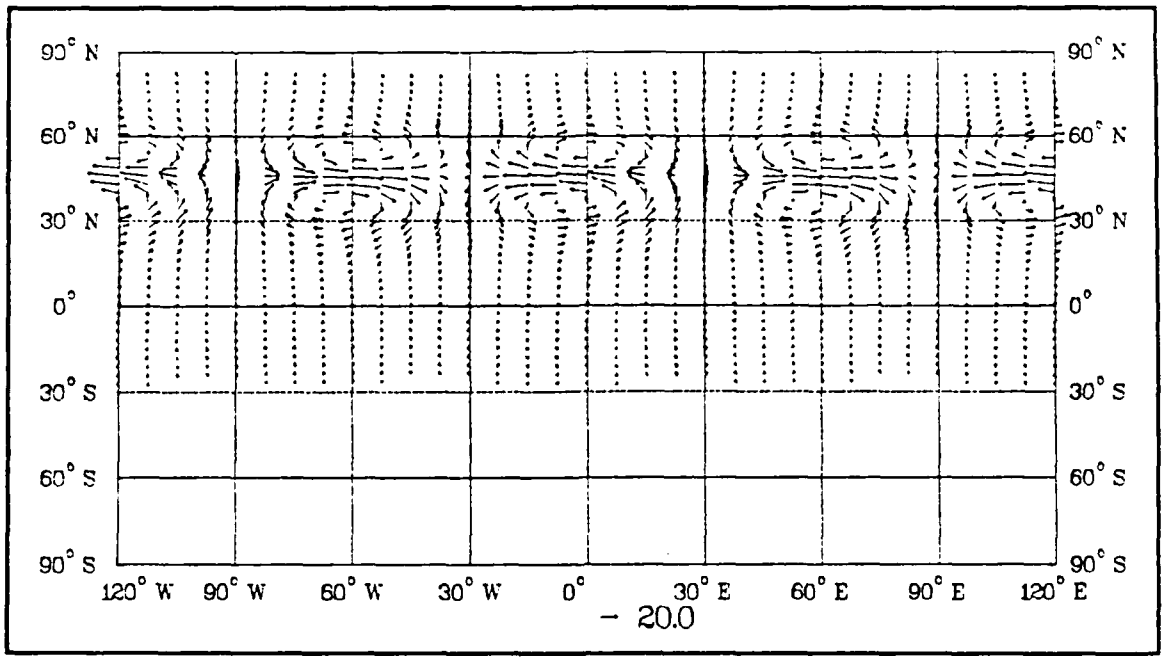

Figure 6.85. Wind Vectors at 24 Hours for Phase III, Experiment 10, Mode 1

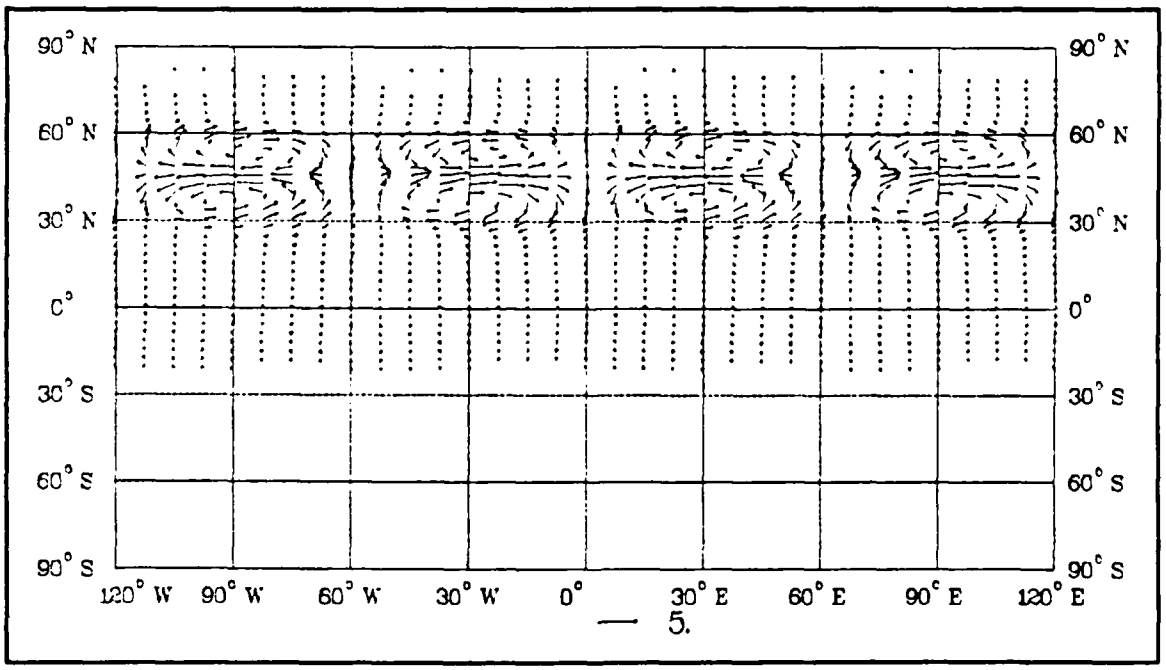

Figure 6.86. Wind Vectors at 24 Hours for Phase III, Experiment 10, Mode 2

2. Experiment 11

In this experiment the forcing is only applied to the thermal equation (Eq. 3.4). After 24 hours a wavenumber three circulation develops in the lowest level (σ = .938), but the circulation is rather chaotic (Fig. 6.87). The circulation remains trapped for the whole time period. After 240 hours (Fig. 6.88) the sinusoidal circulation pattern is still within the source latitudes. It is apparent that the thermal forcing does not play a significant role in producing cold surges in this model. The overall magnitude of the baroclinic mode vector field at 24 hours (not shown) is four times larger than the magnitude of the barotropic field. The larger baroclinic response is similar to the results of Phase I and II.

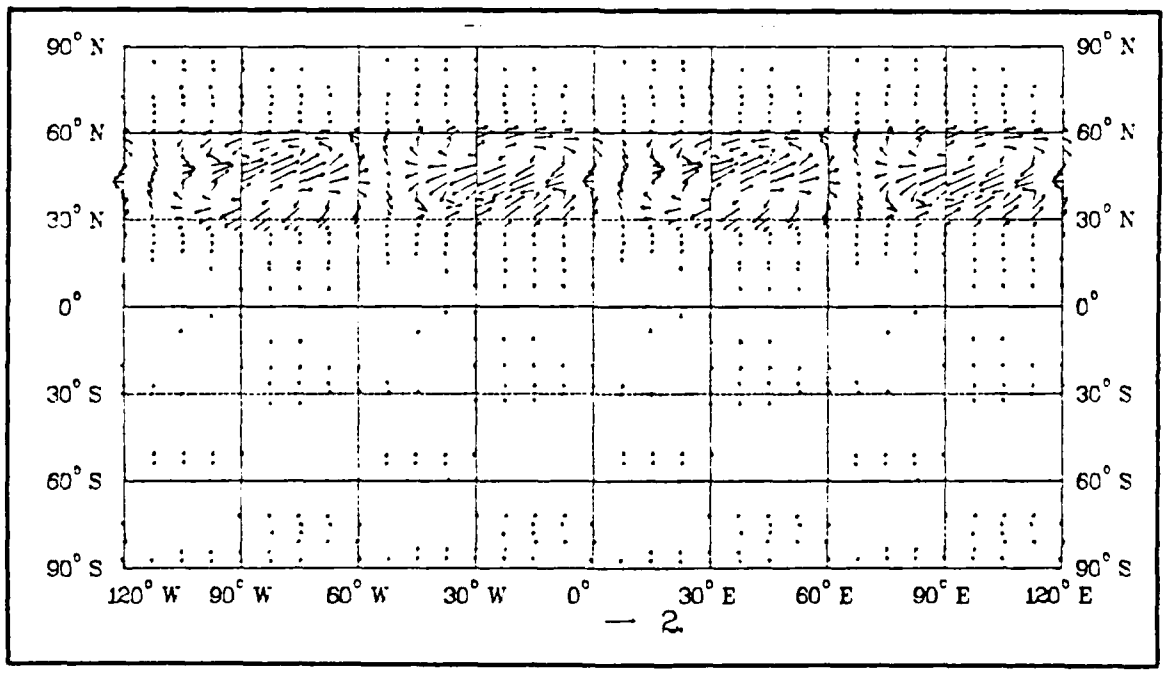

Figure 6.87. Wind Vectors at 24 Hours for Phase III, Experiment 11

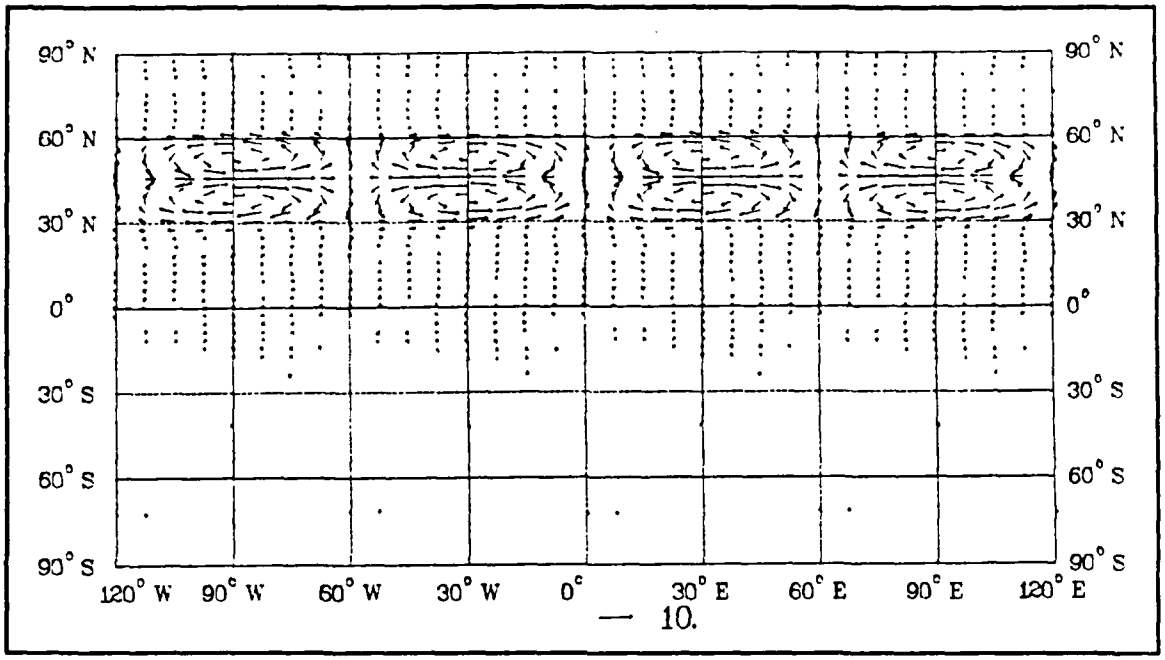

Figure 6.88. Wind Vectors at 240 Hours for Phase III, Experiment 11

3. Experiment 12

In this experiment the forcing is only applied to the vorticity equation (Eq. 3.1). Since the vorticity forcing is dominant, and the thermal forcing does not propagate away from the source, the circulation patterns and magnitudes are not significantly different than the combined thermal and vorticity forcing of Experiment 11.

4. Phase III Summary

The results of Phase III indicate the vorticity forcing is the dominant component in the nonlinear interaction of a planetary wave and a synoptic-scale generic cyclone. The thermal-only forcing does not propagate away from the source and is less intense than the vorticity-only forcing. The vorticity forcing (and thus the combined thermal and vorticity forcing) does produce a northeasterly wind within 48 hours, which is typical of East Asian cold surges. The northeasterly

flow continues into the Southern Hemisphere, which suggests a tropical response to a midlatitude forcing (Lim and Chang, 1987).

VII. CONCLUSION

The objective of this study was to determine whether the nonlinear interaction between a planetary-scale wave (wavenumber four) and a rapidly growing synoptic-scale wave (wavenumber seven) could force a northeasterly cold surge. The nonlinear interaction of these waves produced a wavenumber three forcing. The basic model was a linearized global spectral model with eight levels. Fourteen experiments with three different types of source functions were applied to the thermal and/or vorticity equations. The solutions of each experiment were projected onto the vertical normal modes of the primitive equation model.

The results of each phase of the experiments indicate a midlatitude thermal forcing does not produce a significant cold surge response. The impulse forcing, similar to Lim and Chang (1981), applied to the thermal equation produced a weak cold surge response after 240 hours; however, ten days is longer than the typical two-day surge generation period observed in the East Asian winter monsoon. The difference between the equatorial beta-plane model used by Lim and Chang (1981), and the spherical primitive equation model used in this study will require further explanation. However, the thermal forcing consistently produced a stronger response in the baroclinic mode.

The midlatitude vorticity forcing, on the other hand, produced a stronger response in the barotropic mode. The wavenumber three vorticity forcing produced a significant cold surge response within 48 hours. The cold surge produced by the vorticity forcing is consistent with the observed cold surge in the East Asian winter monsoon.

The lack of cold surge response to a midlatitude thermal forcing, and the significant response to a midlatitude vorticity forcing may be explained by geostrophic adjustment theory. In midlatitude geostrophic adjustment the wind field tends to adjust to the mass field. Thus, when the forcing is prescribed by heating, the local adjustment (to rotational motion) is more complete. When the forcing is prescribed by vorticity, the adjustment will be less efficient and a considerable amount of energy will propagate away in divergent motion. The equatorward propagation studied by Lim and Chang's (1981) theory is through equatorial Rossby waves that have a significant divergent component. Thus, the divergent motion may offer a possible explanation for the different responses to the two types of forcings.

The initial condition of this study did not include any basic current (mean flow). In reality, the cold surge is superimposed on an existing northeasterly monsoonal flow at the surface. It would be interesting to see if the presence of an initial mean flow would alter the results of the forcings. Also, the nonlinear effects of topographic channeling play an important role in the cold surge response. Using some type of topographic barrier may lead to interesting conclusions.

LIST OF REFERENCES

Arakawa, A. and M. J. Suarez, 1983: Vertical differencing of the primitive equations in sigma coordinates. *Mon. Wea. Rev.*, **111**, 34 - 45.

Baker, B. J., 1983: *Numerical simulation of the forcing of monsoon surges by midlatitude baroclinic waves*. Master's Thesis, Naval Postgraduate School, Monterey, CA, September 1985, 109 pp.

Bashford, K. R., 1985: Generation of cold surges. Notes from unpublished Master's Thesis, Naval Postgraduate School.

Boyle, J. S. and T. J. Chen, 1987: Synoptic aspects of the wintertime East Asian monsoon. *Monsoon Meteorology*, edited by C. P. Chang and T. N. Krishnamurti. Oxford University Press, 125 - 160.

Chang, C. P., J. E. Millard and G. T. J. Chen, 1983: Gravitational character of cold surges during Winter MONEX. *Mon. Wea. Rev.*, **111**, 293 - 307.

Eady, E. T., 1949: Long waves and cyclone waves. *Tellus*, **1**, 33 - 52.

Gill, A. E., 1982: *Atmosphere-ocean dynamics*. Academic Press, 662 pp.

Haltiner, G. J. and R. T. Williams, 1980: *Numerical prediction and dynamic meteorology*. John Wiley & Sons, 477 pp.

Harris, N. E., 1985: *Numerical simulation of cold surges*. Master's Thesis, Naval Postgraduate School, Monterey, CA, September 1985, 80 pp.

Huschke, R. E., 1959: *Glossary of Meteorology*. American Meteorological Society, 638 pp.

Lau, K. M. and C. P. Chang, 1987: Planetary scale aspects of the winter monsoon and atmospheric teleconnections. *Monsoon Meteorology*, edited by C. P. Chang and T. N. Krishnamurti. Oxford University Press, 161 - 202.

Lim, H. and C. P. Chang, 1981: A theory for midlatitude forcing of tropical motions during winter monsoons. *Mon. Wea. Rev.*, **38**, 2377 - 2392.

Lim, H. and C. P. Chang, 1987: On the dynamics of midlatitude-tropical interactions and the winter monsoon. *Monsoon Meteorology*, edited by C. P. Chang and T. N. Krishnamurti. Oxford University Press, 405 - 434.

Lindzen, R. S., 1967: Planetary waves on beta-plane. *Mon. Wea. Rev.*, **95**, 441 - 451.

McAtee, M. D., 1984: *Sensitivity of planetary waves to initial conditions and forcing*. Master's Thesis, Naval Postgraduate School, Monterey, CA, December 1984, 61 pp.

Peng, M. S., 1982: *A spectral study of supercritical baroclinic disturbances in a stratified viscous fluid*. Doctoral Thesis, State University of New York at Albany, Albany, NY, June 1982, 140 pp.

Ramage, C. S., 1971: *Monsoon Meteorology*. Academic Press, 296 pp.

INITIAL DISTRIBUTION LIST

		No. Copies
1.	Defense Technical Information Center Cameron Station Alexandria, Virginia 22314-6145	2
2.	Library, Code 0142 Naval Postgraduate School Monterey, California 93943-5002	2
3.	Commander Naval Oceanography Command NSTL Station Bay St. Louis, Mississippi 39522	1
4.	Commanding Officer Fleet Numerical Oceanography Center Monterey, California 93943	1
5.	Commanding Officer Air Force Global Weather Center Offutt Air Force Base, Nebraska 68113	1
6.	Officer-in-Charge Naval Environmental Prediction Research Facility Monterey, California 93943	1
7.	Prof. R. J. Renard, Code 63Rd Naval Postgraduate School Monterey, California 93943-5000	1
8.	AFIT/CIR Wright-Patterson Air Force Base, Ohio 45433-6583	1
9.	Air Weather Service Technical Library Scott Air Force Base, Illinois 62225	1
10.	Captain Randy J. Lefevre Det 1, 2nd Weather Squadron Wright-Patterson Air Force Base, Ohio 45433	2

11. Prof. R. T. Williams, Code 63Wu 5
Naval Postgraduate School
Monterey, California 93943-5000

12. Prof. C. P. Chang, Code 63Cp 2
Naval Postgraduate School
Monterey, California 93943-5000

13. Prof. R. L. Elsberry, Code 63Es 1
Naval Postgraduate School
Monterey, California 93943-5000

14. Dr. M. S. Peng, Code 63Pg 1
Naval Postgraduate School
Monterey, California 93943-5000

15. Dr. M. A. Rennick 1
Martin-Marietta Data Systems
Fleet Numerical Oceanography Center, Building 702
Monterey, California 93943

16. Dr. T. Rosmond 1
Naval Environmental Prediction Research Facility
Monterey, California 93943

17. Prof. Hock Lim 1
Blk 1M Prine Grove
#01-46
Singapore 2159
Republic of Singapore

18. Prof. G. T. Chen 1
Department of Atmospheric Sciences
National Taiwan University
Taipei, TAIWAN 107, R. O. C.

19. Prof. T. Y. Tsay 1
Department of Atmospheric Sciences
National Taiwan University
Taipei, TAIWAN 107, R. O. C.